Research Summary: IAPA Scholarship
Megan E. McGovern

In this report, I will provide a summary of my research accomplishments upon receiving the IAPA scholarship. First, I will discuss the need for my current research. Then, I will provide a brief summary of the prerequisite, background research which was performed prior to receiving the IAPA scholarship. Finally, I will discuss my more recent research accomplishments, which I was able to achieve due in part from the support of the Gallagher Family Memorial Scholarship from the Illinois Asphalt Pavement Association. For referencing convenience, I have included my published research in the Appendix of this report.

My Research: The Need

Cracks in asphalt pavements are expensive and difficult to properly repair. They drastically affect the life span of asphalt pavements, rideability, and lead to millions of dollars of repair and maintenance annually. If left untreated, cracks deteriorate and widen over time, allowing moisture and oxygen to readily infiltrate the pavement system, which can lead to severe pavement damage over time. Oxidative aging has long been recognized as an important contributing factor to cracking of asphalt pavements. As the asphalt concrete is subjected to conditions in the field, it continuously becomes oxidized, leading to material embrittlement with time. Aged pavements are stiffer, more brittle, and relieve stresses much slower than newer pavements. While aged pavements accumulate damage at a faster rate, their crack healing rate also occurs at a slower rate.

A rejuvenator, as the name implies, is a product that aims to restore the physical and chemical properties of aged bitumen. Rejuvenators address the issue of oxidative hardening by softening the aged asphalt via the restoration of the original asphaltenes to maltenes ratio [1-3]. Some examples of rejuvenators are refined tallow, waste vegetable or frying oils, waste motor oils, lube extracts, extender oils, emulsions, soft virgin binders, and bio-binders [1,4,5]. Rejuvenators are generally applied to the surface of existing pavements; therefore, it is essential for the rejuvenator to have the ability to penetrate the surface and diffuse through the aged asphalt. If the rejuvenator lacks this ability, not only will the aged asphalt be unaffected, but the unabsorbed rejuvenator will reduce skid resistance [3,6]. To avoid creating slick, over-coated surfaces, it is often good practice to apply rejuvenators in several coats at a lower application rate [7]. During the diffusion process, the rejuvenator first forms a low-viscosity layer around the layer of aged binder which coats the aggregate. Then, the rejuvenator starts to diffuse into the aged binder, thus softening it. Eventually, all the rejuvenator penetrates into the aged binder and the inner layer becomes less viscous and the outer layer becomes more viscous as the mixture approaches a state of equilibrium [3,6].

Preventive maintenance of pavements is an important aspect of pavement. It is much more cost effective to maintain a pavement in an acceptable state than defer maintenance until damage becomes severe. Thus, preservation entails repairing distresses in the pavement at very early stages, i.e., as they begin to occur. One of the great challenges is determining when a pavement has become vulnerable to cracking. Currently, pavement engineers lack practical tools to determine the proper time for preventive maintenance. Maintenance can entail the application of surface treatments such as the application of rejuvenators, or a more substantial rehabilitation such as pavement milling and resurfacing. Accurate evaluation of aging effects of asphalt concrete could greatly benefit pavement engineers in determining the critical time for applying preventive maintenance measures to extend the pavement life. One such pavement preservation method could entail the use of rejuvenators. Currently, researchers are still pursuing a thorough and quantitative understanding of the effect of rejuvenators. There exists a need for a more reliable method for determining the effectiveness of a rejuvenating agent.

Background on Research Accomplishments

My research has followed a natural trajectory, where the primary goal is to provide pavement engineers with a tool to quickly, accurately, and non-destructively evaluate the oxidative aging level of asphalt concrete pavements. Such a tool would allow pavement engineers to make decisions regarding proper maintenance time, as well as evaluate the effectiveness of these decisions (e.g., evaluate the efficacy of applied rejuvenators). In this section, I will detail the work that has lead up to my current research.

Characterization of Asphalt Concrete using Linear Ultrasonics

To understand the oxidative aging effects on asphalt concrete mixtures, acoustic emissions and ultrasonic tests were conducted in Reference [8]. A set of nine mixtures, encompassing different aging levels ranging from 0 to 72 hours of laboratory oven aging were prepared and tested. Acoustic emission tests were conducted on all specimens, and ultrasonic tests were conducted on specimens aged from 0 to 36 hours. Ultrasonic tests were not performed on specimens aged past 36 hours, as the rough cratered surface texture impeded satisfactory couplant conditions. This study was the first to report frequency dependent ultrasonic velocity and attenuation measurements. Furthermore, this study was the first to report ultrasonic shear wave measurements.

Using the ultrasonic measurements from Reference [8], the dynamic Young's (uniaxial) and shear complex moduli were computed in Reference [9]. There was observed to be a discernible trend of the dynamic modulus with respect to aging. Specifically, it increases from 0 hours to 24 hours and decreases from 24 hours to 36 hours. From this trend, it was concluded that after 24 hours, the binder becomes so stiff that it loses adhesion with the aggregate resulting in an overall decrease in the dynamic modulus. It was observed that the complex modulus results via ultrasonic measurements do not overlap with results from mechanical testing due to scattering effects present in the ultrasonic testing that are not present in the mechanical testing; however, a correlation does exist. It was noted that shear ultrasonic measurements must be carried out, because too much uncertainty exists in trying to guess a suitable Poisson's ratio. Also, frequency dependent ultrasonic measurements must be carried out to eliminate need for mechanical testing. The correlation between the ultrasonic measurements and the amount of aging suggests that this non-destructive method can be successfully employed to detect aging in asphalt concrete.
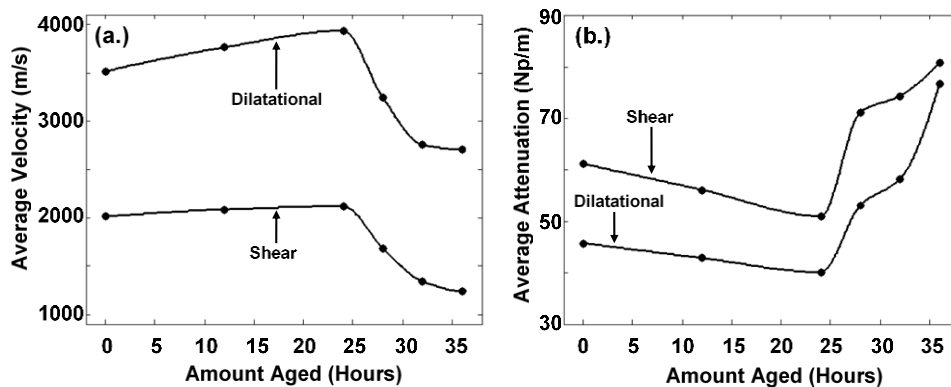
Figure 1. Average across frequency of **(a.)** velocities (m/s) and **(b.)** attenuations (Np/m) for asphalt concrete aged 0 to 36 hours. The average velocity (for both dilatational and shear) increase from 0 to 24 hours and decrease from 24 to 36 hours. The average attenuation (for both dilatational and shear) decreases from 0 to 24 hours and increases from 24 to 36 hours.

The results from References [8] and [9] all exhibit a particular trend, where the properties increase (decrease) with an increase in age until reaching a critical point, after which the data decreases (increases) with age. Furthermore, these results agree with data published in other studies. See Figure 1. These results highlight the importance of the critical point in oxidative aging. Below this critical point, asphalt has the

ability to self-heal micro-flaws. Beyond this critical point, degradation of the pavement occurs rapidly. This behavior can be explained by understanding the two phenomena that occur as the level of oxidative aging in the asphalt concrete increases: 1. The binder stiffness increases and 2. The adhesion between the binder/mastic and aggregates decrease. At low aging levels, i.e., below the critical point, the binder stiffness is the dominating affect on the overall composite stiffness. At higher ageing levels, i.e., above the critical point, the adhesion loss dominates the overall stiffness. The critical point for the mixture-type used in this study was observed to occur at 24 hours of laboratory aging.

Characterization of Asphalt Concrete using Nonlinear Ultrasonics

While the linear acoustic techniques from References [8] and [9] allow the pavement engineer to detect damage at high levels, these techniques are not sensitive to microflaws (i.e., flaws much smaller than the ultrasonic wavelength). For this reason, nonlinear acoustic methods are more suitable for damage detection due to the increased sensitivity to microflaws. In Reference [10], the feasibility of assessing the level of oxidative aging of asphalt concrete was studied using non-collinear wave mixing, a nonlinear acoustic technique. This technique involves the mixing of two ultrasonic waves. In a linear elastic material, the two waves will simply cross paths. However, in a nonlinear elastic medium, such as asphalt concrete, the two waves may interact to produce a third scattered wave. This interaction will only exist under the right conditions. Please refer to Reference [10] for a more detailed discussion on the appropriate conditions. Even in its unaged, virgin state, asphalt concrete belongs to a nonlinear elastic class of materials called mesoscopic materials. As the asphalt concrete is oxidatively aged, it displays increasingly nonlinear behavior. This nonlinear behavior can be monitored by observing some parameters of the third scattered wave (which arose from the interaction). Namely, these parameters include the frequency at which the interaction takes place f_2/f_1 and the efficiency of the interaction, β/β_0. Refer to Reference [10] for a detailed description of these parameters.

Non-collinear wave mixing was performed on a set of asphalt concrete specimens subjected to various amounts of oven-aging from 0 to 36 hours. In order to perform the measurements, angles were cut into the cylindrical gyratory compacted specimens to facilitate the mounting of the transducers and ensure that the waves interacted at the appropriate angle. See Figure 2. It was observed that the frequency ratios changed with the amount of aging. Even in the presence of strong attenuation, the nonlinear scattered wave was detected. It was found that asphalt concrete exhibits nonlinear behavior which increases exponentially with the amount of aging.
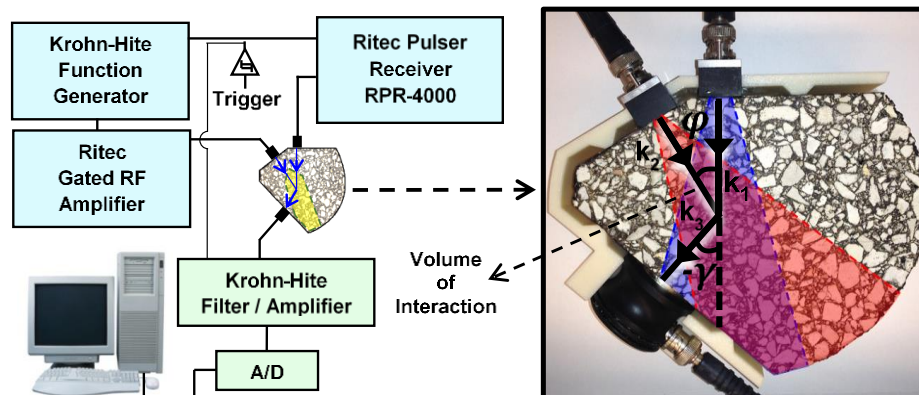

Figure 2. Test samples Schematic diagram of the ultrasonic data collection system illustrating the angle of interaction of the two longitudinal waves and the location of the shear transducer to receive the generated scattered shear wave. The blue and red regions denote the areas of signals k_1 and k_2, respectively, due to beam spread. The region where they overlap is the volume of interaction. Note, the beam spread from k_2 is slightly higher than k_1 due to the difference in frequencies.

For field use, the method presented in Reference [10] is not, in its current state, practical, because it involves coring the pavement and then cutting the sample to the geometry shown in Figure 2. Thus, the goal of Reference [11] was to address this issue and modify the testing configuration to be one-sided. A one-sided configuration would eliminate the need for a core, and thus, extend the method to be truly non-destructive and employable on-site. This was achieved through the use of subsurface dilatational waves. Subsurface dilatational waves are dilatational (compressional) waves that propagate close and parallel to the surface. Dilatational transducers were mounted on variable Plexiglas angle wedges to generate subsurface dilatational waves. The two waves were propagated through a sample set of asphalt concrete specimens of different oxidative aging levels such that they interacted to produce a third scattered nonlinear shear wave, which was received by a third transducer positioned on the same side of the specimen. Please refer to Figure 3, which shows the one-sided configuration. The non-collinear wave mixing technique was thus employed in the same manner as the previous study in Reference [10]. As before, it was verified that the nonlinear wave originated from the wave mixing in the specimen and not the testing instrumentation by using selection criteria. It was found that asphalt concrete exhibits nonlinear behavior which increases exponentially with the amount of aging. The results from this study correlated well with the results from the previous study [10], demonstrating the effectiveness of this technique.

Reference [11] demonstrated that wave-mixing of subsurface dilatational waves could successfully assess the aging level of the pavement; however, prior knowledge of the specimens' linear acoustic properties (*i.e.,* velocity and attenuation) was necessary in order to properly set the incident angle of the wedges. Reference [12] addresses the issue of appropriately setting the incident angle when the acoustic properties of the pavement are unknown via an iterative technique. A "nonlinear-characterization curve" was also introduced, which allows for the amount of oxidative aging to be estimated. The nonlinear-characterization curve is constructed by plotting the two measured nonlinear parameters, i.e., f_2/f_1 versus β/β_0, obtained from the aged sample set in laboratory conditions. See Figure 4. Once this nonlinear-characterization curve is known for a particular mixture, it need not be generated again. A library of these curves could be generated for various mixture-types, so that all the pavement engineer needs to know *a priori*, is the mixture-type of the pavement to be interrogated. The parameters of the pavement (f_2/f_1, β/β_0) can then be measured, superimposed on the nonlinear-characterization curve, and the age determined. To verify the accuracy of the iterative angle technique, a blind study was performed, whereby the samples were tested assuming no prior knowledge about the material properties of the specimen.
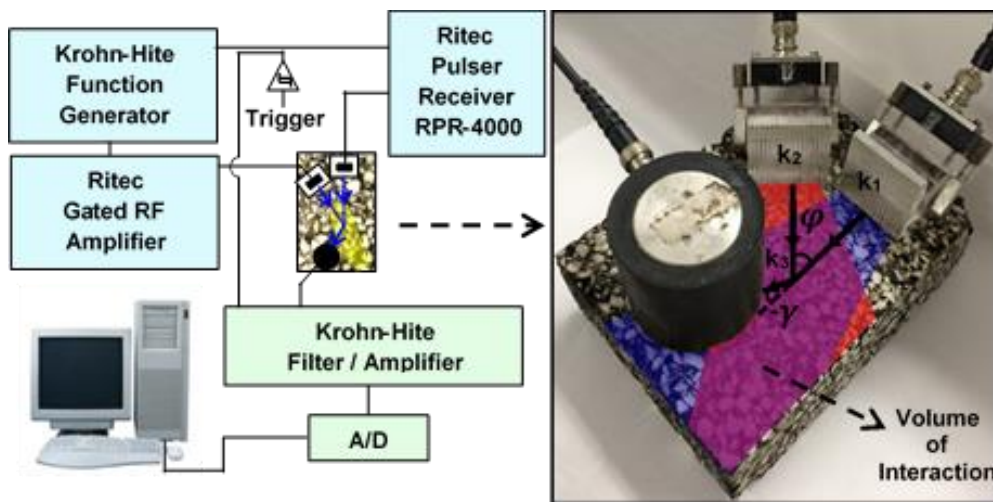
Figure 3. Test samples Schematic diagram of the ultrasonic data collection system illustrating the angle of interaction of the two longitudinal waves and the location of the shear transducer to receive the generated scattered shear wave. The blue and red regions denote the areas of signals k_1 and k_2, respectively, due to beam spread. The region where they overlap is the volume of interaction. Note, the beam spread from k_2 is slightly higher than k_1 due to the difference in frequencies.
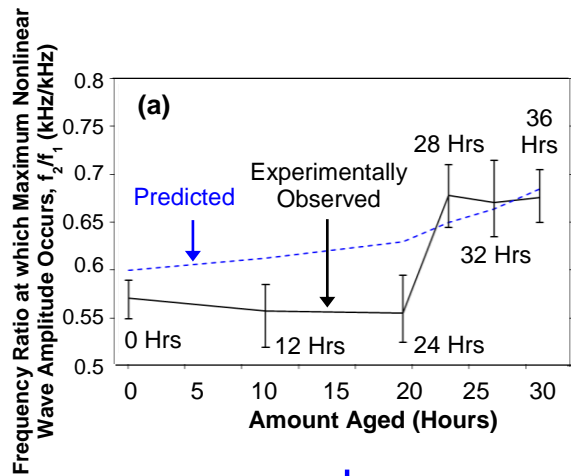
For each aging level, the observed frequency ratio at which the maximum nonlinear wave amplitude occurred, f_2/f_1, and the normalized nonlinear parameter, β/β_0, were used to generate the reference curve

The reference curve only requires knowledge of the existing mixture so that the field measurements can be normalized by the parameters corresponding the virgin mix

The nonlinear parameters, f_2/f_1 and β/β_0, of the asphalt pavement can be experimentally obtained and superimposed on the reference curve to determine the amount of oxidative aging
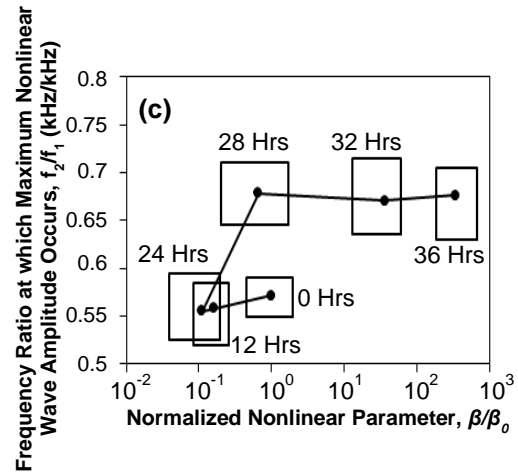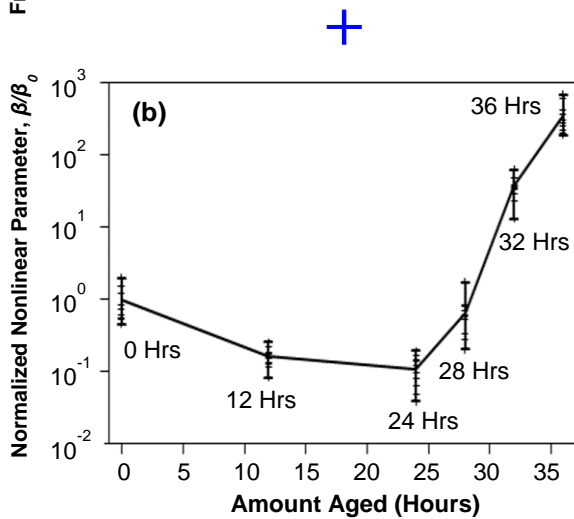
Figure 4. Generation of the reference curve, i.e., the frequency ratio vs. the normalized nonlinear parameter. Please note that (a) and (b) are experimentally determined from specimens with increasing levels of controlled oxidative aging. The data from (a) and (b) is used to create (c).

Research Accomplishments since Receiving IAPA Scholarship

Since receiving the IAPA scholarship, I have been able to expand upon the non-collinear wave-mixing method presented in my previous research. Specifically, I have simplified the one-sided technique [12] to be more practical for field use. I also have studied the ability of the technique presented in Reference [12] evaluate the efficacy of asphalt rejuvenators, which aim to restore the mechanical properties lost due to oxidative aging. Because this approach is capable of assessing the level of oxidative aging, pavement engineers now have the proper tools to not only identify the proper time for maintenance, but they can also treat the pavement and assess the effectiveness of the treatment. A more detailed discussion on this research will now be provided.

In the previous research (see previous section), the non-collinear wave-mixing technique was demonstrated to be a reliable method for assessing the amount of oxidative aging present in AC. Furthermore, the testing-setup can be configured such that only access to one-side (i.e., the top) of the pavement is necessary. An iterative angle technique was introduced to address the issue of the unknown linear acoustic properties, i.e., ultrasonic velocity and attenuation. The iterative angle technique; however, can be tedious and time-

consuming. Thus, in Reference [13], the one-sided technique was modified such that it is quicker and simpler to implement in the field. This was done by using a fixed angle technique. In this technique, an angle is determined for the mixture-type that will be suitable across the desired range of age levels (e.g. 0 to 36 hours). For the mixture-type, age-range, and testing set-up used in this study, the suitable angle was determined to be 73º. It was observed that the fixed angle technique introduces some error in the accuracy of the measurements when compared to the iterative angle technique; however, the error was not so great as to diminish the effectiveness of the test for assessing the age level. To verify the accuracy of the fixed angle technique, a blind study was performed. Please refer to Figure 5, which shows the results from this blind study test superimposed on the nonlinear-characterization curve. This fixed angle technique has the advantage that eliminates the need for determining the incident angle via the tedious and relatively time-consuming iterative angle method, because the test set-up is completely constant across the entire laboratory sample set. This technique therefore has the potential to be developed into an instrument for pavement engineers to use to quickly evaluate the state of the pavement.
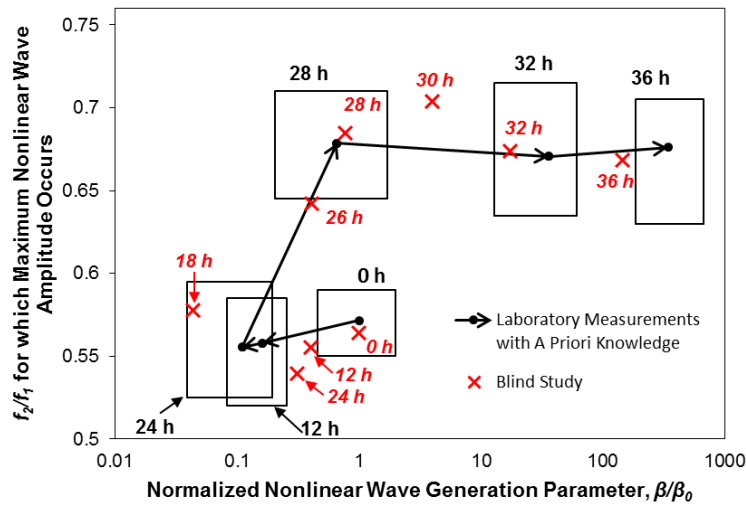

Figure 5. The frequency ratio f_2/f_1 at which interaction occurs vs. the efficiency of the interaction β/β_0 for asphalt concrete specimens subjected to oven-aging. The red x's represent the average of the 10 independent measurements taken from the top surface using the fixed-angle technique, without any prior knowledge of the specimen aging (only the type of mixture was known).

Receiving the Gallagher Family Memorial Scholarship has also allowed me to extend my research to explore the efficacy of rejuvenators on restoring the properties of aged asphalt concrete to the virgin state. In Reference [14], the effectiveness of rejuvenators, *i.e.,* the effective amount of aging of the AC after rejuvenator application, was assessed via the non-collinear wave mixing technique as a function of the dwell time. The data collected from the rejuvenator-coated specimens was compared to the known reference curve to determine the degree of restoration the rejuvenator had on the AC as a function of the dwell time.

Oxidatively aged asphalt concrete specimens were coated with rejuvenator (10% by weight of the binder) and left to dwell for a specific amount of time: 3 to 6 days in 1 day increments, 1 to 8 weeks in 1 week increments, and 12 weeks. Once the dwell time reached the desired amount, the specimen was wiped of any excess rejuvenator, to improve couplant conditions, and immediately ultrasonically tested. The frequency ratio, f_2/f_1, at which the interaction took place and the normalized nonlinear wave generation parameter, β/β_0, were recorded and compared against the nonlinear-characterization curve. See Figure 6. This is the same plot that was created in Reference [11] using asphalt concrete samples (with no rejuvenator) subjected to various amounts of oxidative oven aging. It was observed that the samples with a dwell time of 5 weeks and greater exhibited nonlinear characteristics similar to the reference virgin specimen. From

1 to 4 weeks, the nonlinear parameters became closer to the virgin parameters with each successive week. This indicates that the rejuvenator takes time to chemically act on the aged binder. It is difficult to know whether the observed changes in the specimens are due to a composite effect of the rejuvenator and asphalt concrete, or a result from the rejuvenator chemically acting on the aged binder. The ability of the rejuvenator to fully penetrate and act on the binder was observed to be dependent on the porosity and aggregate structure, and thus varied for each specimen. As a result, some portions of the binder were restored to a greater extent than others. This non-uniform nature was captured via the nonlinear ultrasonic technique.
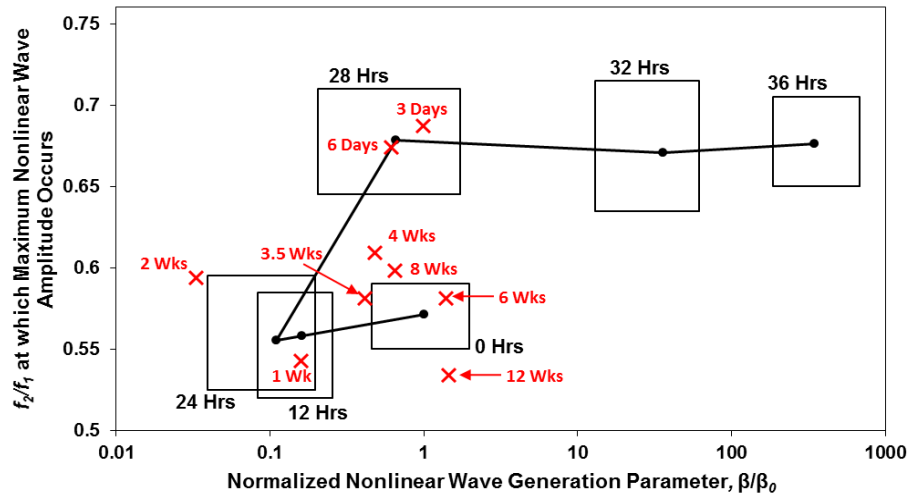
Figure 6. Damage evolution path for increasing levels of aging (solid line and solid dots), as well as the average of five measurements taken on specimens aged 36 hours exposed to rejuvenator for increasing amount of dwell times (crosses) using the iterative-angle technique.
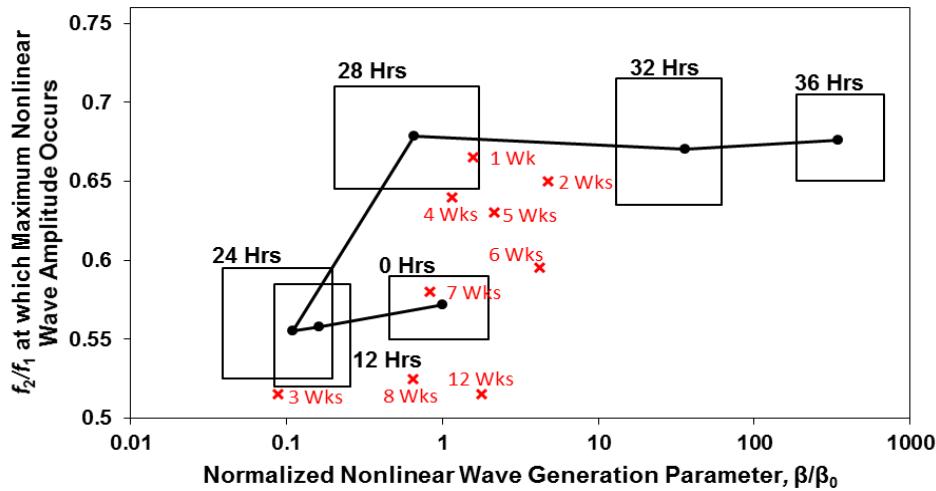
Figure 7. Damage evolution path for increasing levels of aging (solid line and solid dots), as well as the average of five measurements taken on specimens aged 36 hours exposed to rejuvenator for increasing amount of dwell times (crosses) using the fixed-angle technique. Extracted from….

Most recently, the utility of using the fixed angle technique from Reference [13] for testing the efficacy of rejuvenators was studied. Figure 7 shows the results from this study. The results obtained using the fixed-

angle technique agree with the results obtained from the more accurate iterative-angle technique presented in Figure 6, thus, demonstrating the validity of this technique.

Conclusions

I developed a method to nondestructively assess the amount of oxidative aging present in a pavement when there is only access to one side (*i.e.,* the top). Receiving the Gallagher Family Memorial Scholarship has also allowed me to extend this method to be practical for field use by introducing a "fixed angle" technique. A blind study was performed on a sample set of aged asphalt concrete specimens to verify the validity of this method. This research has the potential to lead to an instrument which would allow decision makers to quickly and accurately determine the proper time for rehabilitation/maintenance of pavements. Also, this technique was used to evaluate the efficacy of asphalt rejuvenators, which aim to restore the mechanical properties lost due to oxidative aging. Because this approach is capable of assessing the level of oxidative aging, pavement engineers now have the proper tools to not only identify the proper time for maintenance, but they can also treat the pavement and assess the effectiveness of the treatment.

Acknowledgements

References

1. E. Buenrostro-Gonzalez, H. Groenzin, C. Lira-Galeana and O. C. Mullins, "The Overriding Chemical Principles that Define Asphaltenes," *Energy and Fuels,* vol. 15, pp. 972-978, 2001.
2. J. Shen, S. Amirkhanian and J. A. Miller, "Effects of Rejuvenating Agents on Superpave Mixtures Containing Reclaimed Asphalt Pavement," *Journal of Materials in Civil Engineering,* vol. 19, no. 5, pp. 376-384, 2007.
3. Á. García, E. Schlangen and M. Van de Ven, "Properties of capsules containing rejuvenators for their use in asphalt concrete," *Fuel,* vol. 90, pp. 583-591, 2010.
4. S. N. Nahar, J. Qiu, A. Schmets, E. Schlangen, M. Shirazi, M. van de Ven, G. Schitter and A. Scarpas, "Turning Back Time: Rheological and Microstructural Assessment of Rejuvenated Bitumen," *Transportation Research Board 93rd Anual Meeting: Compendium of Papers,* 2014.
5. D. Oldham, E. H. Fini and T. Abu-Lebdeh, "Investigating the Rejuvenating Effect of Bio-Binder on Recycled Asphalt Shingles," *Transportation Research Board 93rd Annual Meeting: Compendium of Papers,* 2014.
6. E. R. Brown, "Preventative Maintenance of Asphalt Concrete Pavements," National Center for Asphalt Technology, Auburn, AL, 1988.
7. R. E. Boyer, "Asphalt Rejuventators 'Fact, or Fable'," Asphalt Institute, Panama City, FL, 2000.
8. M.E. McGovern, B. Behnia, W.G. Buttlar, and H. Reis, (2013), "Characterization of oxidative aging in asphalt concrete – Part 1: Ultrasonic velocity and attenuation measurements and acoustic emission response under thermal cooling" *Insight Non-Destructive Testing and Condition Monitoring Journal*, Vol. 55, No. 11, pp. 596-604.
9. M.E. McGovern, B. Behnia, W.G. Buttlar, and H. Reis, (2013), "Characterization of oxidative aging in asphalt concrete – Part 2: Estimation of complex moduli" *Insight Non-Destructive Testing and Condition Monitoring Journal*, Vol. 55, No. 11, pp. 605-609.
10. M.E. McGovern, W.G. Buttlar, and H. Reis, (2014), "Characterization of Oxidative Aging in Asphalt Concrete using a Non-Collinear Ultrasonic Wave Mixing Approach," *Insight Non-Destructive Testing and Condition Monitoring Journal*, Vol. 56, No. 7, pp. 367-374.
11. M.E. McGovern, W.G. Buttlar, and H. Reis, (2014), "Estimation of Oxidative Aging in Asphalt Concrete Pavements using Non-Collinear Wave Mixing of Critically Refracted Longitudinal Waves," *Insight Non-Destructive Testing and Condition Monitoring Journal*, Vol. 57, No. 1, pp. 25-34.

12. M.E. McGovern, W.G. Buttlar, and H. Reis, (2015), "Field Estimation of Oxidative Aging in Asphalt concrete Pavements using Non-Collinear Wave Mixing" *Insight Non-Destructive Testing and Condition Monitoring Journal*, Vol. 57, No. 11, pp. 1-10.

13. M.E. McGovern, W.G. Buttlar, and H. Reis, (2015), "Field Assessment of Oxidative Aging in Asphalt Concrete Pavements with Unknown Acoustic Properties," submitted for review towards publication to the *Journal of Construction & Building Materials,* (In Review).

14. M.E. McGovern, N. Farace, W.G. Buttlar, and H. Reis, (2015), "Effectiveness of Rejuvenators on Aged Asphalt Concrete using Ultrasonic Non-Collinear Subsurface Wave Mixing" *Materials Evaluation*, Vol. 73 No. 10, pp. 1365-1376.

15. M.E. McGovern and H. Reis, (2015), "Nondestructive Field Evaluation of Aging Levels of Rejuvenated Asphalt Concrete Pavements" *Transportation Research Board*, (*Recommended for publication—in Press*).

Appendices for IAPA Scholarship Report

The following appendices include the References [1-12, 14] for referencing convenience.

CONCRETE TESTING

Characterisation of oxidative ageing in asphalt concrete – Part 1: Ultrasonic velocity and attenuation measurements and acoustic emission response under thermal cooling

M E McGovern, B Behnia, W G Buttlar and H Reis

Asphalt concrete mixtures with different levels of oxidative ageing, prepared by oven-ageing the mixture at 135ºC for different amounts of time, were used to study the effects of oxidative ageing upon the ultrasonic velocity and attenuation measurements. The embrittlement temperatures, ie low-temperature cracking, of the mixtures with different amounts of oven-aged times were also evaluated by monitoring the acoustic emission response of the specimens when cooled from room temperature to –50ºC. It was observed that the embrittlement temperature increases (ie the onset of embrittlement occurs at a warmer temperature) as the amount of ageing increases. However, the rate-of-change of the embrittlement temperatures with ageing time increases gradually until 24 h of ageing, after which the rate of change significantly increases. It was also observed that both the dilatational and shear velocities increase up to approximately 24 h of ageing, after which they significantly decrease with ageing. Also, both the dilatational and shear attenuation decrease with ageing up to around 24 h of ageing, after which both attenuations strongly increase. The results from both ultrasonic and acoustic emission tests are consistent with results obtained using the mechanical disc-shaped compact tension (DC(T)) fracture tests.

Introduction

Low-temperature cracking in asphalt concrete pavements is a major cause of pavement deterioration. Cracks in asphalt concrete pavements are difficult to properly repair and they drastically affect the life span of pavements and their rideability, leading to millions of dollars worth of repair and maintenance annually. When left untreated, cracks deteriorate and widen over time, allowing moisture and oxygen to readily infiltrate the pavement system, which can lead to severe pavement damage. Oxidative ageing has long been recognised as an important contributing factor to cracking of asphalt pavements. As the asphalt concrete is subjected to environmental conditions, it continuously degrades

Professor Henrique Reis and graduate student Megan E McGovern are affiliated with the Department of Industrial and Enterprise Systems Engineering, University of Illinois at Urbana-Champaign, 117 Transportation Building, 104 S Mathews, Urbana, Illinois 61801, USA.

Professor William G Buttlar and Post-Doctoral Research Associate Behzad Behnia are affiliated with the Department of Civil and Environmental Engineering, University of Illinois at Urbana-Champaign, 117 Transportation Building, 104 S Mathews, Urbana, Illinois 61801, USA.

*Corresponding author. Tel: +1 217 333 1228; Fax: +1 217 244 5705; Email: h-reis@uiuc.edu

due to oxidation at or near the surface. This leads to pavements with graded material properties, where the asphalt layers near the surface have warmer low-temperature cracking properties. To illustrate the effect of oxidative ageing, Figure 1 shows two pictures of the same pavement section: the one on the left was taken immediately after the construction and the one on the right was taken after nineteen months[1]. Comparing the two pavement conditions clearly reveals the difference in pavement surface, texture and colour, which are the result of ageing and climatic weathering. Aged pavements are stiffer, more brittle and relieve stresses at a much slower rate than unaged pavements. While aged pavements accumulate damage at a faster rate, their crack-healing ability is also lower when compared with unaged pavements. The amount of ageing with time varies significantly depending upon the chemical composition of the binder (for example crude source, refining techniques and additives), environmental factors and the characteristics of the mixture (for example asphalt content and air voids), as reported by Lau *et al*[2], Petersen *et al*[3], Thomas[4] and Baek *et al*[5].

Pavement Age: 0 month   Pavement Age: 19 months

Figure 1. Pavement section at the Advanced Testing and Research Engineering Laboratory (ATREL) at the University of Illinois. Immediately after the construction (left) and 19 months after construction (right). Figure reproduced from Dave *et al*[1]

Preventive maintenance of pavements is one important aspect of pavement preservation that is usually overlooked. Preservation entails repairing distresses in pavements at a very early stage, *ie* as they begin to occur. Preventive maintenance can entail the application of surface treatments, such as the application of rejuvenators, or a more substantial rehabilitation, such as pavement milling and resurfacing. One of the great challenges is determining when a pavement has become vulnerable to low-temperature cracking. Currently, pavement engineers lack practical tools to determine the proper time for preventive maintenance. The ability to rapidly and accurately evaluate the level of oxidative ageing in asphalt concrete mixtures, and its effects on pavement performance, would greatly benefit pavement engineers in determining the critical time for preventive maintenance measures to extend pavement life.

The primary goal of this study is to assess the effects of laboratory-induced oxidative ageing upon both the frequency-dependent ultrasonic dilatational and shear velocities and corresponding attenuations, and upon the low-temperature

embrittlement properties, which are estimated using an acoustic emission approach. The obtained results are consistent with the disc-shaped compact tension (DC(T)) fracture test results reported by Braham et al[6,7].

Experimental procedures

Nine asphalt concrete specimens with the same mixture design were prepared following Superpave guidelines and using a gyratory compactor. A 19 mm nominal maximum aggregate size (NMAS) with a target asphalt content of 5.9% by weight of the total mixture was selected for this study. The PG 64-22 binder was utilised as the base binder. The aggregate blend consisted of aggregates from four different stockpiles: 65% of coarse aggregate (CM16), 23% of manufactured sand (FM20), 10.5% of manufactured sand (FM02) and 1.5% of mineral filler (MF).

Mixing of the asphalt concrete mixtures was conducted at 155°C using a standard bucket mixing procedure. Laboratory-ageing of the uncompacted loose asphalt concrete mixtures was performed by placing the loose mixtures in an oven at 135°C for 0, 12, 24, 28, 32, 36, 48, 60 and 72 h. To ensure uniform ageing throughout the sample, the mixtures were hand-stirred every 12 h. Once aged, the mixtures were compacted at 135°C using a servo-controlled gyratory compactor (IPC Servopac) to construct cylindrical specimens 150 mm long and 150 mm in diameter. Each of the compacted gyratory specimens were then cut to obtain two $40 \times 70 \times 135$ mm³ rectangular specimens, which were used for ultrasonic velocity and attenuation measurements, and four half-moon 60 mm-thick samples, which were used to evaluate the acoustic emission response during thermal cooling. Figure 2 shows the geometry and dimensions of the extracted test samples from each of the cylindrical compacted gyratory specimens. To avoid the end-effects induced during compaction and to obtain a smooth surface for sensor placement, a 5 mm layer was trimmed from each end of the cylindrical gyratory compacted specimens. The entire set of aged specimens, ie from virgin specimens to specimens aged up to 72 h, was tested using acoustic emission. However, ultrasonic velocity and attenuation measurements were only performed on specimens aged up to (and including) 36 h. The rough, cratered surfaces of specimens aged past 36 h caused coupling difficulties with the sensors, preventing ultrasonic testing.
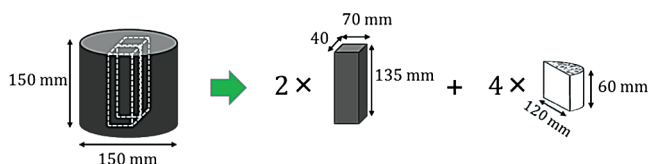

Figure 2. Preparation of asphalt concrete test samples and their dimensions for ultrasonic measurements and acoustic emission tests

Acoustic emission response to thermal cooling

Over the past few decades, acoustic emission (AE) has been utilised extensively to evaluate the fitness-for-service of structures and to characterise microscopic damage in materials[8]. The acoustic emission phenomenon refers to the generation of transient elastic mechanical waves caused by local transient instabilities in the media. When a material is stressed (mechanically or thermally) to a point when inelastic deformation occurs, strain energy is suddenly released in the form of transient elastic mechanical waves. The inelastic deformation is due to local dynamic movements or momentary instabilities (for example microcracks develop). Emitted AE elastic waves propagate outward from the source and can be detected using piezoelectric sensors mounted on the surface of the test sample. Figure 3 schematically illustrates crack generation/propagation along with the corresponding AE wave generation, propagation and detection for a material test sample

under increasing loading conditions. Acoustic emission has already been successfully used to estimate the embrittlement temperatures of virgin and aged asphalt binders, as reported by Apeagyei et al[9], Dave et al[10] and Behnia et al[11], where a review of acoustic emission to characterise asphalt concrete mixtures is provided. Here, the acoustic emission approach is used to estimate the low-temperature embrittlement properties of asphalt concrete mixtures and their dependence upon ageing.
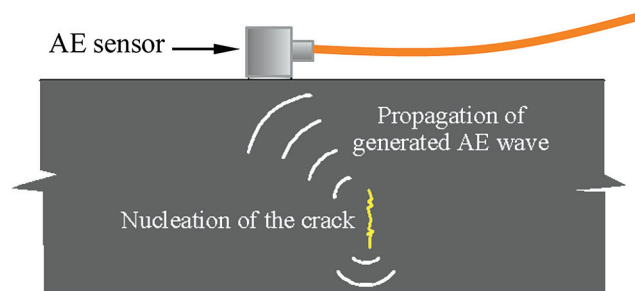

Figure 3. Crack nucleation and propagation and detection of acoustic emission (AE) waves

Each of the AE test samples was positioned inside a cooling chamber (Shuttle portable ULT-25 freezer), see Figure 4(a), and its acoustic emission activity was monitored while the sample was cooled from ambient temperature to –50°C. Figure 4(b) shows the typical temperature *versus* cooling time. As the temperature decreases, the difference in the thermal expansion coefficients between the asphalt mastic and aggregates in the mixture produces progressively higher thermal tensile stresses within the mastic. These thermal tensile stresses eventually result in thermal microcrack formation, which becomes the source of the acoustic emission events, ie acoustic emissions, in the form of transient elastic stress waves that are detected by the AE sensors. Wideband
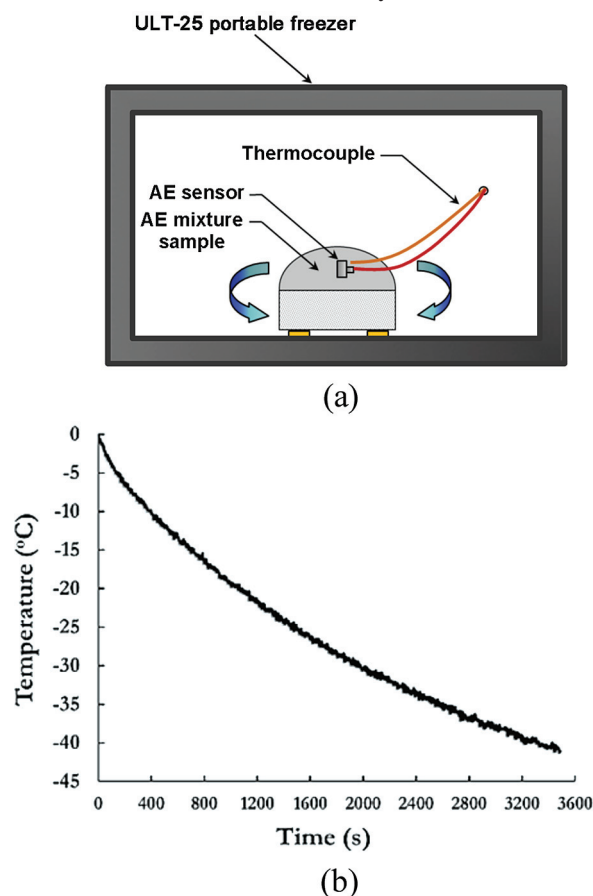

(a)

(b)

Figure 4. (a) Cooling chamber and (b) typical plot of test sample temperature *versus* cooling time during acoustic emission testing

AE sensors (Digital Wave, Model B1025) with a nominal frequency range of 50 kHz to 1.5 MHz were coupled to the specimen surface via high-vacuum grease. The signals from the AE sensors were pre-amplified by 20 dB using broadband pre-amplifiers. The fracture wave detector (FWD) signal conditioning unit was used to further amplify the signal by 21 dB (for a total amplification of 41 dB) and to filter the signal using a 20 kHz high-pass double-pole filter. A 16-bit analogue-to-digital converter (ICS 645B-8) with a sampling frequency of 2 MHz was employed to digitise the AE signals. The digital data was then stored for later processing. The test temperature was monitored and recorded using a K-type thermocouple, which was positioned on the specimen top surface.

Figure 5(a) shows a typical time domain waveform associated with an AE event, while Figure 5(b) shows the corresponding power spectral density. Here, an AE event is defined as an individual waveform having a threshold voltage of 0.1 V and energy equal to or greater than 4 V^2-μs. The event energy is defined by Equation (1), where E_{AE} is the energy of an event with duration time t (μs) and a recorded voltage of $V(t)$:

$$E_{AE} = \int_0^t V^2(t)dt \quad \text{................................(1)}$$
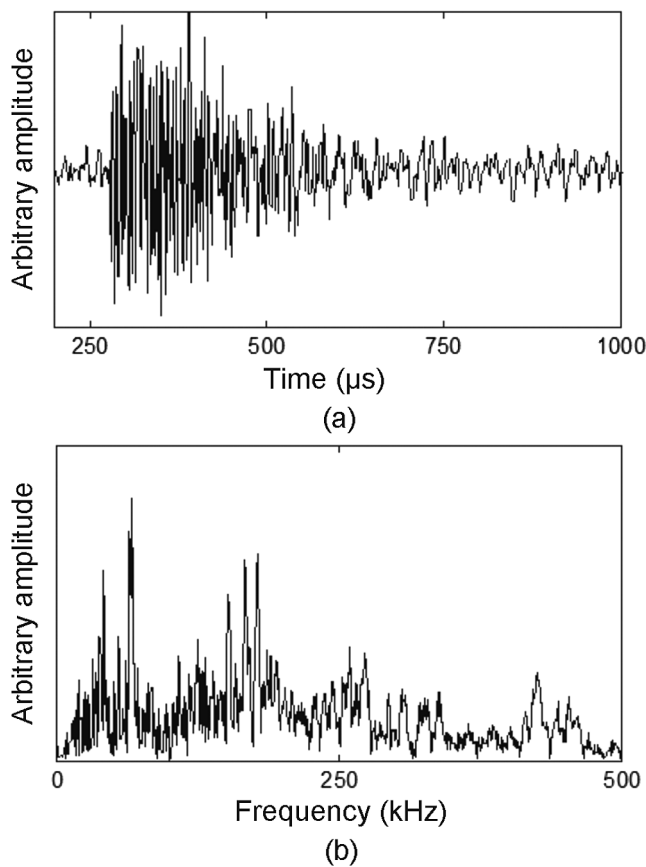

Figure 5. (a) Typical acoustic emission (AE) signal associated with an AE event and (b) corresponding power spectral density curve

A typical plot of AE event counts *versus* temperature for the asphalt concrete samples is shown in Figure 6. There are three distinct regions in the plot: (1) pre-cracking; (2) transition; and (3) stable cracking regions. Using the current filtering, no AE activity is detected in the pre-cracking region. This period occurs prior to the onset of material fracture, during which thermal stresses build up inside the specimen due to differential thermal contraction between the asphalt mastic and aggregates. The 'transition region' begins when thermal microcracking reveals itself via relatively high-energy AE events, which occur immediately after the pre-cracking period starts. Progressively higher thermal stresses in the specimen eventually cause thermal microcracks to develop in the

asphalt mastic, as well as at the interface between asphalt mastic and aggregates. Microcracks result primarily from a combination of asphalt mastic brittleness (at lower temperatures) and from the action of thermally-induced tensile stresses within the material, perhaps enhanced by the stress concentrations at the interface between the mastic and the aggregates.
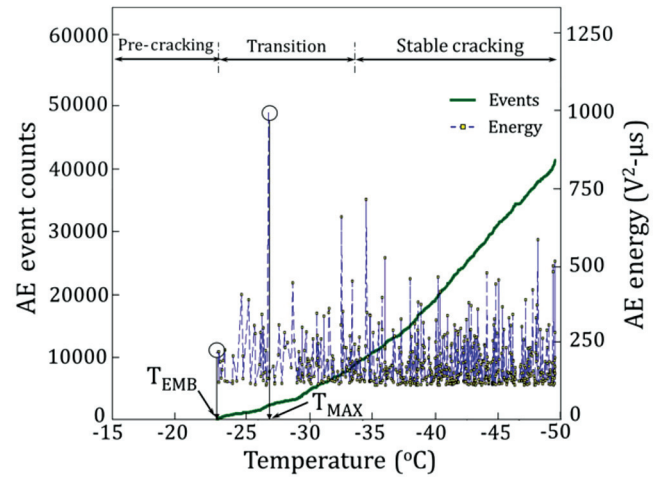

Figure 6. Typical plot of AE event counts and AE event energy *versus* temperature for asphalt concrete samples

The formation of microcracks manifests itself as a cluster of high-amplitude AE elastic waves during the test. The temperature corresponding to the first AE event with an energy level above 4 V^2-μs has been termed the 'embrittlement temperature', as illustrated in Figure 6. It is hypothesised that the embrittlement temperature, T_{EMB}, represents a fundamental material state that is independent of material constraints, sample size (as long as a statistically representative volume or larger is used), as well as sample shape. The 'transition region' can be considered as the region where material behaviour gradually changes from quasi-brittle to brittle state and where resistance to fracture is generally very low, allowing cracks to propagate readily. In Figure 6, the slope of the AE event counts *versus* temperature plot increases until the stable crack region starts, when the slope becomes steep and relatively constant. The 'stable cracking region' usually starts at a very low temperature when the material is brittle and generates a significant amount of AE activity.

Figure 6 also shows the temperature corresponding to the event of maximum energy, ie T_{MAX}. The variability of T_{MAX} is much higher than the variability of the embrittlement temperature T_{EMB}, and it appears to depend upon the microstructure of the mixture. Considering asphalt concrete as a material made of mortar and bricks of different geometry, ie mastic and aggregates, respectively, there exist pockets of mastic of various geometries and size within the material test sample[12]. The T_{EMB} is detected when microcracks are formed, probably at the interface between the mastic and the aggregates, perhaps induced by stress concentrations at the interfaces. Because of the indeterminate nature of the material microstructure, the formation of these microcracks, while releasing some strain energy locally, does not prevent those pockets of mastic from continuing to accumulate thermally-induced tensile strain energy. This strain energy continues to increase as the temperature is reduced until it reaches T_{MAX}. At T_{MAX} the thermal stresses in the mastic equal the mastic fracture strength, which leads to the release of an AE event with relative high energy.

Ultrasonic velocity and attenuation measurements

Pairs of dilatational and shear transducers (Panametrics, models V101 and V151, respectively), with a centre frequency of 500 kHz and a beam diameter of 25.4 mm, were used for the dilatational and shear velocity measurements. In each case, the sending transducer

was coupled to a rectangular-shaped delay line and the receiving transducer was coupled to the opposite side of the asphalt concrete specimen. A function generator (Krohn-Hite, model 5920) was used to generate a five-cycle sinewave toneburst, which swept between 10 kHz and 500 kHz in 5 kHz increments. The generated signal was amplified by a gated amplifier (Ritec, GA-2500A) and used as the input for the sending transducer. The data was sampled at 17 MHz and averaged 25 times to mitigate noise and effects from scatter. Figure 7 shows a schematic diagram of the experimental set-up.
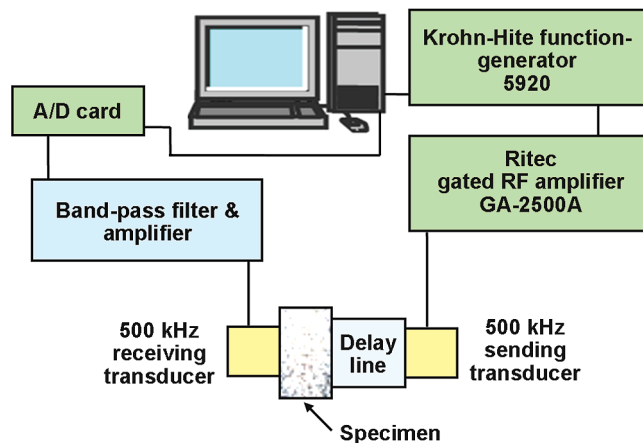
Figure 7. Schematic diagram of experimental set-up for ultrasonic measurements. This set-up was used for measurements across both the width and height of the asphalt concrete specimens

Several methods to estimate velocity exist, including the threshold-crossing method[13], the cross-correlation method[14] and the overlap method[15], which require that the signal retain its shape as it propagates through the medium. However, in the case of asphalt concrete, the waveform does not retain its shape during propagation. As a result, the phase comparison method, credited to Sachse and Pao[16], was chosen because it is relatively insensitive to waveform distortion; however, this method can break down when there is a low signal-to-noise ratio and/or when multiple wave paths arrive at the same time.

Wave propagation through asphalt concrete

As the wave propagates through asphalt concrete, it becomes scattered and distorted. As the wave propagation distance increases, the effects of scatter (hence, the wave shape distortion) also increase. It was observed that across the height of the specimen ($\approx$ 70 mm), the waveform becomes distorted and harder to analyse at higher frequencies. Across the width of the specimen ($\approx$ 40 mm), the wavelength corresponding to lower frequencies is longer than the specimen dimensions, which can lead to erroneous calculations due to phase interference effects. However, when the wavelength is shorter than the specimen dimension and longer than the nominal maximum aggregate size (NMAS), the signal propagates through the medium with relatively small distortion. Here, this range is termed the 'valid range', as shown in Figure 8.

The stochastic nature[17] of asphalt concrete with the two discrete phases, ie mastic and aggregates, where each phase has different acoustic properties, leads to energy scattering and mode conversion. This effect increases with the increase in frequency. The presence of multiple discrete scatterers makes it possible to have multiple mode conversions and multiple paths to the (primary and scattered) wave fields from the source to the observation point. As a result, at some distance from the source, the ultrasonic energy will be travelling in both dilatational and shear modes, regardless of the initial mode at the source. Because dilatational waves travel faster than shear waves, the dilatational energy always arrives first at the observation point. However, assuming a polarised shear wave at the source, it is possible that a fraction of its energy could travel some distance in the faster dilatational wave mode (due to
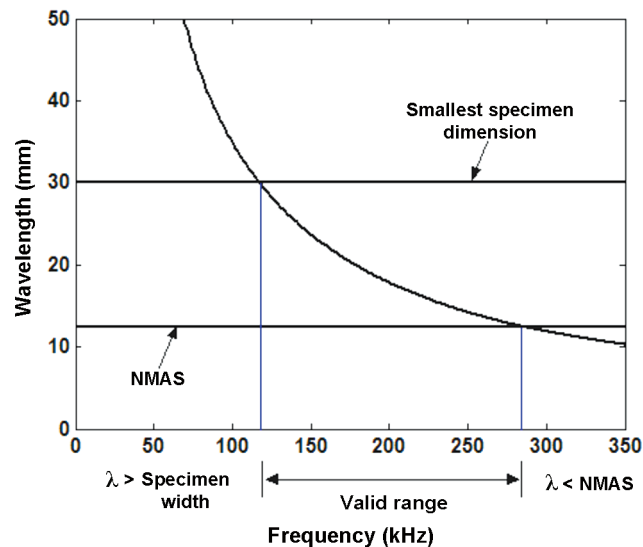
Figure 8. The wavelength (obtained via the velocity) as a function of frequency for the virgin specimen. The 'valid range', ie NMAS < λ < specimen dimension, is the range at which ultrasonic measurements can be taken in a conventional through-transmission format (for example without the use of a delay line). NMAS stands for nominal maximum aggregate size

mode conversion), and a smaller fraction of this dilatational energy could arrive at the observation point in the polarised shear wave mode (also due to mode conversion). Because interactions between the propagating wave and aggregates increase with frequency, the distance that the received shear energy may have travelled in the faster dilatational wave mode may also increase with frequency. This leads to an apparent increase in the measured shear velocity with an increase in frequency.

As a result, to obtain the dilatational velocities, the dilatational portion of the received signal was isolated by partitioning in time (ie windowing) the beginning of the signal, because the dilatational wave mode is the fastest (hence first) arriving wave. However, during the estimation of the shear wave velocity, partitioning of the receiving signal was not performed because it does not isolate the shear portion of the signal. To mitigate this difficulty, the following was carried out: (1) a five-cycle pulse train was used; (2) the smaller dimensions in the specimen were used during the measurements; (3) multiple independent measurements (ten for each of the two similar specimens for a total of twenty measurements) and waveform averaging were performed; and (4) advantage was taken from the polarisation of the shear transducers to filter out, as much as possible, the wave energy arriving in undesirable modes.

Delay line

To overcome the difficulties that arise from the wavelength at lower frequencies being longer than the specimen dimension, a delay line was used. The delay line assures that the transmitted waveform will be fully formed before it propagates through the specimen. A block (72 × 57 × 116 mm³) made of ultra-high molecular weight polyethylene (UHMWPE) was chosen as the delay line because its acoustic impedance is close to the acoustic impedance of the virgin asphalt concrete samples. The dimensions of the delay line were chosen to avoid waveguide effects.

Velocity

The angle of the fast Fourier transform (FFT) was computed from the signals to find the phase. The phase was then unwrapped to account for jumps equal to or greater than 180°. Following Sachse and Pao[16], the phase velocity was then obtained from the following equation:

$$v(f) = \frac{2\pi \cdot f \cdot d_A}{\phi_A(f) - \phi_U(f)} \quad \dots\dots\dots\dots\dots\dots\dots(2)$$

where ϕ_A denotes the phase for the signal passing through the delay line/asphalt set-up, ϕ_U denotes the phase of the signal obtained from using just the UHMWPE delay line, d_A is the distance travelled through the asphalt specimen and f is the frequency. Only the linear portions of the phase spectrum are used to calculate velocity.

Attenuation

The transmitted waves propagate first through the delay line and then through the smallest dimension of the specimen, see Figure 7. The attenuation coefficient can be calculated by comparing the fast Fourier transform (FFT) of the signal passing through the delay line/specimen set-up to a reference signal (for example using only the delay line). At both the delay line/specimen and transducer/specimen interfaces, signal loss also occurs due to an impedance mismatch and imperfect couplant conditions. Neglecting this loss leads to an overestimation of the attenuation values. This loss can be accounted for by measuring the attenuation in the 'valid range' (see Figure 8) via the conventional through-transmission technique (ie using no delay line) and then translating the attenuation measured using the delay line set-up by the appropriate correction value.

Figure 9 shows the four required set-ups and the corresponding amplitudes of the received signals that are required to account for the losses at the interfaces. First, the signal is recorded through the width dimension of the specimen coupled to the delay line, see Figure 9(a). A signal is then recorded through only the delay line, as shown in Figure 9(b). Next, signals are obtained through the width and height dimensions of the specimen without the delay line, see Figures 9(c) and 9(d), respectively. The uncorrected attenuation $\alpha_{uncorrected}$ is determined across all frequencies based on the signals obtained for the set-up with the delay line. Note that this attenuation is an overestimate of the attenuation in the asphalt concrete because it contains the losses from the transducer/asphalt and delay line/asphalt interfaces. Equation (3) shows this uncorrected attenuation, where A_{UA} denotes the amplitude received through the delay line/asphalt set-up, A_U denotes the amplitude received through only the delay line and d_h and d_w denote the height and width of the asphalt concrete specimens, respectively:

$$\alpha_{uncorrected}(f) = -\frac{1}{d_w}\ln\left(\left|\frac{A_{UA}(f)}{A_U(f)}\right|\right) \quad\text{...................(3)}$$

Testing Set-up   Received Signal Amplitude
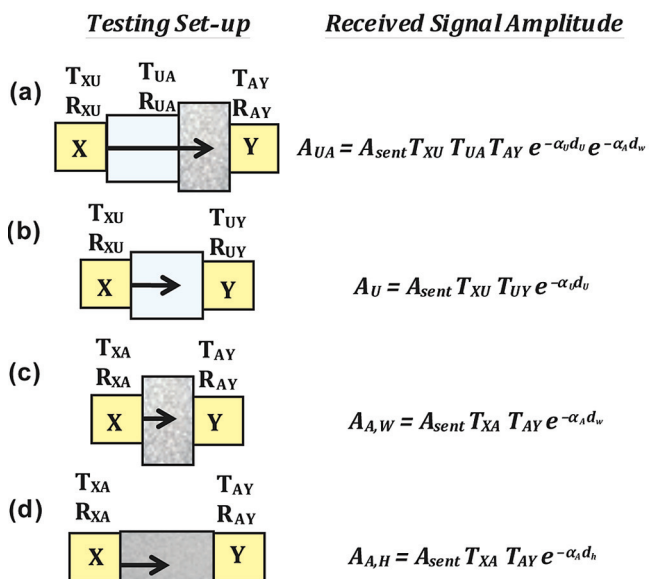
Figure 9. Method to find attenuation coefficients of asphalt concrete test specimens with correction for signal loss at the interface boundaries. A_{sent} **is the signal sent by transducer X, Y is the receiving transducer and subscripts** A **and** U **denote asphalt and delay line, respectively.** T_{IJ} **and** R_{IJ} **denote transmission and reflection coefficients, respectively, between medium I and medium J**

The true attenuation (denoted as α^*), see Equation (4), is then calculated using signals obtained from the set-up without the delay line over the valid region, see Figure 8. Due to the manner in which α^* is estimated, it is independent of the loss at the transducer/asphalt concrete boundaries (assuming consistent couplant conditions). In Equation (4), $A_{A,H}$ and $A_{A,W}$ denote the amplitudes of the waveforms received across the height and the width of the test sample, respectively (without the delay line), see Figure 9:

$$\alpha^*(f) = -\frac{1}{d_h - d_w}\ln\left(\left|\frac{A_{A,H}(f)}{A_{A,W}(f)}\right|\right) \quad\text{.................(4)}$$

To find the amount that $\alpha_{uncorrected}$ needs to be translated (ie corrected), a frequency f^* should be chosen at which to evaluate α^*. This frequency f^* should be chosen from the 'valid range' (see Figure 8), such that the wavelength is shorter than the specimen dimension and longer than the nominal maximum aggregate size (40 mm > λ > NMAS = 19.0 mm). This allows the difference between $\alpha_{uncorrected}$ and α^* at the frequency f^* to be calculated, which is termed as $\alpha_{translate}$. Figure 10(a) provides a graphical representation of this procedure:

$$\alpha_{translate} = \alpha_{uncorrected}(f^*) - \alpha^*(f^*) \quad\text{.................(5)}$$

As the last step, $\alpha_{uncorrected}$ is translated down by $\alpha_{translate}$, ie the uncorrected attenuation values are translated down such that the resulting attenuation is lower in magnitude by the value $\alpha_{translate}$. Figure 10(b) provides a graphical representation of this procedure.

Equation (6) describes the culmination of the procedures outlined above. An example of the attenuation described by Equation (6) is shown as the solid black line in Figure 10(b):
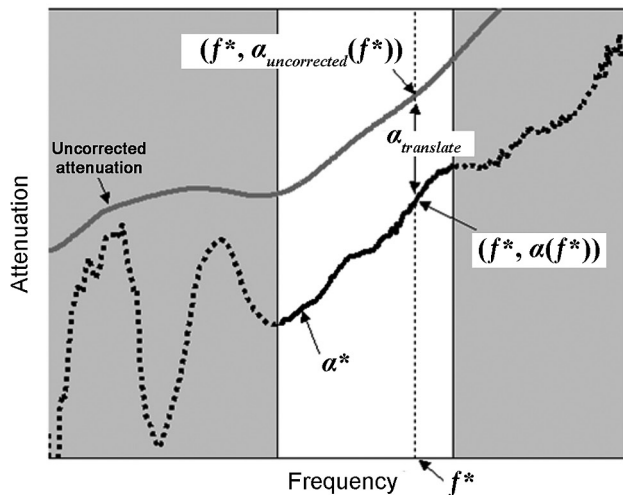
$$\alpha(f) = \alpha_{uncorrected}(f) - \alpha_{translate}$$
$$= \frac{1}{d_w}\ln\left(\left|\frac{A_{UA}(f^*)A_U(f)}{A_U(f^*)A_{UA}(f)}\right|\right) - \frac{1}{d_h - d_w}\ln\left(\left|\frac{A_{A,H}(f^*)}{A_{A,W}(f^*)}\right|\right) \quad\text{...(6)}$$

Results and discussion

Acoustic emission testing was carried out for all asphalt concrete test samples at different ageing levels ranging from 0 to 72 h of oven-ageing. Velocities and the corresponding attenuations were only measured for specimens aged up to 36 h of oven-ageing.

Acoustic emission response to thermal cooling

The temperatures corresponding to the first major event (ie embrittlement temperature), as well as the total number of AE event counts, are presented in Table 1. The embrittlement temperatures of the asphalt mixtures versus ageing time are shown in Figure 11(a). The results reveal that embrittlement temperature increases with ageing time: the higher the ageing time, the warmer the embrittlement temperatures, ie the longer the ageing time, the warmer the temperatures at which the thermally-induced micro-cracks in the asphalt concrete samples start to develop. This can be linked to the age-hardening effects that occur during oven-ageing, which makes asphalt mixtures more brittle and therefore less crack resistant. The rate-of-change of the embrittlement temperatures with respect to ageing time is shown in Figure 11(b). It is observed that initially the average rate of change of T_{EMB} versus ageing time gradually increases from 0 to approximately 24 h, followed by a significant increase from 24 to 36 h. After approximately 36 h of ageing time, the average rate of change of T_{EMB} versus ageing time drops drastically. At this ageing level, it appears that oxidative ageing reactions (ketone, carboxylic acid, quinolone formation, etc) have run their course and that the binder has reached a predominantly glassy state. This leads to a plateau in the T_{EMB} versus ageing time plot for longer ageing times, which indicates that ageing beyond 36 h does not have a significant effect on the
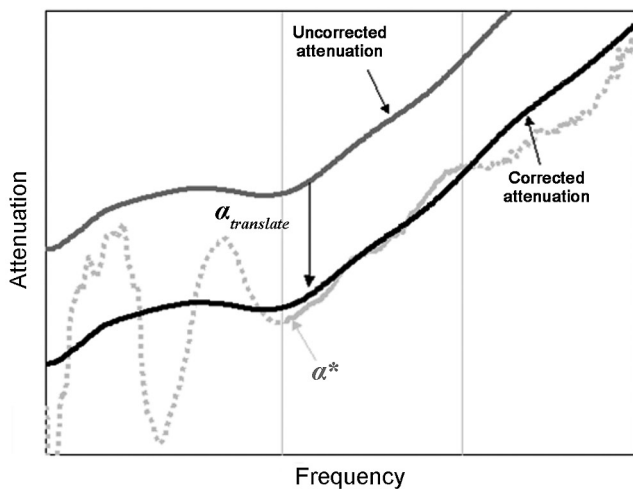
Figure 10. Correction of the attenuation values obtained via the delay line technique in order to account for the losses at the interfaces: (a) choose f^* from the valid range and determine the corresponding $\alpha^*(f^*)$ and $\alpha_{uncorrected}(f^*)$ to obtain $\alpha_{translate}$. The shaded grey regions denote the invalid regions for choosing f^*. The solid black line is α^*. The solid dark grey line is $\alpha_{uncorrected}$; (b) translate the $\alpha_{uncorrected}$ by $\alpha_{translate}$. The attenuation α^* is shown in a very light grey for comparison purposes

cracking resistance of asphalt mixtures. In other words, 36 h of oven-ageing appears to be a threshold up to which the majority of ageing occurs. Furthermore, the significant amount of ageing that occurs after 24 h of oven-ageing time suggests that the oxidative ageing level equivalent to 24 h of oven-ageing may represent a critical point beyond which deterioration of the pavement rapidly accelerates.

Figure 12 illustrates the total number of AE event counts *versus* laboratory ageing time. Results show that the number of AE event counts increases until 12 h of laboratory oven-ageing and then decreases for longer ageing periods; this decrease is particularly significant after 24 h of ageing. Explaining the observed phenomenon requires an understanding of the ageing effects on the internal structure of asphalt concrete mixtures. As a heterogeneous material, the internal structure of the asphalt concrete is influenced by the quality of asphalt mastic inter-particle bonds, as well as the quality of bonds between the aggregates and asphalt mastic. Figure 13 schematically depicts the thermally-induced stresses between the mastic and the aggregates, as well as the adhesive bonds between the particle fines in the mastic.

The behaviour of the oven-aged asphalt concrete mixture includes two important phenomena, which counteract each other. These two phenomena are the increase in binder stiffness and the decrease in
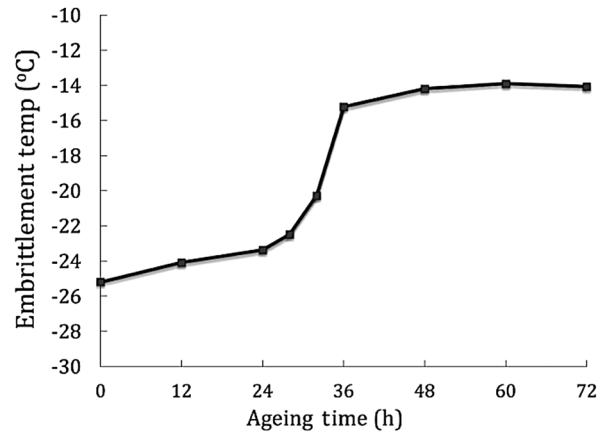
(a)
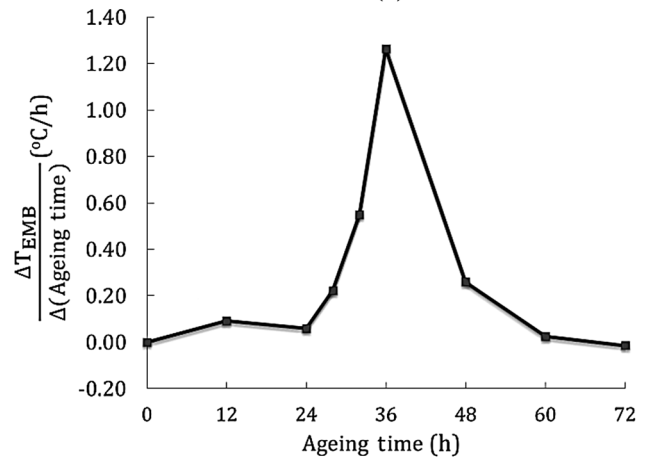
(b)

Figure 11. (a) The embrittlement temperature *versus* oven-ageing time plot; (b) the average rate-of-change of embrittlement temperature *versus* oven-ageing time plot
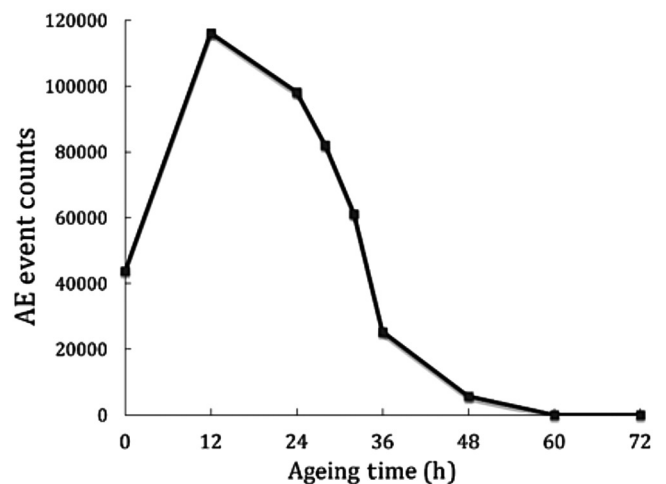

Figure 12. AE event counts *versus* oven-ageing time plot

adhesion of the asphalt binder with increasing ageing, *ie* the ageing of asphalt mixtures increases the stiffness of the asphalt binder while reducing its adhesive properties. Initially, at early stages of ageing, the positive effects of the increase in binder stiffness due to ageing overcome the negative effects of the loss in binder adhesion, which leads to an overall increase in stiffness of the entire composite mixture. As a result, short-term aged compacted samples appear to have a 'stronger' internal structure when compared to virgin asphalt concrete samples. However, for longer ageing times, the deteriorating effects resulting from the reduction in binder adhesion overcome the advantageous effects of increased binder stiffness. This loss in

Table 1. Acoustic emission test results showing the number of AE event counts and embrittlement temperatures

Ageing time (h)	Rep #	Number of AE event counts			T_{EMB} (°C)		
		N_{AE}	Average	CoV %	T_{EMB} (°C)	Average	CoV %
0	#1	44,196			−24.18		
	#2	41,593	43,836	4.29%	−27.31	−25.18	6.99%
	#3	43,424			−25.87		
	#4	46,129			−23.37		
12	#1	134,550			−25.41		
	#2	118,841	116,287	11.76%	−23.01	−24.08	4.90%
	#3	107,414			−24.72		
	#4	104,342			−23.16		
24	#1	89,850			−22.92		
	#2	106,400	98,250	13.97%	−24.85	−23.36	7.33%
	#3	113,000			−21.13		
	#4	83,750			−24.55		
28	#1	99,820			−23.12		
	#2	81,250	82,120	15.38%	−22.07	−22.47	6.25%
	#3	10,310			−23.98		
	#4	77,100			−20.72		
32	#1	73,800			−21.69		
	#2	57,100	61,200	17.03%	−22.39	−20.28	10.33%
	#3	49,400			−19.01		
	#4	64,500			−18.02		
36	#1	20,002			−15.46		
	#2	31,692	25,393	22.16%	−14.23	−15.23	9.09%
	#3	28,535			−17.09		
	#4	21,344			−14.12		
48	#1	5381			−13.69		
	#2	7402	5765	23.94%	−14.79	−14.19	4.06%
	#3	6162			−13.70		
	#4	4113			−14.57		
60	#1	147			−12.83		
	#2	200	145	27.18%	−15.19	−13.89	10.48%
	#3	118			−15.09		
	#4	115			−12.44		
72	#1	138			−11.12		
	#2	91	98	34.32%	−15.96	−14.06	14.98%
	#3	107			−14.07		
	#4	57			−15.09		

binder adhesion properties leads to weaker bonds between the mastic and the aggregates and to weaker bonds between the fines in the mastic, which lead to a weaker internal structure of the composite. This manifests itself as a significant reduction in the number of detectable AE events in the long-term aged asphalt concrete samples.

Figure 12 shows that ageing initially improves the internal structural bonds in the asphalt concrete samples, as the 12 h aged samples exhibit higher AE activity than the virgin samples. When ageing time exceeds 24 h, a drastic drop in the AE event counts occurs, which indicates a weakening in the internal bond structure within the test samples. These observed AE test results are consistent with the fracture test results reported by Braham et al[6] using the disc-shaped compact tension (DC(T))[7]. In their study, the uncompacted samples were aged for 4, 6, 8, 12, 24, 36 and 48 h at 135ºC. These uncompacted samples were then compacted and tested using the DC(T) test to evaluate the fracture cracking resistance of the mixtures. Figure 14, which is reproduced after Braham et al[6], shows the fracture energies of the asphalt concrete samples for different ageing levels. The DC(T) results are consistent with the trend observed using AE testing, ie the fracture energy of each asphalt mixture increases with increasing ageing until it reaches a peak, and then it decreases with increasing ageing.

Ultrasonic velocity and attenuation measurements

Figure 15 shows the velocity and attenuation measurements for each specimen as a function of frequency. Figure 16 also shows the ultrasonic dilatational and shear measurements, presented, however, as a function of both ageing time and frequency. Figure 17 shows the average of each ultrasonic parameter across frequency as a function of ageing.

Referring to Figures 15(a) and 16(a), there is an increase in the dilatational velocity from 30 kHz to ≈100 kHz for all the specimens. After ≈100 kHz, the velocity starts to level out. For the specimens aged for 32 and 36 h, the velocity for frequencies above 250 kHz (ie point A in Figure 15) was difficult to calculate because of the low signal-to-noise ratio caused by increased attenuation. From 0 to 24 h, the velocity (across all frequencies) increases with increasing ageing; however, from 24 to 36 h, the velocity (across all frequencies) decreases with increasing ageing, see Figures 15(a) and 17. As the binder ages its stiffness increases, thus accounting for the increase in velocity. However, after 24 h of ageing, while the binder continues to increase its stiffness with ageing, the integrity of mastic-to-particle adhesion appears to deteriorate. This phenomenon leads to the formation of a diffuse micro-flaw population, which
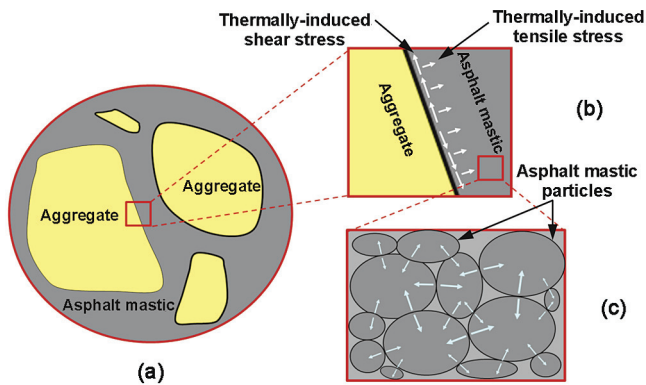
Figure 13. (a) Schematic representation of asphalt concrete as a heterogeneous material composed of aggregates and asphalt mastic; (b) thermally-induced tensile and shear stresses inside mastic at the interface of asphalt mastic and aggregate; and (c) asphalt mastic showing inter-particle adhesive interactions
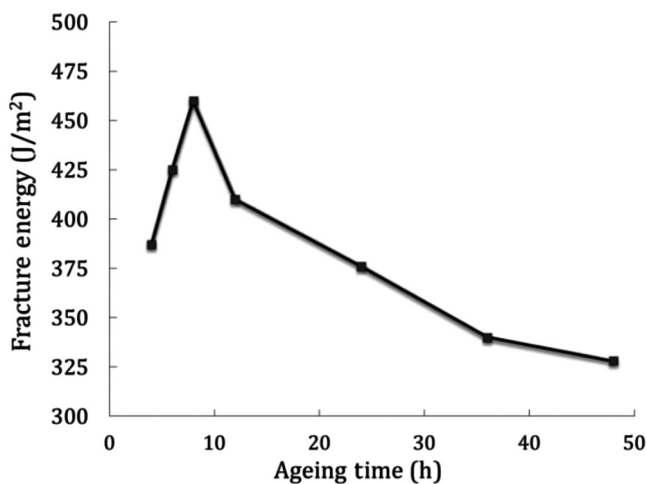

Figure 14. Oven-ageing effects on fracture energy of asphalt concrete samples. Data reproduced from Braham *et al*[12]
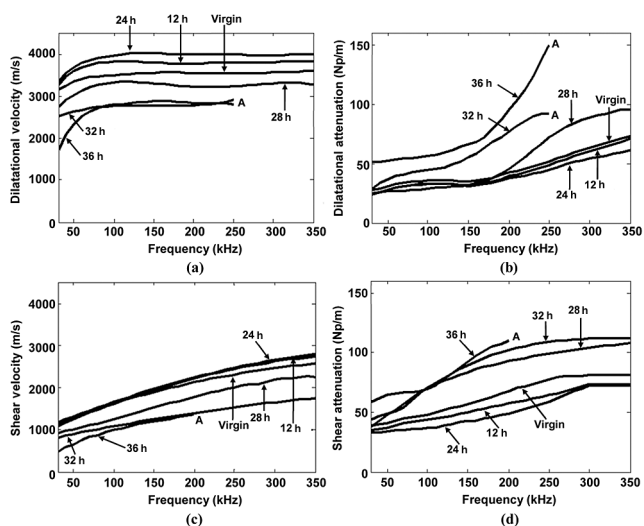

Figure 15. Top row: (a) Dilatational velocities and (b) corresponding attenuations for asphalt concrete samples aged from 0 to 36 h. Bottom row: (c) Shear velocities and (d) corresponding attenuations for asphalt concrete aged from 0 to 36 h. For samples aged 32 and 36 h, the dilatational velocity for frequencies above 250 kHz, *ie* point A, were difficult to calculate because of the low signal-to-noise ratio caused by the increased attenuation. For similar reasons, the shear velocity for the specimen aged 36 h was only calculated up to 200 kHz and the shear attenuation of the specimen aged up to 24 h was determined only up to 300 kHz
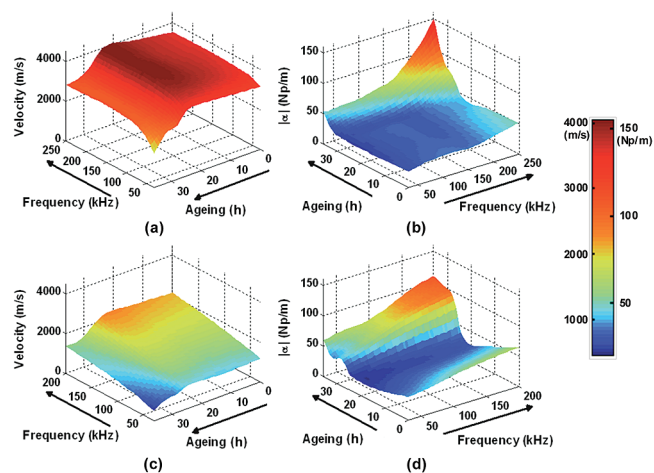
Figure 16. Top row: (a) Dilatational velocity and (b) corresponding attenuation of asphalt concrete mixtures as a function of frequency and oven-ageing hours. Bottom row: (c) Shear velocity and (d) corresponding attenuation of asphalt concrete mixtures as a function of frequency and oven-ageing hours. The surface was fitted using cubic spline interpolation
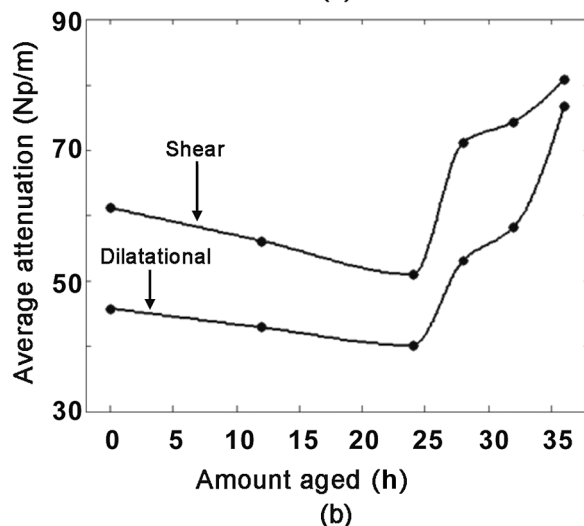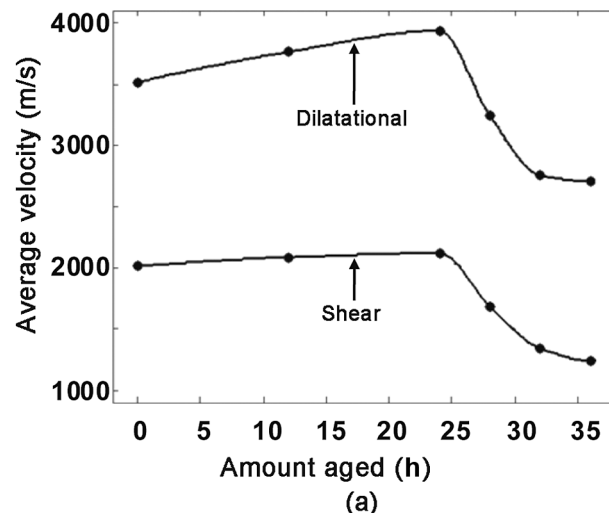
Figure 17. (a) Average across frequency of velocities and (b) corresponding attenuations for asphalt concrete samples aged 0 to 36 h. The average velocity (for both dilatational and shear) increases from 0 to 24 h and decreases from 24 to 36 h. The average attenuation (for both dilatational and shear) decreases from 0 to 24 h and increases from 24 to 36 h

effectively decreases the overall (composite) elastic moduli for longer ageing times, *ie* after 24 h of ageing, which results in lower velocities. The shear velocities tend to increase with increasing

frequency, see Figures 15(c) and 16(c). As a function of ageing, the shear velocities exhibit a similar trend to the dilatational velocities: they increase from 0 to 24 h and decrease from 24 to 36 h, see Figures 15(a) and 15(c) and Figure 17(a).

Figures 15(b) and 16(b) show the magnitude of the dilatational attenuation coefficients as a function of frequency for different specimens. It is observed that as the frequency increases, the attenuation also increases. For all the specimens, the slope of the attenuation changes around 175 kHz, after which the attenuation drastically increases. For the specimens aged 32 and 36 h, the attenuation above 250 kHz was difficult to calculate because of the low signal-to-noise ratio. The magnitude of the shear attenuation coefficients also increases with frequency, see Figure 15(d) and 16(d). Figure 17 shows the dilatational and shear attenuations as a function of ageing, where a decrease in the attenuation from 0 to 24 h and an increase from 24 to 36 h is observed.

Conclusions

The main objective of this study was to explore the effects of oxidative ageing on ultrasonic velocity and attenuation measurements in asphalt concrete mixtures, as well as on their embrittlement temperatures. Nine asphalt concrete specimens with the same mixture design were prepared at different ageing levels ranging from 0 to 72 h. The acoustic emission response to thermal cooling was used to investigate the age-related changes in asphalt concrete embrittlement temperatures for all specimens. Ultrasonic velocity and attenuation measurements were only performed on specimens aged up to 36 h due to sensor coupling difficulties.

It was observed that the dilatational velocity increases with frequency up to 100 kHz, after which it appears to plateau. Because of the stochastic nature of asphalt concrete, the shear velocity also increases with frequency for all specimens. It was also observed that at each frequency the dilatational and shear velocities follow the same trend with respect to the amount of oven-ageing: both the dilatational and shear velocities increase from 0 to 24 h and decrease from 24 to 36 h of oven-ageing. Dilatational and shear attenuation values increase with increasing frequency for all specimens. As a function of ageing, the attenuations decrease from 0 to 24 h and increase from 24 to 36 h of oven-ageing.

This study also shows that the AE-based embrittlement temperatures (T_{EMB}) of asphalt concrete mixtures progressively get warmer with increasing ageing time. This can be attributed to age-hardening effects, which makes asphalt mixtures more brittle and more prone to cracking. It was also observed that the average rate-of-change of the embrittlement temperature with respect to ageing time is not constant. There is a significant increase in T_{EMB} when the ageing time exceeds 24 h. Based on the limited laboratory testing results, 24 h of laboratory ageing appears to be the critical point beyond which deterioration of the asphalt mixture rapidly accelerates. As a result, the field-ageing time equivalent to 24 h of intense laboratory oven-ageing appears to be a proper time to apply preventive pavement maintenance. It was also observed that, unlike the general idea that oven-ageing always weakens the internal structure of the mixture, this study has shown that oxidative ageing initially improves the internal structure of asphalt mixtures to a point beyond which the mixture structure begins to rapidly deteriorate. The same trend was observed in mechanical DC(T) fracture energy testing[6,7] of aged asphalt mixtures.

Acknowledgements

References

1. E V Dave, 'Asphalt pavement ageing and temperature dependent properties using functionally graded viscoelastic model', Doctoral dissertation, University of Illinois at Urbana-Champaign, Urbana, Illinois, 2009.
2. C K Lau, K M Lunsford, C J Glover, R R Davison and J A Bullin, 'Reaction rates and hardening susceptibilities as determined from pressure oxygen vessel ageing of asphalts', Transportation Research Record No 1342, National Research Council, pp 50-57, 1992.
3. J C Peterson, J F Branthaver, R E Robertson, P M Harnsberger, J J Duvall and E K Ensley, 'Effects of physicochemical factors on asphalt oxidation kinetics', Transportation Research Record No 1391, National Research Council, pp 1-10, 1993.
4. K P Thomas, 'Impact of water during the laboratory ageing of asphalt', Road Materials and Pavement Design, Vol 3, No 3, pp 299-315, 2002.
5. C Baek, B S Underwood and Y R Kim, 'Effects of oxidative ageing on asphalt mixture properties', Transportation Research Board, 91st Annual Meeting, No 12-2328, 2012.
6. A F Braham, W G Buttlar, T R Clyne, M O Marasteanu and M I Turos, 'The effect of long-term laboratory ageing on asphalt concrete fracture energy', Journal of the Association of Asphalt Paving Technologists, Vol 78, pp 417-454, 2009.
7. ASTM 7313-07, 'Standard test method for determining fracture energy of asphalt concrete-aggregate mixtures using the disc-shaped compact tension geometry', American Society of Testing and Materials, West Conshohocken, Pennsylvania, 2007.
8. R G Liptai, D O Harris and C A Tatro, 'An introduction to acoustic emission', Acoustic Emission: A Symposium, presented at the December Committee Week, American Society for Testing and Materials, Bal Harbour, Florida, 7-8 December 1971, ASTM International, Vol 505, 1972.
9. A K Apeagyei, W G Buttlar and H Reis, 'Estimation of low-temperature embrittlement for asphalt binders using an acoustic emission approach', Insight – Non-Destructive Testing and Condition Monitoring, The Journal of The British Institute of Non-Destructive Testing, Vol 51, No 3, pp 129-136, 2009.
10. E V Dave, B Behnia, S Ahmed, W G Buttlar and H Reis, 'Low-temperature fracture evaluation of asphalt mixtures using mechanical testing and acoustic emission techniques', Journal of the Association of Asphalt Paving Technologists (AAPT), Vol 80, pp 193-226, 2011.
11. B Behnia, E V Dave, S Ahmed, W G Buttlar and H Reis, 'Investigation of effects of the recycled asphalt pavement (RAP) amounts on low-temperature cracking performance of asphalt mixtures using acoustic emissions (AE)', Transportation Research Record No 2208, pp 64-71, 2011.
12. R A Guyer and P A Johnson, Nonlinear Mesoscopic Elasticity: The Complex Behavior of Granular Media including Rocks and Soil, Wiley-VCH Verlag GmbH & Co KGaA, Weinheim, 2009. ISBN: 978 3 527 40703 3.
13. L Kleeman, 'Ultrasonic sensors', in: The Industrial Electronics Handbook, J Irwin Ed, CRC Press, Boca Raton, IEEE Press, 1996.
14. D R Hull, H E Kautz and A Vary, 'Ultrasonic velocity measurement using phase-slope and cross-correlation methods', Spring Conference of the American Society for Nondestructive Testing, NASA Technical Memorandum, Denver, 1984.
15. E P Papadakis, 'Absolute accuracy of the pulse-echo overlap method and the pulse-superposition method for ultrasonic velocity', The Journal of the Acoustical Society of America, Vol 52, No 3, pp 843-846, 1972.
16. W Sachse and Y-H Pao, 'On the determination of phase and group velocities of dispersive waves in solids', Journal of Applied Physics, Vol 49, No 1, pp 4320-4327, 1978.
17. S Kazimierz, Stochastic Wave Propagation, Elsevier, New York, 1985.

Characterisation of oxidative ageing in asphalt concrete – Part 2: Estimation of complex moduli

M E McGovern, B Behnia, W G Buttlar and H Reis

The estimation of the dynamic Young's (uniaxial) and shear complex moduli based upon ultrasonic measurements are presented. Phase velocities were used instead of group velocities because of the highly attenuative nature of asphalt concrete. It was observed that the dynamic moduli increase from 0 to 24 h and decrease from 24 to 36 h of oven-ageing. The modulus obtained using ultrasonic measurements is also compared with the modulus obtained using the AASHTO recommended mechanical testing procedure. The differences are due to scattering effects, which are present in ultrasonic testing and absent in mechanical testing. It was also observed that, to avoid the uncertainty associated with assuming a suitable value for the Poisson's ratio, both the dilatational and shear velocities and corresponding attenuation measurements must be carried out. Furthermore, to eliminate the need for traditional mechanical testing during the estimation of complex moduli, frequency-dependent ultrasonic measurements must also be carried out. Results indicate that complex moduli are sensitive to the level of ageing in asphalt concrete mixtures.

Keywords: Asphalt concrete, complex modulus, dynamic modulus, oven-ageing, ultrasonic velocity, attenuation.

Introduction

Asphalt concrete is one of the most heavily used materials in pavement infrastructure[1]. When exposed to the environment, its material properties are altered as it undergoes oxidative ageing at, or near, the top surface, which leads to pavements with graded material properties across the pavement thickness. Oxidative ageing leads to stiffening and embrittlement of the asphalt binders, which reduces the healing capacity and increases the rate of microcrack propagation. This leads pavement systems to become more prone to coalesced macrocrack formation and they may begin to develop surface-initiated fatigue cracking. In addition, the brittle pavement surface will be prone to channelling cracks, such as thermal and block cracks. Fatigue, thermal and block cracking lead to an exponential decline in pavement serviceability and a resulting exponential increase in maintenance costs to restore the pavement condition. In a recent study by Islam and Buttlar[2], a rough pavement network was found to add an additional user cost of over $300 per vehicle per 12,000 miles driven. The encouraging news

Professor Henrique Reis* and graduate student Megan E McGovern are affiliated with the Department of Industrial and Enterprise Systems Engineering, University of Illinois at Urbana-Champaign, 117 Transportation Building, 104 S Mathews, Urbana, Illinois 61801, USA.

Professor William G Buttlar and Post-Doctoral Research Associate Behzad Behnia are affiliated with the Department of Civil and Environmental Engineering, University of Illinois at Urbana-Champaign, 117 Transportation Building, 104 S Mathews, Urbana, Illinois 61801, USA.

*Corresponding author. Tel: +1 217 333 1228; Fax: +1 217 244 5705; Email: h-reis@uiuc.edu

from the study was that properly timed maintenance treatments, resulting in a moderately smooth pavement over its life, yields an approximate 50-to-1 return on investment[2].

Pavement engineers face the difficult task of predicting the long-term behaviour of asphalt concrete subjected to field conditions in order to schedule preventive maintenance procedures aimed at ensuring proper pavement performance. Typically, rheology-based testing provides the foundation to understanding asphalt concrete behaviour under various conditions (for example loading, oxidative ageing, etc). These methods for evaluating existing conditions of asphalt concrete pavements are very time consuming, costly and, by themselves, may cause additional damage. As a result, decisions are often based upon visual inspection of deteriorated pavements. Furthermore, ignoring ageing- and temperature-induced property gradients in asphalt concrete pavements may yield significant errors. Complex moduli have the potential to characterise asphalt concrete subjected to field conditions. However, conventional mechanical techniques for the determination of complex moduli in asphalt concrete are also costly and time consuming. As a result, there exists the need for a quick, repeatable and less costly method for the determination of the complex moduli in asphalt concrete.

Previous studies by Velsor *et al*[3], Mounier *et al*[4] and Norambuena-Contreras *et al*[5] have correlated the complex modulus results obtained from ultrasonic tests to results from conventional mechanical tests; however, either the shear velocity was assumed to be constant across frequencies or the unknown Poisson's ratio was assumed. In this study, none of these assumptions are made. Furthermore, the lack of frequency-dependent ultrasonic measurements leads to uncertainties in the construction of the master curve. When velocities are taken at multiple temperatures, they must be shifted using the time-temperature superposition as discussed by Kim[1] and Christensen[6]. If the velocity is not considered to be frequency dependent (*ie* only a single reported value at each temperature), the amount by which it should be shifted (*ie* the shift factor) is unknown. When the shift factor is unknown, comparisons must be made between the ultrasonic data and the data obtained via mechanical testing. Consequently, the need for traditional mechanical testing is not eliminated.

In Part 1 of this study, ultrasonic dilatational and shear velocities and corresponding attenuation measurements were obtained for six different asphalt concrete specimens subjected to different amounts of oven-ageing (*ie* 0, 12, 24, 28, 32 and 36 h of ageing). In Part 2 of this paper, using these ultrasonic measurements, the dynamic uniaxial longitudinal and shear complex moduli for a frequency range of 30 to 350 kHz are estimated, and their dependence upon oxidative ageing is discussed.

Complex moduli – basic theory and measurement techniques

Asphalt concrete is a viscoelastic material, as its material properties are dependent on both time and temperature. Accordingly, its moduli are complex. The complex Young's (uniaxial) modulus is given by Christensen[6] as:

$$E^* = E' + iE'' \quad ....(1)$$

where:

$$E' = |E^*|\cos\varphi$$
$$\quad ....(2)$$
$$E'' = |E^*|\sin\varphi$$

and:

$$|E^*| = \sqrt{(E')^2 + (E'')^2} = \frac{\sigma_0}{\varepsilon_0} \quad ....(3)$$

where σ_0 and ε_0 are the longitudinal stress and strain, respectively. The magnitude of the complex Young's modulus $|E^*|$ is commonly referred to as the dynamic modulus, where the storage modulus is denoted by E', the loss modulus is denoted by E'' and φ is the phase angle, which can be found as:

$$\varphi = \tan^{-1}\frac{\mathrm{Im}[E^*]}{\mathrm{Re}[E^*]} = \tan^{-1}\frac{E''}{E'} \quad ....(4)$$

Figure 1 shows a graphical representation of the complex moduli. The complex shear modulus is analogous to the uniaxial modulus by simply substituting the uniaxial moduli parameters for the shear moduli parameters G^*, G', G'' and $|G^*|$ in the above equations.
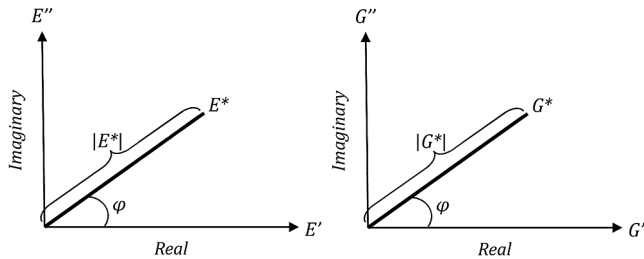
Figure 1. Graphical representation of complex Young's modulus. The naming conventions are as follows: |E*| ≡ dynamic modulus, E* ≡ complex modulus, E' ≡ storage modulus, E'' ≡ loss modulus and φ ≡ phase angle

Mechanical complex modulus test

Conventional techniques for measuring the dynamic modulus of asphalt concrete involve mechanical tests such as the compressive dynamic modulus test and the indirect tension test, as described by Kim[1]. Here, the focus will be on the compressive dynamic modulus test. The American Association of State Highway and Transportation Officials (AASHTO) standard[7] AASHTO T 342-11 details the compressive dynamic modulus test procedures for determining the dynamic modulus and phase angle of asphalt concrete over a range of frequencies and temperatures. The set-up consists of a servo-hydraulic loading frame with the capability of applying a sinusoidal compressive loading at a specified frequency (for the range of 0.1 to 25 Hz). The system contains an environmental chamber, which is used to control the temperature of the asphalt concrete specimen during testing. The specimen consists of a core extracted from a cylindrical gyratory compacted specimen (150 mm tall, 102 ±2 mm diameter). Four linear variable differential transformers (LVDT) are placed at four locations around the circumference of the asphalt concrete specimen (90º apart) to measure the average axial deformation. A load cell measures the applied load. The master curve is constructed by performing tests at temperatures of −10, 4.4, 21.1, 37.8 and 54ºC for sinusoidal loading at frequencies of 0.1, 0.5, 1.0, 5, 10 and 25 Hz for each temperature.

Ultrasonic parameters and the complex moduli

The complex moduli can be related to the ultrasonic parameters via the dilatational and shear phase velocities and corresponding attenuations. The group velocities and attenuations can also be used to calculate the complex moduli; however, the group velocity loses

its meaning when there is high attenuation as the 'wave packet' does not maintain its shape. The Poisson's ratio is a function of the shear to dilatational complex velocity ratio. Thus, to obtain the complex moduli, it is necessary to have the dilatational ultrasonic parameters (*ie* dilatational velocity and attenuation measurements) and either the Poisson's ratio or the shear ultrasonic parameters (*ie* shear velocity and attenuation measurements).

The elastic viscoelastic correspondence principle, as discussed by Christensen[6], makes it possible to use complex material properties in the solution of the elastic wave equation, see Kinsler *et al*[8]. Following Christensen[6] and Kinsler *et al*[8], the one-dimensional complex wave equation is written as:

$$\frac{d^2u}{dx^2} = \frac{1}{c^*(i\omega)^2}\frac{d^2u}{dt^2} \quad ....(5)$$

where $c^*(i\omega)$ is the complex phase velocity, ω is the circular frequency, t is time, x is the propagation direction and $u(x,t)$ is the particle motion. The solution to the equation (in terms of real and imaginary components) is:

$$u(x,t) = U_0 e^{i(\omega t - k^*x)} = U_0 e^{k''x}e^{i(\omega t - k'x)} \quad ....(6)$$

The second exponential term in the above equation is the familiar term describing the wave propagation in the x-direction, while the first exponential term is a decay term. The real and imaginary components of the complex wave number[8] are as follows:

$$k' = \mathrm{Re}(k^*) = \frac{\omega}{c(\omega)} \quad ....(7)$$
$$k'' = \mathrm{Im}(k^*) = -\alpha(\omega)$$

The complex phase velocity is related to the complex wave number as:

$$c^*(\omega) = \frac{\omega}{k' + ik''} = \frac{1}{\dfrac{1}{c(\omega)} - i\dfrac{\alpha(\omega)}{\omega}} \quad ....(8)$$

where $c(\omega)$ is the real phase velocity and $\alpha(\omega)$ is the real attenuation. Both of these quantities can be measured via conventional ultrasonic techniques. If the attenuation coefficient approaches zero, then the complex phase velocity is simply the real portion (measured) of the phase velocity. In other words, the phase velocity is only complex in the presence of attenuation.

The complex Young's modulus E* can be related to the complex velocities[9] as follows:

$$E^* = \rho(c_L^*)^2 \frac{3(c_L^*)^2 - 4(c_S^*)^2}{(c_L^*)^2 - (c_S^*)^2} \quad ....(9)$$

where ρ is the material density. The complex shear modulus G* can be written as follows:

$$G^* = \rho(c_S^*)^2 \quad ....(10)$$

and the complex Poisson's ratio is given by:

$$v^* = \frac{1 - 2\left(\dfrac{c_S^*}{c_L^*}\right)^2}{2\left[1 - \left(\dfrac{c_S^*}{c_L^*}\right)^2\right]} \quad ....(11)$$

Experimental results

The real components of the ultrasonic dilatational and shear phase velocities and their corresponding attenuations were measured experimentally and presented in Part 1 of this study. In this study,

these ultrasonic velocities and attenuation measurements are used to determine the complex moduli. Furthermore, comparisons are also made between the complex moduli obtained via the ultrasonic technique and the conventional mechanical approach as recommended by the American Association of State Highway and Transportation Officials[7] (AASHTO).

Using the ultrasonic velocity and attenuation data obtained in Part 1 of this study, Figure 2 shows the dynamic uniaxial modulus $|E^*|$ and the dynamic shear modulus $|G^*|$ as a function of frequency for different amounts of ageing of the asphalt concrete test samples. From this point forward, the dynamic modulus will be called $|E^*|_{specimen}$, where the subscript denotes the specimen according to the amount of ageing to which it was subjected. As the frequency increases, $|E^*|$ increases for all specimens. For example, for the frequency range of 30 to 350 kHz, $|E^*|_{virgin}$ increases from ≈ 5 to ≈ 28 GPa. This increase in $|E^*|_{virgin}$ is greater than what would be obtained from a corresponding mechanical test. This discrepancy can be attributed to scattering energy losses, which are absent in the AASHTO recommended mechanical test procedure.

As expected, $|E^*|$ follows the same trend as the velocities with respect to the amount of ageing: $|E^*|$ increases from 0 to 24 h and

decreases from 24 to 36 h of oven-ageing time. Although the binder becomes stiffer as it ages, it also loses adhesion properties, which leads to a decrease in bonding between the mastic and aggregates, and to weaker bonds between the fines and the binder in the mastic. After 24 h of ageing, this phenomenon results in a decrease of the overall composite (asphalt concrete mixture) stiffness. The complex shear modulus G^* follows similar trends to E^*.

The phase angle decreases with increasing frequency for all specimens, see Figure 3. Typically, the same trend is also observed in mechanical testing; however, discrepancies still exist. In mechanical testing, the phase angle is larger at lower frequencies and approaches zero with increasing frequencies. Via ultrasonic testing, the phase angle decreases with increasing frequencies; however, it seems to reach an asymptote at approximately 14°. This asymptote is likely to be caused by the scattering energy losses at higher frequencies. There is no discernible trend with respect to ageing.
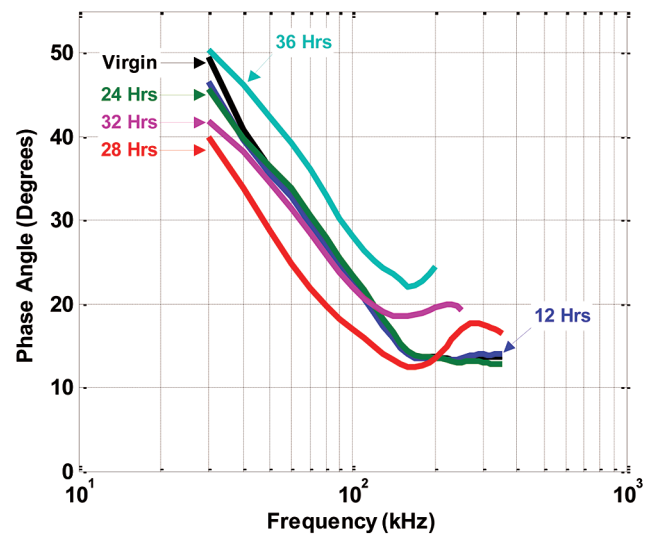
Figure 3. Phase angle (degrees) as a function of frequency for specimens subjected to various amounts of oven-ageing (0 to 36 h)

Figure 4 contains the complex Poisson's ratio as a function of frequency. The real component of the Poisson's ratio decreases with increasing frequency. The imaginary component decreases with increasing frequency from 30 to 190 kHz; above 190 kHz it increases with increasing frequency.

Comparison with mechanical tests

Figure 5(a) shows the dynamic modulus $|E^*|$ obtained using both the conventional mechanical testing method and the ultrasonic method. In Figure 5(a), only the raw ultrasonic data was used during the estimation of the dynamic modulus using the ultrasonic approach. Figure 5(a) shows that the complex modulus obtained via the ultrasonic approach does not fully coincide with the modulus obtained using the conventional mechanical tests. The observed differences are mainly a consequence of the ultrasonic velocities and attenuation measurements being affected by ultrasonic scattering at relatively higher frequencies, while scattering does not affect the results when conventional mechanical tests are used to evaluate $|E^*|$. The presence of wave scattering causes some differences because of the following two reasons: (1) scattering increases the measured attenuation with frequency; and (2) the measured shear velocity is dependent upon frequency, which corresponds to a change in the Poisson's ratio. If scattering effects were not present during ultrasonic wave propagation, the attenuation would be lower and the shear velocity would not be frequency dependent, which would lead to a nearly constant Poisson's ratio. As a result, lowering the attenuation and forcing the Poisson's ratio to be constant (*ie* forcing the shear velocity to be constant) should allow
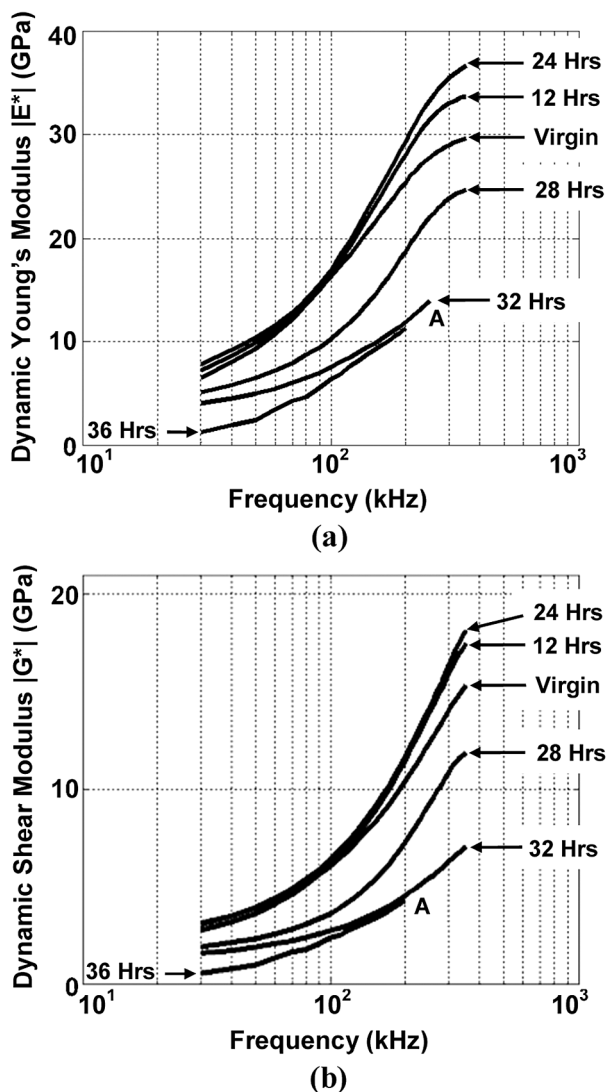

Figure 2. (a) Dynamic Young's modulus $|E^*|$ and (b) dynamic shear modulus $|G^*|$ as a function of frequency for specimens subjected to various amounts of ageing (0 to 36 h) computed using ultrasonic dilatational and shear velocity and attenuation measurements. For 32 and 36 h of ageing, attenuation for frequencies above 200 kHz, for example point A, were difficult to calculate because of the low signal-to-noise ratio caused by the increased attenuation
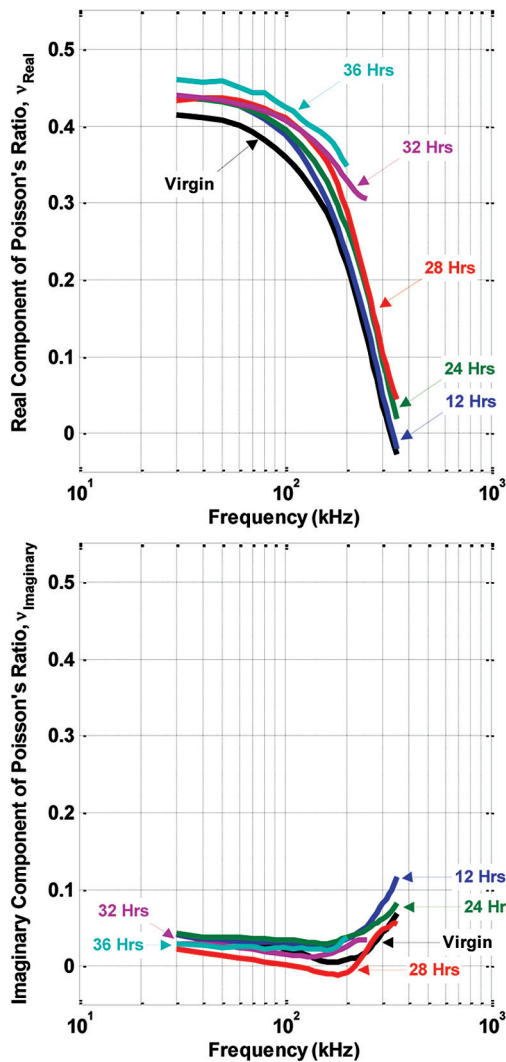
Figure 4. Real component (top) and imaginary component (bottom) of Poisson's ratio as a function of frequency for specimens subjected to various amounts of oven-ageing (0 to 36 h)

for the two methods to coincide.

Figure 5(b) is included to illustrate some of the traditional (and possibly unwarranted) assumptions encountered in the literature. Figure 5(b) shows the mechanical data along with the ultrasonic data, with the following major assumptions: (1) the attenuation is arbitrarily decreased by 20 Np/m; and (2) the shear velocity is forced to remain constant. Based on scattering effects, it might be possible to characterise how much the attenuation should be shifted. It is observed that attenuation does not play a significant role in the determination of these curves because the complex velocity is a function of the attenuation normalised by the angular frequency $\frac{\alpha(\omega)}{\omega}$ (see Equation 8). Thus, for high frequencies (*ie* the ultrasonic range), this ratio is a small number. However, the uncertainty with the second assumption arises in choosing a proper value for the shear velocity, which, empirically, varies with frequency. Since the dilatational velocities are nearly constant, the second assumption corresponds to a constant Poisson's ratio. Figure 6 shows the relationship between the Poisson's ratio and shear velocity for a constant dilatational velocity (mean of higher frequencies), *ie* selecting a constant shear velocity is equivalent to selecting a constant Poisson's ratio. Figure 5(b) shows the ultrasonic results with an arbitrary reduction in attenuation of 20 Np/m for multiple assumptions of the shear velocity (within the measured range), see Figure 6.

The phase angle measured via the ultrasonic approach is higher

(a)

(b)
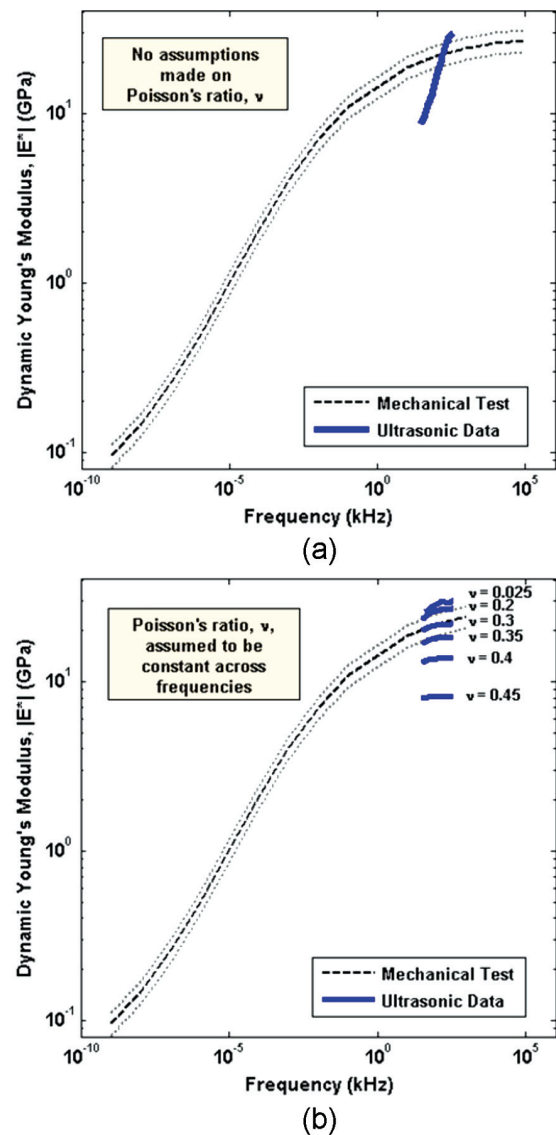
Figure 5. The dynamic modulus |E^*| (GPa) obtained via conventional mechanical testing (grey dashed line) compared with the |E^*| obtained via the ultrasonic method based on: (a) no assumptions made; and (b) the Poisson's ratio, v, is assumed to be constant and an arbitrary decrease in attenuation of 20 Np/m is assumed for both the dilatational and shear waves
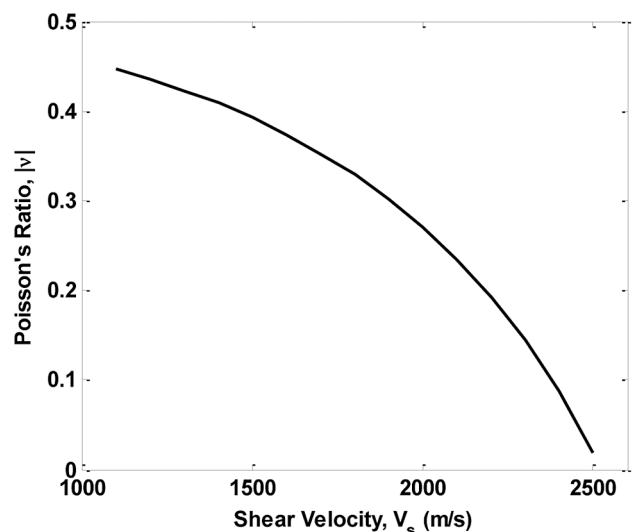
Figure 6. The mean Poisson's ratio as a function of shear velocity in unaged specimen for frequencies above 100 kHz (where the dilatational velocity is relatively independent from frequency)

than the phase angle obtained using the traditional mechanical testing, mainly because of the ultrasonic wave scattering. For the same reasons, the Poisson's ratio, which is a function of the complex dilatational and shear velocities, exhibits similar discrepancies due to scattering.

Construction of the master curve

Previous studies, Velsor[3], Mounier *et al*[4] and Norambuena-Contreras *et al*[5], have measured the group velocity at different temperatures without considering frequency dependency; thus, the velocity at each temperature was a discrete value. When constructing the master curve, it is necessary to shift the data using the time-temperature superposition[1,6]. Shifting the data, however, requires that the shift factor be known. If velocity measurements are not taken with respect to frequency, then the only way to obtain the shift factor is by comparing it to a known master curve, *ie* to a model fitted to data obtained via conventional mechanical testing. Consequently, the need for mechanical testing is not eliminated. To construct the master curve based solely upon ultrasonic data, both velocities and the corresponding attenuations must be known with respect to a range of frequencies.

Correlation with other tests

In a comparison of the results of all the tests presented, it is observed that all the test results reach a peak (or trough) at some level of oven-ageing time. Until it reaches this critical ageing time, the structural response (for example stiffness) typically increases with ageing, after which it decreases. The amount of ageing at which these peaks (or troughs) occur varies slightly between tests. Based on the results from the ultrasonic and acoustic emission tests, this threshold appears to be around 24 h of oven-ageing for this mixture. For example, as the amount of ageing increases, both the ultrasonic dilatational and shear velocities increase until 24 h of ageing, after which they decrease with increasing ageing. The magnitude of the ultrasonic attenuation follows a comparable trend, where it decreases from 0 to 24 h, after which it increases with increasing ageing. The rate of change of the embrittlement temperatures (obtained using AE), with respect to ageing time, increases relatively slowly until 24 h of ageing, after which it rapidly increases; see Part 1 of this study. This response of asphalt concrete with ageing is also supported by the results using the disc-shaped compact tension (DC(T)) fracture tests. Published data using the DC(T) tests also indicates that the fracture energy increases up to a critical ageing time (~10 h of oven-ageing), after which it decreases; see Figure 14 in Part 1 of this study.

Conclusions

Complex moduli were calculated for asphalt concrete specimens subjected to various amounts of oven-ageing time (0, 12, 24, 28, 32 and 36 h) using the ultrasonic velocity and attenuation measurements presented in Part 1 of this study. The complex moduli calculated via ultrasonic testing are compared with the complex moduli obtained via conventional mechanical testing. The discrepancies observed between the two methods are due to the scattering effects, which exist in ultrasonic wave propagation and are absent in mechanical testing. It is observed that to avoid the uncertainty of 'assuming' the value of the Poisson's ratio, both ultrasonic dilatational and shear velocities and the corresponding attenuation measurements need to be obtained as a function of frequency. It is also noted that frequency-dependent ultrasonic measurements must be made to calculate frequency-dependent complex moduli, otherwise the need for the conventional mechanical testing to estimate the complex moduli is not eliminated.

The correlation between the complex moduli and the amount of ageing suggests that this non-destructive method can be successfully employed to evaluate the effects of oxidative ageing in asphalt concrete. It was observed that, across all frequencies, the dynamic modulus increases from 0 to 24 h and decreases from 24 to 36 h of oven-ageing. From this trend, it can be concluded that after 24 h, the binder's increase in stiffness with ageing and its decrease in adhesive properties, which leads to debonding between the mastic and the aggregates and to bond deterioration among the fines in the mastic, results in an overall decrease in the dynamic modulus of the overall mixture. Results from the ultrasonic complex moduli are consistent with results obtained using DC(T) fracture energy tests and with AE-based embrittlement temperatures obtained during cooling from room temperature to –50ºC. Therefore, an acoustic-based approach has the potential to be used as a pavement field inspection/monitoring tool. First, evaluation/characterisation of asphalt concrete properties and their gradation through the pavement thickness could be made using extracted field cores. In the end, embedded wireless sensor nodes could be used to monitor the pavement response to the environment without core extraction.

References

1. Y R Kim, Modeling of Asphalt Concrete, McGraw-Hill, American Society of Civil Engineers, New York, 2009.
2. M Islam and W G Buttlar, 'Effect of pavement roughness on user costs', Journal of the Transportation Research Board, National Research Council, Vol 2285, pp 47-55, 2012.
3. J K Van Velsor, L Premkumar, G Chehab and J L Rose, 'Measuring the complex modulus of asphalt concrete using ultrasonic testing', Journal of Engineering Science and Technology Review, Vol 4, No 2, pp 160-168, 2011.
4. D Mounier, H D Benedetto and C Sauzéat, 'Determination of bituminous mixtures linear properties using ultrasonic wave propagation', Construction and Building Materials, Vol 36, pp 638-647, 2012.
5. J Norambuena-Contreras, D Castro-Fresno, A Vega-Zamanillo, M Celaya and I Lombillo-Vozmediano, 'Dynamic modulus of asphalt mixture by ultrasonic direct test', NDT&E International, Vol 43, pp 629-634, 2010.
6. R Christensen, Theory of Viscoelasticity: An Introduction, Second Edition, Academic Press, New York, 1982.
7. AASHTO, 'Standard method of test for determining the dynamic modulus of hot mix asphalt (HMA)', American Association of State Highway and Transportation Officials (AASHTO), T 342-11, 2011.
8. L E Kinsler, A R Frey, A B Coppens and J V Sanders, Fundamentals of Acoustics, 4th edition, John Wiley and Sons Inc, Hoboken, 1976.
9. ASTM, 'Standard test methods for measuring ultrasonic velocity in materials', Annual Book of ASTM Standards, E494-10, 2010.

Characterisation of oxidative ageing in asphalt concrete using a non-collinear ultrasonic wave mixing approach

M E McGovern, W G Buttlar and H Reis

A study to assess oxidative ageing of asphalt concrete using non-collinear wave mixing of two dilatational waves is presented. Criteria were used to assure that the detected scattered wave originated via wave interaction in the asphalt concrete and not from non-linearities in the testing equipment. These criteria included the frequency and propagating direction of the resultant scattered wave and the time-of-flight separation between the two primary waves and the resulting scattered wave. It was observed that asphalt concrete exhibits non-linear behaviour. It was also observed that the non-linear response decreases with increased ageing until approximately 24 h of ageing, after which the non-linear response exponentially increases. This observation is consistent with previous studies, including the acoustic emission response to thermal loading, and with changes in the dynamic modulus and fracture energy with increasing ageing.

Introduction

Although possessing remarkable toughness in its original state, asphalt concrete (AC) becomes brittle and prone to damage with time, in the form of costly pavement cracking. The time required to reach an unacceptable level of embrittlement depends upon a number of factors and varies widely from pavement to pavement, even within a given region and mixture type. Given the annual costs associated with repair of pavement damage caused by mechanical and thermal loads, considerable interest exists in testing methods to estimate damage in AC mixtures. Current methods to evaluate the existing conditions of AC pavement surfaces for sustainability-based pavement asset management are based upon the binder's rheological properties and are time consuming, costly and, by themselves, may cause additional damage.

Oxidative ageing is a key contributor to the deterioration of asphalt concrete pavements[1,2]. Exposure to environmental conditions causes gradual oxidative ageing of the asphalt concrete, where the highest aged material is located at the surface, while the material at the bottom of the pavement is significantly less aged. Over time, increasing ageing at the surface leads to a pavement with graded material properties through its thickness, where the material near the surface has warmer embrittlement temperatures and higher stiffness compared to the bottom of the pavement. Increasing ageing also results in significant loss of adhesion between the binder, aggregates and fines, which contributes to an increase in the micro-flaw population in the mastic and at the interfaces between the mastic and the aggregates[3]. As the pavement is subjected to thermal loads (for example cold climates and temperature cycling) and mechanical loads (for example traffic loads), microcracks develop and coalesce to form larger cracks. Repeated loading and exposure to environmental conditions eventually leads to significant deterioration of asphalt concrete pavements. Although surveys are conducted to monitor the condition of pavements and to determine when preventative or corrective maintenance is necessary, accurate assessment of the amount of pavement deterioration has remained a challenge. Clearly, there is a need for a rapid *in-situ* non-destructive evaluation technique capable of assessing the level of oxidative ageing in the top layers of asphalt concrete pavements.

Conventional acoustic and ultrasonic structural health monitoring methods, including traditional guided wave studies, are based upon principles that are valid under the assumption of linear elasticity. These include the effects of reflection, scattering, transmission and loss of energy by material absorption and by leakage to adjacent systems, as in the case of guided wave systems. Under these assumptions, the presence of defects leads to phase or amplitude variation of the ultrasonic wave (signal), keeping the frequency of the receiving wave the same as the frequency of the wave emitted by the sending transducer. In non-linear ultrasonics, the frequency of the received wave differs from the frequency of the emitted wave (*ie* from the frequency of the wave generated by the sending transducer), implying that a non-linear transformation of ultrasonic wave energy by the media has occurred, as in harmonic generation[4-7].

In linear elastic wave propagation, superposition holds: two or more waves can cross paths and their resultant (in the region where they cross paths) is the addition (*ie* superposition) of those waves. However, superposition does not hold when the media is non-linear. Because of the presence of higher-order terms in the non-linear equations of motion, when two waves cross paths, *ie* intersect, a third wave, *ie* a scattered wave, may arise. However, in order for a strong scattered wave to occur, resonance and polarisation conditions must be met[8-20].

Using equilibrium conditions and virtual work, the third-order non-linear equations of motion were developed by Murnaghan[8] in 1951. He proposed a set of third-order elastic constants (TOECs), which are commonly referred to as *l*, *m* and *n*. In 1954, Landau and Lifshitz[9] suggested using the relationship between the stress tensor and the elastic energy function as the basis for deriving the non-linear equations of motion and proposed a different set of TOECs, referred to as *A*, *B* and *C*; the derivation was carried out by Goldberg[10] in 1961. The two sets of TOECs are linear combinations of each other. In 1963, Jones and Kobett[11] solved the third-order non-linear elastic equations of motion and developed criteria for the occurrence of a scattered wave. Experimentally, elastic non-linear behaviour has been observed for a variety of materials using the non-collinear wave mixing approach for a broad range of ultrasonic

Professor Henrique Reis* and graduate student Megan E McGovern are affiliated with the Department of Industrial and Enterprise Systems Engineering, University of Illinois at Urbana-Champaign, 117 Transportation Building, 104 S Mathews Avenue, Urbana, Illinois 61801, USA.

Professor William G Buttlar is affiliated with the Department of Civil and Environmental Engineering, University of Illinois at Urbana-Champaign, 205 N Mathews Avenue, Urbana, Illinois 61801, USA.

*Corresponding author. Tel: +1 217 333 1228; Fax: +1 217 244 5705; Email: h-reis@uiuc.edu

frequencies[12-23]. Non-collinear wave mixing has proved useful in a variety of practical applications, which include the determination of higher-order elastic constants[14], and in the inspection and detection of material degradation, such as plastic deformation and fatigue damage accumulation in metals[19] or ageing in polymers[17]. Johnson and Shankland[12,13] also reported scattered waves as a result of the non-linear interaction of two intersecting waves of different frequencies in crystalline rock and developed criteria to assure that the scattered wave is due to non-linearities in the material response and not caused by non-linearities inherent in the instrumentation used.

Distributed damage, such as damage induced by fatigue, typically consists of phenomena initially affecting the material at many locations in the form of local variations in the material microstructure. In metals such as aluminium, these local variations in microstructure consist of fatigue-induced entanglement of dislocation substructures, such as the sidebands. These sidebands, which accumulate at the grain boundaries, produce strain localisation, which eventually leads to microcrack initiation with an increased number of fatigue cycles. While these local changes in microstructure do not change macroscopic elastic moduli or produce variations in linear acoustic parameters, such as acoustic velocity and attenuation, the stress field in the dislocation(s) creates a local non-linear stress-strain response in the localised volume of the dislocation(s). These local variations in the microstructure on the scale of single grains develop before the initiation of a visible crack. This degradation of the material significantly reduces the material's resistance to crack growth when microcracking coalescence occurs at a later time. The ultimate strength of most structural materials is limited by the presence of these microscopic microstructural variations, *ie* defects, which can be produced by mechanical or thermal loading and subsequently serve as nuclei of the fracture process. Because these nuclei (local variations) are significantly shorter than the acoustic wavelength at the frequencies normally used in ultrasonic non-destructive evaluation, linear acoustic parameters (*ie* attenuation, velocities, etc) are usually not sensitive enough to detect this kind of microscopic degradation of the material structural integrity.

In addition to the non-linear behaviour of the individual constituents of asphalt concrete, *ie* binder, crushed stone and fines, the presence of micro-flaws in the composite structure causes a non-linear distortion in the propagating wave. As the asphalt concrete is subjected to oxidative ageing, two counter-acting effects take place within the mastic (binder + fine material). The stiffness of the mastic increases with ageing, while the adhesive properties of the mastic decrease. Until a critical amount of ageing, the positive effects of the increased stiffness overcome the negative effects of the reduction in adhesion. Beyond this critical point, the adhesion loss becomes the dominating effect. The loss in adhesion leads to weaker bonds between the mastic and the aggregates and between the fines in the binder, which leads to a weaker internal structure of the composite. This degradation of the material significantly reduces the material's resistance to crack growth later when microcracking coalescence occurs. The ultimate strength is limited by the presence of these micro-flaw populations, which will then serve as nuclei of the fracture process. As in metals, the presence of these micro-flaw populations causes a non-linear distortion in the propagating wave. Therefore, as the oxidative ageing of the asphalt increases, the material displays increasingly non-linear behaviour. Air voids, which are also present in the material based on standard design mixture guidelines, may also have a similar effect on the propagating wave.

Using linear ultrasonics, McGovern *et al*[24,25] studied the effects of oxidative ageing of asphalt concrete mixtures upon the acoustic emission response during thermal cooling and upon both ultrasonic longitudinal and shear velocities and corresponding attenuations. In this study, the non-linear behaviour of asphalt concrete as a function of laboratory-induced oxidative ageing is investigated by a non-collinear wave mixing approach, using two dilatational waves similar to the methodology used by Johnson and Shankland[12,13]. For the purpose of comparison, the asphalt concrete mixtures and the different levels of oxidative ageing are the same in both studies[24,25].

Asphalt concrete and its non-linear mesoscopic nature

Asphalt concrete belongs to a class of materials that have non-linear mesoscopic elasticity (NME). For example, rocks, soils and powdered aluminium have non-linear mesoscopic elasticity (NME)[26,27]. This class of materials typically has a bricks-and-mortar character. In these materials, the bricks (quartz grains in the case of rocks and crystallites, such as quarts, feldspar and clay particles, in the case of soils) interface with one another across a distinctive, elastic phase, which behaves as the mortar (a system of asperities in the case of rocks and a system of fluid layers and fillets in the case of wet soil). For these materials, the typical elastic modulus is an order of magnitude smaller than the corresponding modulus of the bricks. Having ten times as much displacement and about 10% of the volume means that the mortar, while only a minor phase in terms of volume concentration, is responsible for much of the compliance in the composite and may carry strains as high as two orders of magnitude greater than the strains in the bricks or rigid particle phase.

This behaviour has also been observed in asphalt concrete mixtures, where the bricks are the aggregates (*ie* crushed stone) and the mortar is the asphalt binder, which is approximately 5% by volume. Asphalt binders exhibit both linear and non-linear viscoelastic behaviour and the level of non-linearity increases with stress or strain levels[28-35]. Masad *et al*[33-35] found the average binder strain range to be 9 to 12 times the mixture strain, and that the binder maximum strain can be as high as 90 times that of the mixture strain; this induces non-linear behaviour in the binder and consequently in the mixture as well. Masad *et al*[35] also studied the viscoelastic response of un-aged and aged binders. The non-linear response of binders and mixtures was also studied by Delgadillo[36], and a comprehensive investigation on low-temperature cracking in asphalt pavements was carried out by Marasteanu *et al*[37]. Clearly, in addition to thermal cracking induced by the thermal stresses during cooling, the high level of stresses and strains in the binder will increase the non-linear response of the asphalt concrete mixture.

Specimen preparation and linear characterisation

Six gyratory compacted asphalt concrete specimens were prepared using PG 64-22 binder with a target asphalt content of 5.9% by weight of the total mixture. The aggregate structure had a nominal maximum aggregate size (NMAS) of 9.5 mm and it consisted of aggregates from four different stockpiles: 65% of coarse aggregate (CM16), 23% of manufactured sand (FM20), 10.5% of manufactured sand (FM02) and 1.5% of mineral filler (MF). This mixture design followed Superpave guidelines.

The asphalt concrete mixtures were mixed using a standard bucket mixing procedure at a temperature of 155ºC. The mixtures were oxidatively aged by placing the uncompacted mixtures in an oven at 135ºC. Each of the six specimens was subjected to a different amount of ageing, namely 0, 12, 24, 28, 32 and 36 h. Ageing beyond 36 h was not carried out because the rough, cratered surfaces of specimens aged past 36 h caused coupling difficulties with the sensors, preventing ultrasonic testing. To ensure uniformity of the ageing process (*ie* uniform exposure to oxygen), the mixtures were hand-stirred every 12 h.

Cylindrical specimens (150 mm in height and with 150 mm diameters) were created by compacting the aged mixtures with a servo-controlled gyratory compactor (IPC Servopac) at a temperature of 135°C. Each of the cylinders was cut to obtain a 5 cm-thick cylinder, see Figure 1. Appropriate angles were then cut into the cylinders so that the transducers could be mounted directly onto the flat faces of the specimen. Figure 1 shows the geometry and dimensions of the extracted test samples from each of the cylindrical compacted gyratory specimens.
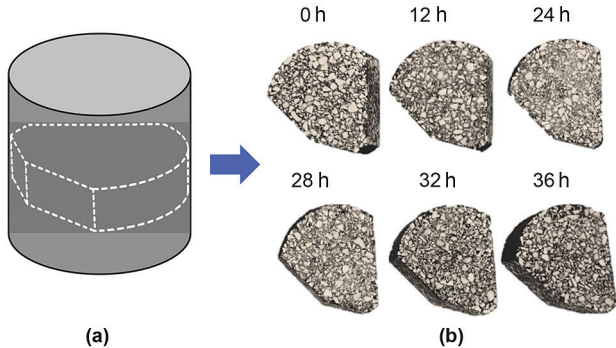
Figure 1. Geometry of test specimens: (a) gyratory compacted specimen; and (b) extracted test specimens with different levels of oven ageing at 135ºC. The angles at which these specimens were cut were such that the sending and receiving transducers were positioned at the appropriate angles to satisfy resonance and polarisation conditions, see Figure 3

In a previous study[24,25], ultrasonic phase velocity and attenuation measurements for dilatational and shear waves were taken on six specimens constructed with the same mixture design and oxidatively aged using the same process as described above (see Figure 2). These ultrasonic results are presented as a function of frequency and ageing amount. It can be seen that the velocity (over all frequencies) increases with increased ageing until 24 h of ageing; after 24 h, the velocity decreases with increased ageing. Similarly, the attenuation (over all frequencies) decreases with increased ageing until 24 h of ageing, after which it increases with increased ageing. Please refer to McGovern *et al*[24,25] for a more detailed discussion on these results.
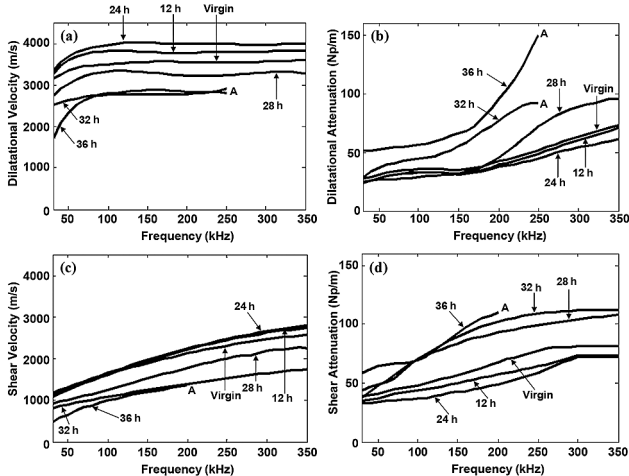
**Figure 2. Velocities and corresponding attenuations. Top row: (a) dilatational velocities and (b) corresponding attenuations for asphalt concrete samples aged from 0 to 36 h. Bottom row: (c) shear velocities and (d) corresponding attenuations for asphalt concrete aged from 0 to 36 h. For samples aged 32 and 36 h, the dilatational velocity for frequencies above 250 kHz, *ie* point A, were difficult to calculate because of the low signal-to-noise ratio caused by the increased attenuation. For similar reasons, the shear velocity for the specimen aged 36 h was only calculated up to 200 kHz and the shear attenuation of the specimen aged up to 24 h was determined only up to 300 kHz. *Reprinted with permission from McGovern et al[24]*

Using a non-collinear wave mixing approach

Jones and Kobett[11] considered the scattered wave that may result from the interaction of two primary monochromatic waves. The two waves travelling in directions k_1 and k_2, with frequencies f_1 and f_2, respectively, may be dilatational and/or shear (polarised either in or out of the k_1-k_2 plane) and may interact to produce a scattered dilatational or shear wave with a sum $(f_1 + f_2)$ or difference $(f_1 - f_2)$ frequency, which propagates in the k_3 direction.

The polarisation of the scattered shear wave depends on the type and polarisation of the two primary waves. In addition to resonance conditions, polarisation conditions must also be met in order for interaction to be possible for a given set of primary waves. As a result, there are only a finite set of possible interaction cases; out of fifty-four potential non-linear scattered waves (resulting from nine possible interaction cases of different bulk primary waves), only nine potential non-linear scattered waves satisfy both the resonance and polarisation conditions. In this study, only the non-collinear interaction of two dilatational waves is considered, where two dilatational waves (k_1,f_1 and k_2,f_2) are forced to interact to produce a scattered shear wave ($k_3 = k_1 - k_2, f_3 = f_1 - f_2$). For resonance and polarisation conditions to be met, the following equations need to be satisfied:

$$\cos[\varphi] = \left(\frac{c_l}{c_t}\right)^2 \left[1 - \frac{1}{2}\frac{f_1}{f_2}\left(1 - \frac{c_t^2}{c_l^2}\right)\left(\frac{f_2^2}{f_1^2} + 1\right)\right] \quad \text{............}(1)$$

$$\tan[\gamma] = \frac{-f_2 \sin[\varphi]}{f_1 - f_2 \cos[\varphi]} \quad \text{............}(2)$$

In Equations (1) and (2), f_1 and f_2 denote the frequencies of the two primary dilatational waves travelling in directions k_1 and k_2, respectively, c_l and c_t denote the dilatational and shear velocities, respectively, φ is the angle between k_1 and k_2, and γ is the angle between k_1 and k_3. For the case described by the above two equations, the non-linear scattered wave is polarised in the k_1-k_2 plane. To assure that the scattered wave originates from the non-linear interaction in the material and not from non-linearities inherent to the testing instrumentation, Johnson and Shankland[11,12] proposed three criteria: (1) frequency – the frequency of the observed scattered wave must match the frequency predicted by theory; (2) amplitude – the amplitude of the scattered wave must be proportional to the product of the amplitudes of the primary waves; and (3) directionality – the propagating direction of the scattered wave must match the direction predicted by theory (Equations (1) and (2)). In this study, the experimentally-observed time-of-arrival of the scattered wave is also considered, which should closely 'match' the time-of-arrival predicted using ray-path analysis.

Experimental set-up

Prior to cutting the asphalt concrete specimens, the appropriate angles must be chosen such that wave interaction occurs and the resulting scattered wave is received. The reader is referred to Equations (1) and (2). The frequency ratio f_2/f_1, interaction angle φ and scattered wave angle γ are all interdependent quantities. In other words, once one parameter is chosen (for example φ), the other two (for example γ and f_2/f_1) are set. Typically, this task is relatively simple: for a known set of ultrasonic material properties (*ie* dilatational and shear velocities/attenuations), one parameter can be chosen, in consequence setting the other two. Then, the specimen dimensions can be selected and appropriate angles cut into the specimen.

In this study, the goal is to use the non-collinear wave mixing approach to estimate the ageing level of asphalt concrete. It follows that the testing set-up should be the same for all specimens. The ultrasonic velocities vary with the level of ageing, which complicates the matter of choosing the appropriate testing

set-up (ie specimen dimensions, interaction/scattered angles and frequencies) that will work across all aged specimens. To assess the specimen ageing, a testing set-up will be chosen based on the virgin specimen parameters. Determining a final testing set-up is an iterative process, where the goal is to find one testing set-up that meets the conditions, which will now be outlined.

Interaction angle, φ

The interaction angle will be chosen such that all six specimens (0 to 36 h of ageing) will interact at the same angle, resulting in different f_2/f_1 and γ for specimens having different ageing levels. The interaction angle will be chosen based solely on its effects on the scattered wave angle and frequency ratio.

Primary and scattered wave frequencies

The primary wave frequencies should be chosen such that the waves propagate with minimal distortion (due to scattering and attenuation) and generate a non-linear scattered wave with the same characteristics. To achieve this, the wavelength of the propagating wave should be larger than the aggregate size. The nominal maximum aggregate size for this mix is 9.5 mm. The upper frequency bound for shear waves is 110 kHz, which corresponds to a shear wave wavelength ($\approx$ 9.5 mm) through the 36 h-aged specimen. The dilatational waves have wavelengths greater than 9.5 mm for all ages for the measured frequency range ($\leq$350 kHz). Furthermore, the two primary wave frequencies should be chosen such that their resulting velocities are similar, to be consistent with the theory presented in Equations (1) and (2).

Above 100 kHz, the dilatational wave velocities all tend to plateau (see Figure 2). Thus, the frequencies of the primary waves should be chosen to be greater than 100 kHz, because Equations (1) and (2) were derived with the assumption that k_1 (f_1) and k_2 (f_2) have the same velocity. Above 200 kHz, the attenuation increases dramatically. In fact, for specimens aged 36 h, a signal could not be detected through the thickness of 30 mm above 250/200 kHz for dilatational/shear waves. Therefore, the primary wave frequency should be restricted to 200 kHz or below. It is difficult to detect shear waves below 50 kHz with the transducers employed in the set-up; as a result, the scattered shear wave should have a frequency above 50 kHz.

Therefore, the primary waves should be chosen within a frequency range of 100 to 200 kHz, and the resulting scattered shear wave should be within a frequency range of 50 to 110 kHz. Also, the scattered wave frequency (f_3) should have a sufficient separation from the primary wave frequencies (f_1 and f_2), so that they can be easily separated in the frequency domain. Of course, the choice of frequencies should also consider the effects it has on the interaction and scattered wave angles.

Scattered wave angle, γ

All specimens will be cut according to the conditions specified using the virgin parameters. The amount of deviation between the angle for which the specimens are cut and the actual scattered angles will affect how well the scattered wave is received. For this reason, a case should be found that minimises the difference in scattered wave angles between the virgin specimen and the other aged specimens, so that even if the receiving transducer is not oriented in the ideal location it can still receive the non-linear scattered wave.

Specimen dimensions

Asphalt concrete is highly attenuative (see Figure 2), which will greatly diminish the amplitudes of the primary and scattered waves as they propagate through the specimen. This attenuation loss should be minimised by minimising the distance through which the wave propagates to ensure that the scattered non-linear wave can be detected by the receiver. The propagation distances should be at

least one wavelength long, such that the waves are stabilised by the time they interact. For simplicity, k_1 and k_2 can be chosen to have the same propagation distances.

The non-linear wave generation parameter, β

To characterise the non-linearities in the asphalt concrete with respect to ageing, a non-linear wave generation parameter is introduced. The amplitude of the scattered wave is proportional to the product of the primary wave amplitudes at the time of interaction[14,15]. The primary waves suffer attenuation as they propagate through the specimen before they interact, and the scattered wave is further attenuated as it travels to the receiver. Accounting for the attenuation, the received amplitude of the scattered wave can be described by the following expression (assuming perfect coupling conditions):

$$A_{age}^{(k_3)} = \beta_{age} A_{sent}^{(k_1)} A_{sent}^{(k2)} \exp\left[-\left(\alpha^{(k_1)}+\alpha^{(k_2)}\right)D_{k_1 k_2}\right]\exp\left[-\alpha^{(k3)}D_{k_3}\right]$$

where:

$$\beta \equiv \text{conversion efficiency}$$
$$A_{sent}^{(k_n)} \equiv \text{Transmitted amplitude of } k_n \text{ (volts)}$$
$$\alpha^{(k_n)} \equiv \text{Attenuation coefficient of } k_n \left(\frac{Np}{m}\right)$$
$$D_{kn} \equiv \text{Propagation distance of } k_n \text{ (}m\text{)}$$

The conversion efficiency parameter β is a dimensionless parameter, which accounts for the fraction of the interacting waves that is converted to the scattered wave. The propagation distances are approximated via a straight ray-path assumption. The attenuation coefficients were measured empirically.

Normalising the amplitude by the attenuation, and denoting it by:

$$A_{age}^{*(k_3)} = \frac{A_{age}^{(k_3)}}{\exp\left[-\left(\alpha^{(k_1)}+\alpha^{(k_2)}\right)D_{k_1 k_2}\right]\exp\left[-\alpha^{(k_3)}D_{k_3}\right]}$$

then:

$$A_{age}^{*(k_3)} = \beta_{age} A_{sent}^{(k_1)} A_{sent}^{(k_2)}$$

Assuming that variations in the coupling conditions between testing set-ups can be neglected, the transmitted amplitudes of the primary waves $A_{sent}^{(k_1)}$ and $A_{sent}^{(k_2)}$ will be the same for all tests performed. As a result, the conversion efficiency parameter for the aged mixture, β_{age}, can be normalised by the conversion efficiency parameter for the virgin, ie unaged, mixture, β_0, to characterise increasing levels of ageing:

$$\frac{\beta_{age}}{\beta_0} = \frac{A_{age}^{*(k_3)}}{A_0^{*(k_3)}}$$

By way of the above formulation, the non-linear wave generation parameter is independent of the attenuation, so that it represents the conversion efficiency of the energy transferred from the primary waves interacting to produce the scattered non-linear wave. Thus, this parameter is a good indicator of the material's inherent non-linear behaviour.

Experimental description

Using the considerations outlined in the previous section, the specimens were cut so that two longitudinal transducers could be mounted on the faces of the specimens and generate two longitudinal primary waves (k_1 and k_2) that interact at 31° to produce a non-linear scattered shear wave, which is received at –42° with respect to k_1. These angles were chosen based on virgin specimen properties and used for all six specimens. Table 1 contains the theoretical values

Table 1. Average dilatational and shear velocities (between 140-200 kHz), corresponding frequency ratio f_2/f_1 and scattered wave angle γ for an interaction angle φ of 31°. For time-of-flight calculations, the shear velocity at the scattered wave frequency f_3 is also presented

Amount aged (h)	Dilatational velocity mean (140-200 kHz) c_L (m/s)	Shear velocity mean (140-200 kHz) c_S (m/s)	Velocity ratio c_S/c_L	Interaction angle φ (°)	Frequency ratio f_2/f_1	Angle of scattered wave γ (°)	Scattered wave frequency $f_3 = f_1 - f_2$ (kHz)	Shear velocity at f_3 c_S (m/s)
0	3559	1992	0.560		0.700	−42*	60	1384
12	3785	2066	0.546		0.710	−43	58	1334
24	4005	2088	0.521	31*	0.724	−44	55.2	1343
28	3285	1629	0.496		0.738	−46	52.4	1013
32	2780	1313	0.472		0.751	−47	49.8	904
36	2868	1273	0.444		0.764	−49	47.2	648

*Note: The specimens (for all ages) were all cut to the angles determined for the virgin specimen. Care was taken to find a case where the difference in the scattered wave angle was minimal (ie $\gamma_{36h} - \gamma_{Virgin} = 7°$) so that the receiving transducer could detect the scattered wave for all specimens. Keeping the angles constant causes the frequency ratio at which the non-linear wave interaction occurs to shift.

for all aged specimens. The velocities used to calculate the velocity ratio were computed using the mean velocities across 140-200 kHz (see Figures 1 and 3). This set-up avoids complications that arise with the implementation of wedges (for example refracted angle, generation of multiple refracted modes, etc). The specimen dimensions were cut such that k_1 and k_2 will propagate a distance of 5 cm and k_3 will propagate a distance of 4 cm. A plastic template was created using a 3D printer to ensure reproducibility of transducer placement between tests. The plastic template supported the asphalt concrete specimens using three screws to minimise the contact area between the test specimens and the supporting structure surface.

A pulser-reciever (Ritec RPR 4000) was used to generate and amplify a 15-cycle sinusoidal signal at $f_1 = 200$ kHz. This signal (k_1) was sent to a dilatational wave transducer (Panametrics V413, centre frequency 500 kHz). A function generator (Krohn-Hite Model 5920) was used to generate an 8-cycle sinusoidal wave, which swept from $f_2 = 110$ kHz to 180 kHz in 1 kHz increments. This signal (k_2) was amplified using a gated amplifier (Ritec GA-2500A) and sent to another dilatational wave transducer (Panametrics V413, centre frequency 500 kHz). The number of cycles in the tonebursts was chosen to ensure the intersection of the primary dilatational waves within the specimen, see Figure 3 for transducer placement. The scattered shear wave (k_3) was received by a shear transducer (Panametrics V1548, centre frequency 100 kHz), filtered/amplified by a 4-pole Butterworth filter (Krohn-Hite model 3945) and then sent to the computer for data acquisition.

Data acquisition consisted of three steps: (1) operating the two sending transducers simultaneously; (2) individually operating only the first sending transducer; and (3) individually operating only the second sending transducer. To obtain the non-linear

Figure 3. Schematic diagram of the ultrasonic data collection system illustrating the angle of interaction of the two longitudinal waves and the location of the shear transducer to receive the generated scattered shear wave. The blue and red regions denote the areas of signals k_1 and k_2, respectively, caused by the beam spread. The overlap region is the volume of interaction. Note that the beam spread from k_2 is slightly higher than from k_1 due to the difference in frequencies

scattered wave, ie the difference signal, the signals obtained from operating the sending transducers individually, ie one at a time, were subtracted from the signal obtained when operating the two sending transducers simultaneously. The remaining signal will now be referred to as the difference signal. The difference signal, ie the scattered shear wave, resulting from the non-linear interaction of the two intercepting waves, is very low in amplitude due to: (1) the low conversion efficiency of the interaction between the two primary dilatational waves; (2) the inherent dispersion in the asphalt concrete (especially at high frequencies); and (3) the presence of the dominating, ie large amplitude, primary waves in the imperfect subtraction (a portion of the signal energy is lost in the conversion to the non-linear scattered wave; this leads to the signal resulting from the addition of the signals obtained when the dilatational transducers are operated individually being larger than the signal obtained when the two longitudinal transducers are operated simultaneously). To circumvent the low amplitude and maximise the ability to detect the scattered wave, the following steps were taken: (1) a high sample rate (50 MHz) was used in order to avoid trigger jitter, as suggested by Johnson and Shankland[13]; and (2) to mitigate the scattering effects, an average of 500 waveforms were collected. For each ageing level, 10 independent measurements were taken, which required removal of the three sensors, removal of the used couplant and subsequent application of new couplant and repositioning of the three sensors.
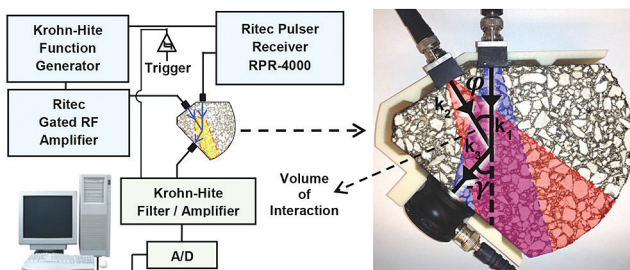
Experimental results

To ensure that the received wave is a scattered wave resulting from non-linear interaction between the primary waves within the specimen, the following selection criteria (proposed by Johnson and Shankland[12,13]) were used, ie amplitude, directionality, frequency, and time-of-arrival criteria.

Amplitude criterion

The amplitude of the non-linear signal must be proportional to the product of the amplitude of the primary dilatational waves. An experiment was conducted where it was observed that, as the voltage of the primary waves was increased, the amplitude of the non-linear signal also increased in a manner proportional to the amplitudes of the primary waves.

Directionality criterion

The propagating direction of the scattered wave must match the propagating direction predicted by theory. The geometry of the samples was selected using the virgin parameters shown in Table 1, which were calculated using Equations (1) and (2). As a result,

since the scattered non-linear wave was received, the directionality criterion was satisfied. Care was taken to ensure that even though the scattered wave angle γ for the aged specimens deviated from the virgin scattered wave angle, it still hit the transducer face.

Frequency criterion

The frequency of the non-linear scattered wave must closely match the frequency predicted by theory (*ie* $f_3 = f_1 - f_2$ at the appropriate value of f_2/f_1). The experimental set-up is based on virgin specimen properties; therefore, for each aged specimen, the frequency ratio at which interaction takes place will vary. To verify that the non-linear interaction took place at the predicted frequency ratio, the amplitude of the non-linear scattered wave was monitored as f_2 was swept and f_1 was held constant. The maximum amplitude of the non-linear scattered wave should occur when f_2 reaches the frequency where f_2/f_1 matches the ratio predicted by the theory (Figure 4).
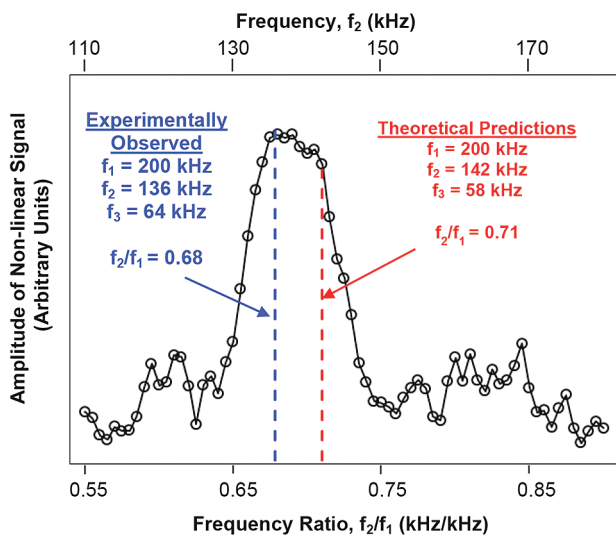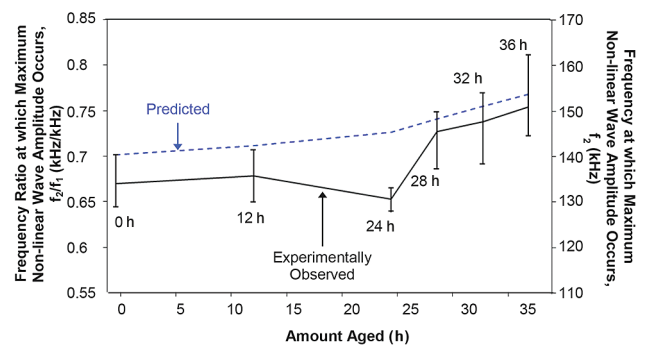

Figure 4. Experimentally-obtained amplitude of scattered shear wave, *ie* difference signal ($f_3 = f_1 - f_2$) as f_2 is swept from 110 kHz to 180 kHz (f_2 / f_1 = 0.55 to 0.90), while f_1 is held constant at 200 kHz. This analysis was performed for all specimens to obtain the data shown in Figure 5. The plot shown above is from the specimen oven-aged for 12 h and shown as a representative case. The dashed blue line represents the experimentally observed maximum and the dashed red line represents the theoretically predicted maximum, which was obtained using the experimentally-determined velocity data

The amplitude of the scattered wave may be measured by taking the fast Fourier transform (FFT) of the difference signal and recording the amplitude at the appropriate frequency (f_3) as f_2 was swept. Because the frequency of the non-linear scattered wave, *ie* f_3, changes with the amount of ageing of the specimen, instead of monitoring the f_3 amplitude via taking the FFT, a 4th-order Butterworth bandpass filter (30-90 kHz) was used. These filter limits ensured that the primary waves were filtered out as well as any other very low frequencies. Recording the difference wave amplitude over a finite band of frequencies (instead of a discrete point as it is done with the FFT method) ensured that even when f_3 changed (with ageing), the k_3 amplitude could still be monitored. It was verified that filtering with such a broadband filter and taking the FFT yielded nearly the same results for the amplitudes. For the different specimens, the non-linear frequencies were theoretically predicted to be: $(f_3)_0$ = 60 kHz; $(f_3)_{12}$ = 58 kHz; $(f_3)_{24}$ = 55 kHz; $(f_3)_{28}$ = 55.4 kHz; $(f_3)_{32}$ = 49.8 kHz; and $(f_3)_{36}$ = 47.2 kHz. Accordingly, for the chosen angle of interaction, the non-linear scattered wave should reach a maximum amplitude in the different specimens when: $(f_2/f_1)_0$ = 0.700; $(f_2/f_1)_{12}$ = 0.710; $(f_2/f_1)_{24}$ = 0.724; $(f_2/f_1)_{28}$ = 0.738; $(f_2/f_1)_{32}$ = 0.751; and $(f_2/f_1)_{36}$ = 0.764.

Data collected from the specimen aged 12 h is shown in Figure 4 as a representative example of the measured amplitude of the filtered difference signal (*ie* the non-linear scattered wave amplitude). As f_2 is swept, the non-linear wave amplitude reaches a maximum at f_2/f_1 = 0.68 (f_2 = 136 kHz). This is close ($\approx$ 4% difference) to the predicted value of f_2/f_1 = 0.71 (f_2 = 142 kHz). Theoretically, the amplitude of the received shear wave should have vanished when f_2 deviates from 136 kHz. The width of the amplitude curve shown in Figure 4 is probably due to wave scattering induced by the presence of the stochastic nature of the aggregate structure, which leads to different propagation paths of the wave energy and to the large interaction volume. The relatively large interaction volume and the stochastic nature of the asphalt concrete structure, *ie* aggregate-binder matrix, may have the effect of smearing the theoretical frequency ratio over a range of values centred about the theoretically-predicted value[21,22]. The theory assumes the test sample material to be isotropic and homogeneous and the two interacting longitudinal waves to be monochromatic.

The frequency ratios at which the maximum non-linear wave amplitudes occurred were recorded from all the measured data and plotted as a function of specimen ageing, as shown in Figure 5. The theoretical prediction was calculated using the mean of the measured velocities across 140 to 200 kHz and is denoted by the dashed line. The measured amplitudes of the scattered waves, corresponding to specimens with different ageing levels, reach a maximum close to the theoretical predictions (Table 2). The largest deviation from the theoretical prediction is for the case with 24 h of ageing (8.65% difference). Even though the 36 h had a low percent difference (1.18%), it had the highest standard deviation amongst the measurements. Although there is a statistically significant observable trend for the experimentally-observed frequency ratio as a function of ageing, it is not very sensitive, as the errors are high relative to the change with ageing.

Figure 5. Experimentally-observed frequency ratio at which the maximum non-linear scattered wave amplitude occurs. The theoretical amplitude was predicted (see Equations (1) and (2)) using the experimentally-obtained dilatational and shear velocities

Table 2. Experimentally-obtained and theoretically-predicted frequency ratios corresponding to the maximum amplitude of the scattered wave

Amount aged (h)	Experimentally recorded mean f_2/f_1	Standard deviation of experimental results (kHz)	Theoretical f_2/f_1	% difference
0	0.67	0.0200	0.70	4.61
12	0.68	0.0199	0.71	4.25
24	0.66	0.0080	0.724	8.65
28	0.73	0.0209	0.738	1.81
32	0.74	0.0275	0.751	1.01
36	0.75	0.0282	0.764	1.18

Time-of-arrival

Finally, the results were also viewed in the time domain to see whether a time separation existed. If the non-linear signal originated from the equipment, for example the function generator, amplifiers, transducers, etc, a separation in time between the primary waves and the difference signal should not exist. In other words, the non-linear signal inherent to instrumentation should arrive at the same time as the primary waves. However, when the difference signal is due to non-linear wave mixing within the asphalt concrete, a time separation should exist. The theoretical time of arrival of the difference signal, *ie* scattered wave, can be calculated assuming mean velocities, see Table 1, and a straight ray-path analysis.

As a representative example, Figure 6 shows a set of time domain records obtained from the asphalt concrete specimen aged for 36 h: (a) when both sending transducers are operating simultaneously; (b) when the sending transducers are operated individually, one at a time; and (c) the resulting scattered wave, *ie* the difference signal. The theoretical arrival time for the difference signal is found to be 81.5 µs, which matches closely ($\approx 8.8\%$ difference) with the observed arrival time of 74.9 µs. The stochastic nature of the asphalt concrete also causes disparities in the independent measurements, as even a slight variation in the placement of the transducers can alter the paths of the travelling waves.
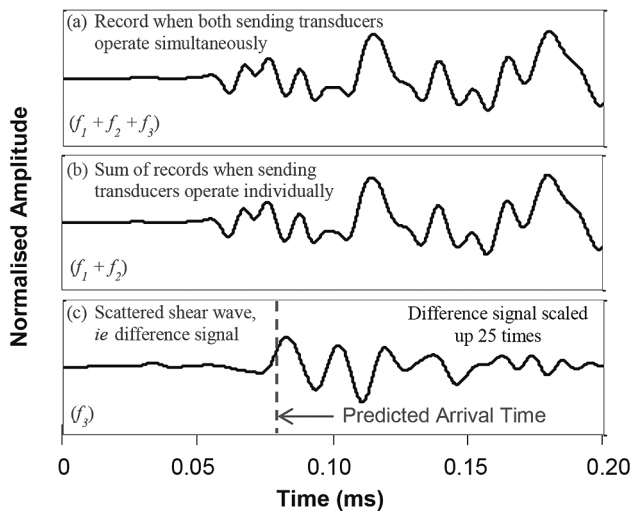
Figure 6. Time domain records required to obtain the non-linear scattered shear wave: (a) time record obtained when both sending transducers were operated simultaneously; (b) time record obtained when sending transducers were operated one at a time and the received waveforms added; and (c) non-linear scattered wave, *ie* the difference signal, obtained from subtracting the signals obtained from operating the sending transducers individually from the signal obtained when operating the two sending transducers simultaneously. The theoretically-predicted time of arrival for the difference signal matches closely (~8.8% difference) with the experimentally-observed time of arrival. The records are all normalised by the maximum amplitude of the record in (b). The difference signal was scaled up 25 times

The non-linear wave generation parameter, β

The non-linear scattered wave generation parameter, β, is an indicator of the conversion efficiency of the energy transferred from the primary waves, due to the non-collinear interaction, to produce the scattered non-linear wave. Figure 7 shows β normalised by β_0 (corresponding to the virgin mixture). The normalised parameter decreases with an increased amount of ageing until 24 h, when it begins to exponentially increase with increasing ageing. Similar trends have been observed in other experiments, such as fracture energy obtained via DC(T) tests, acoustic emission responses and dynamic modulus estimates via ultrasonic tests, in which the behaviour of asphalt concrete as a function of ageing has been studied[24-25].
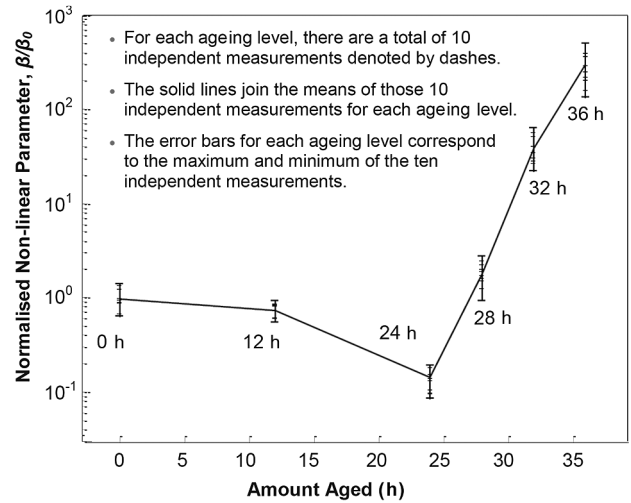
Figure 7. Normalised non-linear parameter, β, *versus* different levels of oven-ageing. The parameter β is normalised with the parameter, β₀, which corresponds to the virgin, *ie* unaged, mixture. For each ageing level, each of the ten independent measurements required removal of the three sensors, removal of the used couplant, and subsequent application of new couplant, and reposition of the three sensors

Due to the nature of the experimental set-up (parameters were based upon the material properties of the virgin specimen), the scattered wave will not always hit the received transducer in the best possible manner (*ie* normal incidence at the transducer centre), and the experimentally-measured beta parameter will be affected by this deviation. However, since the scattered wave hits the receiving transducer increasingly off-centre and at an angle as ageing increases, the measured values of β may increasingly be an underestimate of its true value as ageing increases. Figure 2 shows that the attenuation increases drastically with ageing. Should attenuation not be taken into account, the observable trend of the non-linear wave amplitude with respect to ageing shown in Figure 7 will be less pronounced. However, accounting for attenuation reveals that the asphalt concrete exhibits increasingly strong non-linear behaviour with ageing.

Conclusions

Asphalt concrete test samples were manufactured with various amounts of laboratory-induced oven ageing and assessed using a non-linear ultrasonic approach involving the mixing of two non-collinear dilatational waves. A non-linear scattered wave was observed as a result of the interaction of two intersecting waves in the asphalt concrete specimens, even though the material is highly attenuative and dispersive. Criteria were used to confirm that the detected scattered wave originated as a result of wave interaction in the asphalt concrete and not from non-linearities in the testing instrumentation. A non-linear wave generation parameter was defined to describe the conversion efficiency of energy from the primary waves into the non-linear scattered wave. By monitoring the non-linear wave generation parameter, it was observed that the non-linearities exhibited by the asphalt concrete decrease until about 24 h of ageing, after which the non-linear response increases exponentially with increasing ageing. The observed non-linear response has the potential of being used for the assessment of oxidative ageing of asphalt concrete, including durability and damage accumulation due to thermal and mechanical loading and other environmental conditions.

Acknowledgements

References

1. E R Brown, P S Kandhal, F L Roberts, Y R Kim, D Lee and T W Kennedy, Hot Mix Asphalt Materials, Mixture, Design, and Construction, Third Edition, NAPA Research and Education Foundation and NCAT, Maryland, 2009.

2. R Y Kim, Ed, Modelling of Asphalt Concrete, American Society of Civil Engineers Press, Chicago, and McGraw Hill, New York, 2009.

3. E T Hagos, 'The effects of ageing on binder properties of porous asphalt concrete', MS Thesis, Technical University of Delft, The Netherlands, 2008.

4. J H Cantrel and H Salama, 'Acoustoelastic characterisation of materials', International Materials Review, Vol 36, pp 125-145, 1991.

5. J H Cantrel and W T Yost, 'Non-linear ultrasonic characterisation of fatigue microstructures', International Journal of Fatigue, Vol 23, pp 487-490, 2001.

6. J Kim, J Jacobs, J Qu and J W Littles, 'Experimental characterisation of fatigue damage in nickel-based super alloy using non-linear ultrasonic waves', Journal of the Acoustical Society of America, Vol 120, pp 1266-1273, 2006.

7. C Pruell, J Kim, J Qu and L J Jacobs, 'Evaluation of plasticity-driven material damage using Lamb waves', Applied Physics Letters, Vol 91, 231911, 2007.

8. F D Murnaghan, Finite Deformation of an Elastic Solid, John Wiley & Sons Inc, New York, 1951.

9. L D Landau and E M Lifshitz, Theory of Elasticity, Second Edition, Pergamon Press, New York, 1970.

10. Z A Goldberg, 'Interaction of plane longitudinal and transverse elastic waves', Soviet Phys Acoust, Vol 6 (3), pp 306-310, 1960.

11. G L Jones and D R Kobett, 'Interaction of elastic waves in an isotropic solid', Journal of the Acoustical Society of America, Vol 35 (1), pp 5-10, 1963.

12. P A Johnson, T J Shankland, R J O'Connell and J N Albright, 'Non-linear generation of elastic waves in crystalline rock', Journal of Geophysical Research, Vol 92 (B5), pp 3597-3602, 1987.

13. P A Johnson and T J Shankland, 'Non-linear generation of elastic waves in granite and sandstone: continuous wave and travel time observations', Journal of Geophysical Research, Vol 94 (B12), pp 17729-17733, 1989.

14. L H Taylor and F R Rollins, 'Ultrasonic study of three-phonon interactions. I. Theory', Physical Review, Vol 136 (3A), pp A591-A596, 1964.

15. F R Rollins, L H Taylor and P H Todd, 'Ultrasonic study of three-phonon interactions. II. Experimental results', Physical Review, Vol 136 (3A), pp A597-A601, 1964.

16. A J Croxford, P D Wilcox, B W Drinkwater and P B Nagy, 'The use of non-collinear mixing for non-linear ultrasonic detection of plasticity and fatigue', Journal of the Acoustical Society of America, Vol 126 (5), pp EL117-EL122, 2009.

17. A Demcenko, R Akkerman, P B Nagy and R Loendersloot, 'Non-collinear wave mixing for non-linear ultrasonic detection of physical ageing in PVC', NDT&E International, Vol 49, pp 34-39, 2012.

18. F R Rollins, 'Phonon interactions and ultrasonic frequencies', Proceedings of the IEEE, Vol 53 (10), pp 1534-1539, 1965.

19. R W Dunham and H B Huntington, 'Ultrasonic beam mixing as a measure of the non-linear parameters of fused silica and single-crystal NaCl', Physical Review, Vol 2 (4), pp 1098-1107, 1970.

20. L K Zarembo and V A Krasilnikov, 'Non-linear phenomena in the propagation of elastic waves in solids', Soviet Physics, Vol 13, No 6, pp 778-797, 1970.

21. P B Nagy, 'Fatigue damage assessment by non-linear ultrasonic materials characterisation', Ultrasonics, Vol 36, pp 375-381, 1998.

22. P A Johnson, B Zinszner and P N J Rasolofosaon, 'Resonance and elastic non-linear phenomena in rock', Journal of Geophysical Research, Vol 101 (B5), pp 11553-11564, 1996.

23. M E McGovern and H Reis, 'Linear and non-linear characterisation of limestone rock using non-collinear ultrasonic wave mixing', Health Monitoring of Structural and Biological Systems 2014, edited by Tribikram Kundu, Proceedings of SPIE, Vol 9064, pp 906404-1-906404-15, 2014.

24. M E McGovern, B Behnia, W G Buttlar and H Reis, 'Characterisation of oxidative ageing in asphalt concrete – Part 1: Ultrasonic velocity and attenuation measurements and acoustic emission response under thermal cooling', Insight, Vol 55, No 11, pp 596-604, 2013.

25. M E McGovern, B Behnia, W G Buttlar and H Reis, 'Characterisation of oxidative ageing in asphalt concrete – Part 2: Complex moduli estimation', Insight, Vol 55, No 11, pp 605-609, 2013.

26. R A Guyer and P A Johnson, 'Non-linear mesoscopic elasticity: evidence for a new class of materials', Vol 52, No 4, Physics Today, American Institute of Physics, pp 30-36, 1999.

27. R A Guyer and P A Johnson, Non-Linear Mesoscopic Elasticity: The Complex Behaviour of Granular Media including Rocks and Soil, Wiley-VCH Verlag GmbH & Co KGaA, Weinheim, 2009. ISBN: 978 3 527 40703 3.

28. L A Ostrovsky and P A Johnson, 'Dynamic non-linear elasticity in geomaterials', Rivista del Nuovo Cimento, Vol 24, No 7, pp 1-46, 2001.

29. P A Johnson, B Zinszner and P N J Rasolofosaon, 'Resonance and elastic non-linear phenomena in rock', Journal of Geophysical Research, Vol 101, No B5, pp 11553-11564, 1996.

30. J D Ferry, Viscoelastic Properties of Polymers, John Wiley and Sons Inc, New York, 1961.

31. C Y Cheung and D Cebon, 'Deformation mechanisms of pure bitumen', Journal of Materials in Civil Engineering, pp 117-129, 1997.

32. C Y Cheung and D Cebon, 'Thin-film deformation behaviour of power-law creeping materials', Journal of Engineering Materials, pp 1138-1152, 1997.

33. S Kose, M Guler, H U Bahia and E Masad, 'Distribution of strains within hot-mix asphalt binders – applying imaging and finite element techniques', Transport Research Board, Paper No 00-1391, pp 21-27, 2000.

34. E Masad, N Somadevan, H U Bahia and S Kose, 'Modelling and experimental measurements of strain distribution in asphalt mixes', Journal of Transportation Engineering, Vol 127, No 6, pp 477-485, 2001.

35. E Masad, C-W Huang, G Airey and A Muliana, 'Non-linear viscoelastic analysis of unaged and aged asphalt binders', Construction and Building Materials, Vol 22, pp 2170-2179, 2008.

36. R Delgadillo, 'Non-linearity of asphalt binders and their relationship with asphalt mixture permanent deformation', PhD Thesis, University of Wiscosin, Madison, 2008.

37. M Marasteanu, A Zofka, M Turos, Xinjun Li, R Velasquez, Xue Li, W Buttlar, G Paulino, A Braham, E Dave, J Ojo, H Bahia, C Williams, J Bausano, A Gallistel and J McGraw, 'Investigation of low-temperature cracking in asphalt pavements', National Pooled Fund Study 776, Technical Report MN/RC 2007-43, Minnesota Department of Transportation, St Paul, Minnesota, 2007.

Estimation of oxidative ageing in asphalt concrete pavements using non-collinear wave mixing of critically-refracted longitudinal waves

M E McGovern, W G Buttlar and H Reis

A study using non-collinear ultrasonic wave mixing of subsurface longitudinal waves for the assessment of oxidative ageing in asphalt concrete samples with increasing levels of oven ageing is presented. The use of subsurface waves allows for non-destructive interrogation of bituminous structures when only one side of the test specimen is available for testing, such as asphalt concrete pavements. The following criteria were used to verify that the non-linear wave originated within the test specimen due to the non-collinear wave mixing, and not from non-linearities inherent to the testing instrumentation: (1) frequency; (2) amplitude; (3) propagation direction; and (4) time-of-flight separation. It was observed that the non-linear response of the asphalt concrete mixtures decreases with ageing until about 24 h of oven ageing, after which it increases exponentially with ageing. These results correlated well with the results from previous studies, demonstrating the effectiveness of this technique. Potential applications of the technique for the health monitoring of asphalt pavement surfaces are presented.

1. Introduction

Asphalt concrete (*ie* asphalt) pavements are continuously subjected to environmental and loading conditions, which can seriously degrade their structural integrity. Oxidative ageing plays a major role in the degradation[1,2] and it occurs in a non-uniform manner, *ie* the top exposed portion of the pavement is significantly more degraded than the bottom, which is protected by the upper layers of the pavement. As a result, the pavement becomes a graded structure through its thickness, where the top layer is the most oxidised. There exists the need for a non-destructive technique to assess the level of oxidative ageing that the pavement has undergone. In a previous study[3], a technique involving the use of non-collinear wave mixing of bulk ultrasonic waves was presented as a means to non-destructively evaluate the oxidative ageing in asphalt concrete. It was demonstrated that the technique can be used successfully to estimate the amount of oxidative ageing by means of a non-linear wave generation parameter. However, the technique requires that the test be performed on specimens cut to a geometry dictated by the ideal sensor placement (*ie* normal incidence) for through-transmission wave propagation. For use in the field, this would require removal of a portion of the pavement for testing. To be truly non-destructive, the method should be such that it can be performed on the pavement requiring access to only one side, *ie* the pavement surface. Since most of the damage is located at the top layer, a non-destructive technique to evaluate the surface and subsurface (*ie* directly below the surface in the bulk of the medium) of pavements would prove useful in assessing the level of oxidative damage and may aid the decision making process for the maintenance and rehabilitation of pavements.

The non-linear behaviour of a material (for example non-linear constitutive relationship, micro-cracks, etc) leads to non-linear distortion of the ultrasonic waves as they propagate through the medium due to the presence of higher-order terms in the non-linear acoustic wave equation[4-21]. In the case of multiple overlapping waves, interaction between the waves may take place. The non-collinear ultrasonic wave-mixing technique[11-21] involves transmitting two monochromatic waves into a medium simultaneously so that they intersect. These two intersecting waves are termed the primary waves and may be longitudinal or shear waves. If the material exhibits non-linear behaviour, when these two primary waves cross paths at particular angles they can interact to produce a third wave, termed a 'scattered non-linear wave'. For a strong scattered wave to occur, resonance and polarisation conditions must also be met. The resultant scattered non-linear wave may be of a different type (*ie* longitudinal or shear), propagate in a different direction and have a different frequency than the two primary waves. This interaction does not take place in linear materials, where the resulting wave field is simply the linear superposition of the two waves. McGovern *et al*[3] provide a brief literature review on the use of non-collinear wave mixing.

Asphalt concrete has been shown in a previous study[3] to exhibit non-linear behaviour at room temperature. The non-linear behaviour can arise from a multitude of sources, including its brick-and-mortar structure (asphalt concrete belongs to a class of materials that have non-linear mesoscopic elasticity[22,23]) and the presence of micro-cracks and air voids. Furthermore, the two basic constituents of asphalt concrete, crushed stone and asphalt binder (*ie* bitumen), also behave non-linearly[24-34]. In the case of asphalt binder (*ie* bitumen), which is a naturally-occurring, refined and

● *Submitted 06.07.14 / Accepted 13.10.14*

Professor Henrique Reis* and graduate student Megan E McGovern are affiliated with the Department of Industrial and Enterprise Systems Engineering, University of Illinois at Urbana-Champaign, 117 Transportation Building, 104 S Mathews Avenue, Urbana, Illinois 61801, USA.

Professor William G Buttlar is affiliated with the Department of Civil and Environmental Engineering, University of Illinois at Urbana-Champaign, 205 N Mathews Avenue, Urbana, Illinois 61801, USA.

*Corresponding author. Tel: +1 217 333 1228; Fax: +1 217 244 5705. Email: h-reis@uiuc.edu

processed material, non-linear viscoelastic behaviour arises due to its complex chemical morphology. This includes varying proportions of asphaltenes (rigid, brittle, elastic component), resins (viscous component, contributing to temperature- and stress-dependency) and oils (fluid, possibly volatile, low-viscosity component)[1]. As asphalt concrete is subjected to oxidative ageing, the non-linearities in the material change with the amount of ageing. For instance, the lower molecular weight or volatile components present in freshly placed asphalt can dissipate with time, or 'volatilise', rendering the material stiffer and changing its degree of non-linearity. It has already been shown[3] that the non-linear behaviour (defined by a non-linear wave generation parameter, which represents the amount of primary wave energy converted to the non-linear scattered wave) decreases as the material is aged, until it reaches a critical amount of ageing, after which the non-linear behaviour increases exponentially. In summary, as the asphalt concrete is subjected to oxidative ageing, the stiffness of the binder increases with the volatilisation of low molecular weight fractions, and at progressively higher levels of ageing the adhesion between the aggregates, fines and binder decreases, yielding an increase in the micro-flaw population in the mastic and at the mastic-aggregate interfaces[35]. It appears that the evolution of ageing in asphalt concrete first leads to an increase in linearity (volatilisation of oils and resins, lowering stress dependency of response), followed by a progression towards non-linearity (an increase in micro-flaw population through over-stiffening and subsequent volumetric contraction of the binder around rigid aggregates and reduced adhesion).

Critically-refracted longitudinal (or subsurface longitudinal) waves are longitudinal bulk waves that travel nearly parallel to the free surface of a bulk medium[36]. Subsurface waves have the advantage that they propagate in the bulk of the medium (ie right below the surface) and can still be detected at the surface. These waves can be generated by employing angle wedge transducers set to an angle close to or equal to the critically-refracted angle governed by Snell's Law[37]. Prior to 1979, others[38-40] had observed what at times was termed the 'fast surface wave', which travelled at the speed of a bulk wave and arose when the incident angle was set above the critical angle. The first theoretical studies on the beam pattern of longitudinal subsurface waves were performed by Basatskaya and Ermolov[41] in 1979. They also studied the resulting beam pattern when the incident angle was set slightly above and below the first critical angle and made recommendations on how to utilise these waves to best inspect defects in materials. In 1988, Pilarski and Rose[42] demonstrated the feasibility of using subsurface longitudinal waves to characterise materials. Langenberg et al[43] were the first to perform a numerical study of the wave field of subsurface longitudinal waves in 1990. In 1991, Junghans and Bray[44] experimentally characterised the subsurface longitudinal wave beam profile generated by high-angle longitudinal wave probes. From 1996 to 2001, a number of studies utilising subsurface waves to measure residual stresses in various mechanical components and materials were also performed by Bray and others[45-47] using acoustoelastic theory. Most recently, in 2013, Chaki and Demouveau[48] experimentally and numerically characterised the beam profile of the longitudinal subsurface wave. The results from their study revealed that the displacement amplitude of the critically-refracted longitudinal wave reaches a maximum at an incident angle slightly larger than the critical angle.

In this study, the non-linear behaviour of asphalt concrete as a function of laboratory-induced oxidative ageing is investigated using a non-collinear wave mixing of two critically-refracted longitudinal waves, and employing a methodology used by Johnson and Shankland[12,13]. Results are also compared with those from a previous study[3] to demonstrate the feasibility of using the non-collinear wave mixing method in conjunction with critically-refracted longitudinal waves to characterise the oxidative ageing of bituminous infrastructure when there is only access to one side of the test specimen, for example the pavement surface.

2. Specimen preparation and linear characterisation

Six asphalt concrete (ie asphalt) specimens were prepared with the same mixture of 9.5 mm nominal maximum aggregate size and a target asphalt binder (ie bitumen) content of 5.9% by weight of the total mixture. The binder used was PG 64-22 and the aggregates were from four different stockpiles, including: 65% coarse aggregate (CM16); 23% manufactured sand (FM20); 10.5% natural sand (FM02); and 1.5% mineral filler (MF). Mixing was carried out using a standard bucket mixing procedure at a temperature of 155ºC. The mixtures were then subjected to oxidative ageing by placing them in an oven at 135ºC. Each mixture was aged a different amount of time: 0, 12, 24, 28, 32 and 36 h. Beyond 36 h of oven ageing using this protocol, the surfaces of the specimens become very rough and irregular, preventing ultrasonic testing due to poor coupling conditions between the sensor and specimen. Thus, no specimens were aged past 36 h. This is believed to be a reasonable upper limit on lab conditioning, as 36 h of oven ageing at 135ºC was found to represent a very severe ageing condition in a study where the fracture properties of lab-aged specimens were compared to field-aged specimens[49]. In addition, an oven ageing level of 24 h at 135ºC was found to represent the field ageing threshold where surface cracking begins to occur and rapidly increases with age.

The laboratory-prepared mixtures used in this study were hand-stirred every 12 h to create a more uniform exposure of the mixture to oxygen (ie a more uniform ageing process). Six cylindrical specimens (180 mm height and 150 mm diameter) were created by compacting the aged mixtures with a servo-controlled gyratory compactor (IPC Servopac) at a temperature of 135ºC. Each cylinder was cut to obtain a rectangular prism with dimensions 155 × 175 × 50 mm. Figure 1 shows the geometry and dimensions of the extracted test samples from each of the cylindrical compacted gyratory specimens.
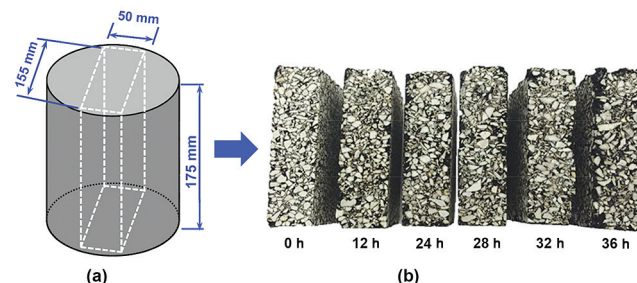

Figure 1. Test specimens: (a) gyratory compacted and (b) test specimens with different levels of oven ageing. See Figure 3

Six asphalt specimens constructed using the same mixture design and levels of oxidative ageing via the process described above were characterised using linear ultrasonics in a previous study[50,51]. In that study, the ultrasonic phase velocities and attenuations for

longitudinal and shear waves were determined as a function of frequency. For more details on the linear characterisation, please refer to McGovern *et al*[50,51].

3. Critically-refracted longitudinal (subsurface) wave

Critically-refracted longitudinal waves are often referred to as subsurface longitudinal waves. These two names will be used interchangeably in this paper. Longitudinal subsurface waves have the properties of a bulk longitudinal wave, while still being able to be detected at the surface. In contrast to surface waves, subsurface longitudinal waves have the advantage that they are insensitive to surface defects and exist well into the bulk of the material[36]. Thus, subsurface waves can be employed to characterise material properties right below the surface where the most ageing in the asphalt concrete pavement is present. Critically-refracted longitudinal waves are generated at the first critical angle, governed by Snell's Law[37]:

$$\frac{\sin \theta_{inc}}{c_i} = \frac{\sin \theta_L}{c_L} \quad \text{.................................... (1)}$$

where c_L and c_i are the longitudinal velocities of the asphalt medium and incident wedge material, respectively, θ_{inc} is the incident angle and $\theta_L = 90^o$ (*ie* $\sin \theta_L = 1$) for the case of critical refraction, refer to Figure 2.
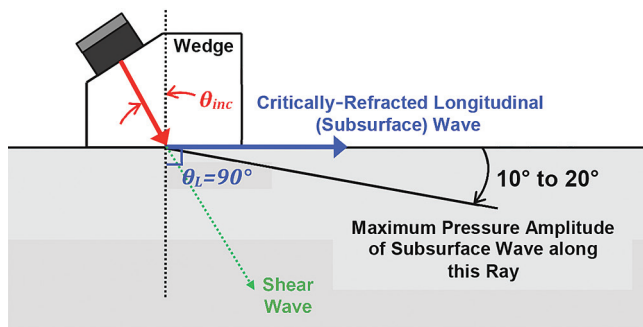
Figure 2. Schematic diagram of transmitted signals through angle wedges with an incident angle equal to the first critical angle to generate the critically-refracted longitudinal (subsurface) waves. The main lobe has a maximum energy at the surface and maximum pressure amplitude (*ie* displacement) along the ray 10° to 20° below the surface

The beam pattern of longitudinal subsurface waves was theoretically studied by Basatskaya and Ermolov[41]. They found that the beam pattern of the subsurface wave is comprised of many lobes. At the critically-refracted angle, most of the energy in the main lobe is contained at the surface, but the maximum displacement occurs at an angle below the surface (for example ≈18° below the surface for steel). Note that the portion of the wave on the free surface is not purely longitudinal due to the stress-free boundary conditions at the surface. When the incident angle is slightly larger than the critical angle, the main lobe becomes narrower and the maximum displacement moves closer to the surface. As the angle is further increased beyond the critical angle, the side lobes start to dominate in amplitude over the main lobe. For incident angles slightly smaller than the critical angle, the main lobe moves away from the surface. Chaki *et al*[48] verified these results via a numerical study and found that the energy of the subsurface wave is maximum at the surface for an incident angle of about 1° greater than the first critical angle.

4. Assessment of oxidative ageing using non-collinear wave mixing

Consider two monochromatic, plane, elastic waves travelling in directions k_1 and k_2 with frequencies f_1 and f_2, respectively. These two waves, termed the primary waves, can be longitudinal or shear polarised in or out of the k_1-k_2 plane. In the presence of non-linearities (for example non-linear elastic medium, cracks, etc), these two primary waves can interact to produce a third wave, *ie* a scattered wave, travelling in the direction k_3 with frequency f_3. The polarisation of the resultant scattered wave (often referred to as the non-linear wave) will depend on the polarisations of the two primary waves. The conditions for which the two primary waves interact to produce a strong scattered wave were derived by Jones and Kobett[11]. A non-linear scattered wave results from the interaction of the two primary waves if resonance and polarisation conditions are met[11]. There are nine possible interaction cases of bulk waves for which these conditions are met. In this study, the case where two longitudinal waves interact to produce a scattered shear wave is utilised. The resonance and polarisation conditions for this case are met when the following two equations are satisfied:

$$\cos[\varphi] = \left(\frac{c_l}{c_t}\right)^2 \left[1 - \frac{1}{2}\frac{f_1}{f_2}\left(1 - \frac{c_t^2}{c_l^2}\right)\left(\frac{f_2^2}{f_1^2} + 1\right)\right] \text{............ (2)}$$

$$\tan[\gamma] = \frac{-f_2 \sin[\varphi]}{f_1 - f_2 \cos[\varphi]} \quad \text{.............................. (3)}$$

where c_i and c_t denote the longitudinal and shear wave velocities of the medium, respectively, f_1 and f_2 are the frequencies of the two primary waves, φ is the interaction angle between k_1 and k_2, and γ is the angle between k_1 and k_3. The resulting scattered shear wave is polarised in the k_1-k_2 plane. The frequency ratio f_2/f_1, interaction angle φ and scattered wave angle γ are all interdependent quantities. In other words, once one parameter is chosen (for example φ), the other two (for example γ and f_2/f_1) are set.

Selection criteria, as proposed by Johnson and Shankland[12,13], can be used to ensure that the measured non-linearities occur as a result of the interaction between the two primary waves and not as a result of possible non-linearities of the testing equipment. These criteria are: (1) frequency – the frequency of the observed scattered wave must match the frequency predicted by theory; (2) amplitude – the amplitude of the scattered wave must be proportional to the product of the amplitudes of the two interacting primary waves; and (3) directionality – the propagation direction of the scattered wave must match that predicted by the theory. In addition, the time-of-arrival of the scattered wave should agree with its predicted theoretical arrival time.

4.1 Choosing the experimental set-up

For the placement of the transducers/wedges, appropriate angles must be chosen (using Equations (2) and (3)) such that wave interaction occurs resulting in a scattered wave. For many materials, this task is relatively straightforward: once the linear ultrasonic material properties (*ie* longitudinal and shear velocities/attenuations) have been characterised, one parameter can be chosen (for example φ), subsequently fixing the other two (for example γ and f_2/f_1). Then, the specimen dimensions can be selected and the sensors positioned appropriately. For this study, the linear ultrasonic properties of the asphalt specimens vary as a function of the oxidative ageing level. If the ultimate goal of this technique is to be used as a means to characterise the level of oxidative ageing, then

the testing set-up should be one which will work across all aged specimens. Here, to assess the specimen ageing, a testing set-up is chosen based on the virgin specimen parameters. Determining a final testing set-up is an iterative process, where the goal is to find one testing set-up that meets the conditions outlined below.

Incident angle, θ_{inc}

The incident angle of the angle wedges should be chosen such that the two subsurface longitudinal waves, which propagate nearly parallel to the free surface, are generated in the specimen. Based on the literature[41,48], the best incident angle to achieve a strong longitudinal subsurface wave is at about 1° greater than the first critically-refracted angle. Table 1 lists the first critical angle for each aged specimen, which were found using Equation (1).

Interaction angle, φ

The interaction angle should be the same for all six specimens (0 to 36 h of ageing). This will result in different f_2/f_1 and γ for each level of ageing; therefore, the interaction angle should be chosen based on its effects on the scattered wave angle and frequency ratio. Furthermore, the size of the angle wedges (40×45 mm) limits how small the interaction angle can be while still maintaining a minimal propagation distance of the two primary waves (to limit attenuation effects). This should be taken into consideration when choosing the interaction angle.

Primary and scattered wave frequencies

The frequencies should be chosen such that the primary waves propagate with minimal distortion (due to scattering and attenuation) and generate a non-linear scattered wave with the same characteristics. Scattering effects can be mitigated by choosing the frequencies such that the wavelength is larger than the maximum aggregate size (9.5 mm). Attenuation effects can be lessened by choosing frequencies below which the attenuation becomes too high to receive a discernible signal. The frequencies should also be chosen such that the resulting scattered wave frequency (f_3) is sufficiently separated from the two primary wave frequencies (f_1 and f_2), so that they can be easily separated in the frequency domain.

Furthermore, f_1 and f_2 should be chosen such that their velocities are similar, to match with the theory presented in Equations (1) and (2) (which assumes that k_1 (f_1) and k_2 (f_2) have the same velocity). Based on these considerations, the primary waves should be chosen within a frequency range of 100 kHz to 200 kHz, and the resulting scattered shear wave should be within a frequency range of 50 kHz to 110 kHz. McGovern et al[3] provide a more detailed discussion on the process used to establish the frequencies used for this particular set of aged asphalt concrete samples.

Scattered wave angle, γ

The transducer/wedge placement is the same for all specimens and is chosen based on the parameters of the virgin material, ie unaged specimen. The amount of deviation between the angle for which the receiving transducer is placed and the actual scattered angles will affect how well the non-linear scattered wave is received. For this reason, a case should be found that minimises the difference in scattered wave angles between the virgin specimen and the other aged specimens, so that even if the receiving transducer is not oriented in the ideal location it can still receive the non-linear scattered wave. The face of the receiving transducer used in this study is quite large (diameter ≈ 44 mm), which allows for the scattered wave angle for the aged specimens to deviate from the virgin scattered wave angle and still strike the transducer face.

Propagation distances and specimen dimensions

Asphalt concrete is a highly attenuative material, which greatly diminishes the amplitudes of the primary and scattered waves as they propagate through the specimen. This attenuation loss should be minimised by minimising the distance through which the wave propagates to ensure that the scattered non-linear wave can be detected by the receiver. The propagation distances should be at least one wavelength long, such that the waves are stabilised by the time they interact. For simplicity, k_1 and k_2 can be chosen to have the same propagation distances. The specimens' dimensions satisfied the constraints imposed by these propagation distances.

Table 1. Average dilatational and shear velocities (between 120-200 kHz), corresponding frequency ratio f_2/f_1 and scattered wave angle γ for an interaction angle φ of 47°. For time-of-flight calculations, the shear velocity at the scattered wave frequency f_3 is also presented

Amount aged (h)	Average dilatational velocity (120 - 200 kHz) c_L (m/s)	Average shear velocity (120 - 200 kHz) c_S (m/s)	First critical incident angle* $\theta_{cr} = \theta_{inc} - 1°$ (°)	Velocity ratio c_S/c_L	Interaction angle φ (°)	Frequency ratio f_2/f_1	Angle of scattered wave γ (°)	Scattered wave frequency $f_3 = f_1 - f_2$ (kHz)	Shear velocity at f_3 c_S (m/s)
0	3554	1943	50	0.547		0.600	−37***	80.0	1510
12	3792	2007	46	0.529		0.613	−38	77.4	1467
24	4007	2030	43	0.507	47***	0.630	−39	74.0	1482
28	3284	1576	56	0.480		0.650	−40	70.0	1108
32	2780	1282	78**	0.461		0.664	−42	67.2	969
36	2861	1240	72	0.433		0.685	−43	63.0	786

* The wedges were set to have an incident angle 1° greater than the critically-refracted angle based on the work carried out by Chaki et al[48].

** An incident angle of 79° was too large an angle to be achieved with the angle wedges, so an incident angle of 76° was used instead.
  Note: this angle is within error of the angle predicted by velocity measurements.

*** For all aged specimens, the sensors were positioned to the angles determined for the virgin specimen. Care was taken to find a case where the difference in the scattered wave angle was minimal (ie $\gamma_{36h} - \gamma_{Virgin} = 6°$) so that the receiving transducer could detect the scattered wave for all specimens. Keeping the angles constant causes the frequency ratio at which the non-linear wave interaction occurs to shift.

4.2 The non-linear wave generation parameter, β

A normalised non-linear generation parameter $\dfrac{\beta_{age}}{\beta_0}$ was previously introduced[3] to characterise the non-linearities in the asphalt concrete with respect to ageing. The formulation of the non-linear wave generation parameter is such that material attenuation is taken into consideration. Thus, it reflects a measure of the material's inherent non-linear behaviour as it represents the conversion efficiency of the energy transferred from the two primary waves interacting to produce the scattered non-linear wave.

The amplitude of the scattered wave is proportional to the product of the amplitudes of the two primary waves at the time of interaction[14,15]. Assuming perfect couplant conditions and accounting for the attenuation suffered by the primary and scattered waves, the received amplitude of the scattered non-linear wave is described by the following equation:

$$A_{age}^{(k_3)} = \beta_{age} A_{sent}^{(k_1)} A_{sent}^{(k2)} \exp\left[-\left(\alpha_{age}^{(k_1)} + \alpha_{age}^{(k_2)}\right)D_{k_1 k_2}\right]\exp\left[-\alpha_{age}^{(k_3)}D_{k_3}\right] \ ... (4)$$

where:

$\beta_{age} \equiv$ Conversion efficiency

$A_{sent}^{(k_n)} \equiv$ Transmitted amplitude of k_n (Volts)

$\alpha_{age}^{(k_n)} \equiv$ Attenuation coefficient of $k_n \left(\dfrac{Np}{m}\right)$

$D_{kn} \equiv$ Propagation distance of k_n (m).

The conversion efficiency β_{age} is a dimensionless parameter that accounts for the fraction of the interacting waves that is converted to the scattered wave for a particular ageing level. Straight ray paths can be assumed for the propagation distances. The attenuation coefficients for asphalt concrete were measured and presented in McGovern et al[50,51] for each ageing level. It was shown[50] that the attenuation coefficient increases drastically with the amount of ageing. Accounting for the attenuation in a highly attenuative material (for example asphalt concrete) is very important. If attenuation is not accounted for, it affects the observable trend of the non-linear wave amplitude with respect to ageing. Of course, in doing so, one must be certain that a non-linear scattered wave is indeed detected by using the selection criteria, which will be outlined in a subsequent section. Thus, the amplitude can then be normalised by the attenuation and denoted by:

$$A_{age}^{*(k_3)} = \dfrac{A_{age}^{(k_3)}}{\exp\left[-\left(\alpha^{(k_1)} + \alpha^{(k_2)}\right)D_{k_1 k_2}\right]\exp\left[-\alpha^{(k_3)}D_{k_3}\right]} = \beta_{age} A_{sent}^{(k_1)} A_{sent}^{(k_2)} \ .... (5)$$

The transmitted amplitudes of the primary waves ($A_{sent}^{(k_1)}$ and $A_{sent}^{(k_2)}$) will be the same for all tests performed if the changes in the couplant conditions between testing set-ups are negligible. Thus, using Equations (4) and (5), β_{age} can be normalised by the conversion efficiency parameter for the virgin material, β_0, to characterise ageing:

$$\dfrac{\beta_{age}}{\beta_0} = \dfrac{A_{age}^{*(k_3)}}{A_0^{*(k_3)}} \ .... (6)$$

The parameter $\dfrac{\beta_{age}}{\beta_0}$ in Equation (6) is the normalised non-linear wave generation parameter and it characterises the amount of ageing with respect to the virgin (unaged) sample.

5. Experimental description

Figure 3 shows a schematic representation of the experimental set-up. Two longitudinal transducers (Panametrics V413, centre

frequency 500 kHz) were mounted on plastic variable angle wedges. The wedges were set at an angle such that the incident angle was 1º greater than the critically-refracted angle for each specimen in order to generate subsurface longitudinal waves. The angle was measured using a digital protractor with an accuracy of 1º. Table 1 shows the appropriate incident angles for each specimen. The wedges were positioned such that the interaction angle between the two primary waves was $\varphi = 47º$ and both k_1 and k_2 propagated a distance of 8.2 cm (from the centre of each angle wedge to the centre of the volume of interaction) before interacting. The scattered non-linear wave propagated a distance of 4 cm (from the centre of the volume of interaction to the centre of the receiving transducer face) and was received by a third longitudinal transducer (Panametrics V1011, centre frequency 100 kHz), which was mounted using normal incidence on the surface in the path of k_3 ($\gamma = -37º$ with respect to k_1). The placement of the sending/receiving transducers was based on the angles (φ and γ) calculated for the virgin specimen properties. The same transducer placement was used for all six specimens. Table 1 contains the theoretical values for all aged specimens. The velocities used to calculate the velocity ratio were computed using the mean velocities across 120-200 kHz. A plastic template was created using a 3D printer to ensure reproducibility of the transducer placement between tests.
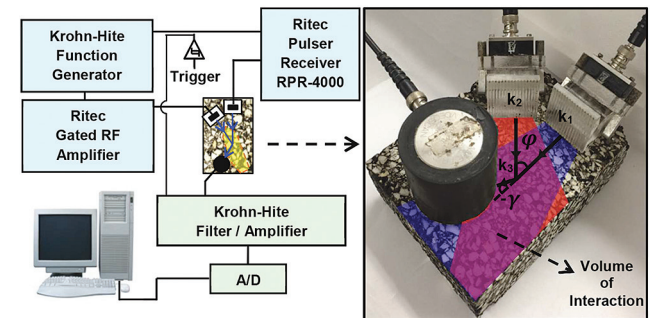

Figure 3. Schematic diagram of the ultrasonic data collection system illustrating the angle of interaction of the two primary longitudinal waves and the location of the receiving longitudinal transducer to receive the generated scattered shear wave. The blue and red regions denote the areas of signals k_1 and k_2, respectively, due to beam spread. The region where they overlap is the volume of interaction. Note that the beam spread from k_2 is slightly higher than k_1 due to the difference in frequencies

A 15-cycle sinusoidal signal with a frequency of $f_1 = 200$ kHz was generated and amplified with a pulser-receiver (Ritec RPR 4000) and sent to one of the angle wedge mounted longitudinal transducers. An 8-cycle sinusoidal wave was generated by a function generator (Krohn-Hite Model 5920) and amplified by a gated amplifier (Ritec GA-2500A). This signal was swept from $f_2 = 100$ kHz to 180 kHz in 1 kHz increments and sent to the other angle wedge mounted longitudinal transducer. The number of cycles in the tonebursts was chosen to ensure the intersection of the primary longitudinal waves in the specimen. The received scattered shear wave was filtered by a 4-pole Butterworth filter (Krohn-Hite model 3945), amplified and sent to the computer for data acquisition.

The generated scattered non-linear wave is very small in amplitude due to the low conversion efficiency of the primary wave energy used to generate the scattered wave[14,15] and the high attenuation due to scattering in the asphalt concrete. Furthermore, the time-of-flight is such that much of the scattered non-linear wave is superimposed with the primary waves. To extract the

non-linear scattered wave, the following steps were taken during data acquisition: (1) data was collected while the two transducers were operated simultaneously; (2) data was collected while one transducer was individually operated; and (3) data was collected while the other transducer was individually operated. The non-linear signal was obtained by subtracting the signals from steps (2) and (3) from the signal obtained in step (1). The remaining signal (*ie* the difference signal) should be the non-linear scattered wave; however, the subtraction is imperfect, mainly because a portion of the energy from the primary waves is used to create the scattered non-linear wave. Therefore, the signal obtained from simultaneous operation of the two sending transducers has an amplitude slightly lower than the sum of the signals obtained when the transducers were operated individually. As a result of the imperfect subtraction, a portion of the primary waves is in the subtracted signal. This was addressed by applying a filter to the difference signal to filter out much of the primary wave contribution.

To maximise the ability to detect the scattered wave and to mitigate scattering effects, an average of 500 waveforms was taken. To avoid trigger jitter, a high sample rate (50 MHz) was used[12,13]. Ten independent measurements were taken for each specimen. Each independent measurement consisted of removing the sensors/ wedges and couplant, applying new couplant and placing the sensors/wedge back into position.

6. Experimental results

The selection criteria proposed by Johnson and Shankland[12,13] were used to verify that the non-linear wave was generated as a result of the interaction between the two primary waves and not from the testing apparatus. The collected data was only used after it satisfied these selection criteria, as described below.

To verify that the amplitude of the non-linear scattered wave was proportional to the product of the amplitudes of the two primary waves, a small experiment was conducted. It was observed that as the voltage of the primary waves was increased, the amplitude of the non-linear signal also increased in a manner proportional to the amplitudes of the primary waves. The propagation direction of the scattered wave (*ie* γ) must match the propagation direction predicted by the theory. The placement of the sensors was selected using the virgin parameters shown in Table 1 (using Equations (2) and (3)), but care was taken to minimise the difference between the virgin scattered angle γ and the scattered angle for the other ageing levels to ensure that the receiving transducer was in the path of the non-linear scattered wave for all the specimens. As a result, since the scattered non-linear wave was received, the directionality criterion was satisfied.

To ensure that the frequency of the scattered wave matches that predicted by the theory (*ie* $f_3 = f_1 - f_2$ at the appropriate f_2/f_1), the amplitude of the non-linear scattered wave was monitored as f_2 was swept and f_1 was held constant. The maximum amplitude of the non-linear scattered wave should occur when f_2 reaches the frequency where f_2/f_1 matches the ratio predicted by the theory. The amplitude was measured by passing the difference signal through a bandpass (30-90 kHz) filter as f_2 was swept. The selected bandpass frequency range ensured that the primary waves were filtered out as well as any very low frequencies. Alternatively, the amplitude of the scattered wave could have been measured by taking the fast Fourier transform (FFT) of the difference signal and recording the amplitude at the appropriate frequency (f_3) as f_2 was swept; however, this would require f_3 to be the same across all aged specimens. Since the experimental set-up was such that the interaction angle

was held constant (*ie* based on virgin specimen properties), the predicted frequency ratio at which interaction occurred varied. Recording the difference wave amplitude over a finite band of frequencies (instead of a discrete point as is the case with the FFT method) ensured that even when f_3 changed (with ageing), the k_3 amplitude could still be monitored. It was verified that filtering with such a broadband filter and taking the FFT yielded nearly the same results for the amplitudes. For the experimental set-up, the non-linear frequencies for all six specimens were theoretically predicted to be: $(f_3)_0 = 80$ kHz, $(f_3)_{12} = 77.4$ kHz, $(f_3)_{24} = 74.0$ kHz, $(f_3)_{28} = 70.0$ kHz, $(f_3)_{32} = 67.2$ kHz and $(f_3)_{36} = 63.0$ kHz. Accordingly, the non-linear scattered wave was predicted to reach a maximum amplitude when: $(f_2/f_1)_0 = 0.600$, $(f_2/f_1)_{12} = 0.613$, $(f_2/f_1)_{24} = 0.630$, $(f_2/f_1)_{28} = 0.650$, $(f_2/f_1)_{32} = 0.664$ and $(f_2/f_1)_{36} = 0.685$.

Figure 4 shows a representative example of the recorded non-linear scattered wave amplitude as f_2 was swept. The example shown is from the virgin specimen. The amplitude was predicted to reach a maximum when $f_2/f_1 = 0.6$ (*ie* $f_2 = 120$ kHz). The experimental data shows that the amplitude actually reached a peak at $f_2/f_1 = 0.575$ (*ie* $f_2 = 115$ kHz). The theoretical and experimental values are quite close with only a 4.1% difference (*ie* 5 kHz). Theoretically, the non-linear amplitude should only occur for a particular (*ie* theoretically predicted) frequency ratio. In reality, the non-linear amplitude plotted as a function of the frequency ratio has a finite width. This width can be attributed to the large interaction volume (due to beam spread) and to wave scattering caused by the stochastic nature of the aggregate structure, which leads to different propagation paths of the wave energy. The theory assumes that the two interacting longitudinal waves are monochromatic and that the test sample material is isotropic and homogeneous. The deviation of the real testing conditions from theory has the effect that the non-linear wave amplitude is spread over a range of values centred about the theoretically-predicted frequency ratio. Frequency ratios at which the maximum amplitudes of the non-linear signal occurred are plotted as a function of ageing in Figure 5. The predicted values
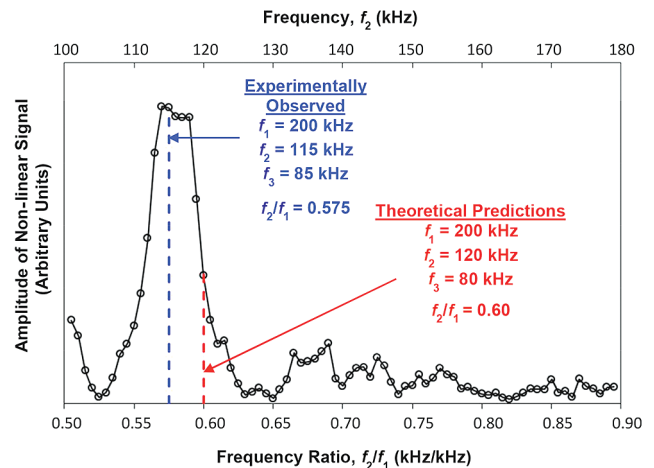
Figure 4. Experimentally-obtained amplitude of scattered shear wave, *ie* difference signal, $(f_3 = f_1 - f_2)$ as f_2 is swept from 100 kHz to 180 kHz $(f_2/f_1 = 0.50$ to $0.90)$ while f_1 is held constant at 200 kHz. This analysis was performed for all specimens to obtain the data shown in Figures 5 and 7. The plot shown above is from the specimen oven aged for 12 h and shown as a representative case. The dashed blue line represents the experimentally-observed maximum and the dashed red line represents the theoretically-predicted maximum, which was obtained using the experimentally-determined velocity data

Figure 5. Experimentally-observed frequency ratio at which the maximum non-linear scattered wave amplitude occurs. The theoretical values were predicted (see Equations (2) and (3)) using the experimentally-obtained dilatational and shear velocities

were calculated using the mean velocities (120 kHz to 200 kHz) and are denoted in Figure 5 by the dashed line. The experimentally-observed frequency ratios closely match the theoretical predictions, as shown in Table 2. The largest deviation from the theoretical prediction is for 24 h ($\approx$12% error). This larger deviation is most likely to be caused by the ageing process. The mixtures were oven aged before compaction. The specimen mixtures were hand-stirred every 12 h to create a more uniform ageing process. The 12 h-aged specimen did not benefit from being hand stirred. It is possible that the mixture used for this specimen was not as homogeneous in terms of ageing; without the benefits of being hand stirred, the oxidised layers at the surface of the mixture material protected the remaining material from being oxidised.
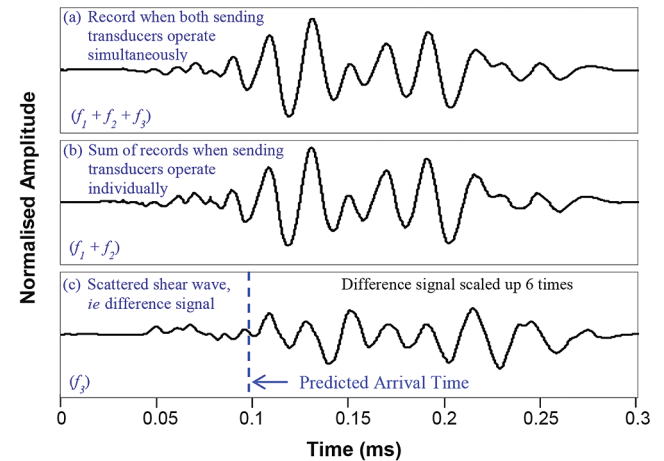
To further validate that the non-linear scattered wave is a result of non-linear wave-mixing inside the sample and not a result of the testing apparatus, the time domain records were also examined. Non-linearities generated by the testing equipment will have the same arrival time as the primary waves, whereas non-linearities arriving from wave-mixing in the specimen will have an arrival time corresponding to the paths dictated by the transducer placement and scattered wave angle γ (Equation (3)). Thus, a time separation between the primary waves and the non-linear scattered wave should exist, and the experimental time-of-arrival of the scattered wave should match its theoretical time-of-arrival. The theoretical time-of-arrival of the difference signal, *ie* scattered wave, can be calculated assuming mean velocities, see Table 1, and a straight ray-path analysis.

Figure 6 shows the time domain records for the specimen aged 36 h as a representative example. The time domain records shown are for the cases when: (a) the transducers were operated simultaneously; (b) the transducers were operated individually and their time domain

records were summed; and (c) the difference between the records obtained in (a) and (b). The theoretical time-of-flight of the non-linear scattered wave was calculated assuming straight ray paths. The primary velocities were calculated using the mean longitudinal velocity between 120 kHz to 200 kHz. The shear wave velocity (at the appropriate frequency) was used for the non-linear scattered wave velocity. The predicted arrival time (0.0982 ms) of the non-linear scattered wave matched closely ($\approx$4.7% difference) with the experimentally-observed arrival time (0.1028 ms).


Figure 6. Time domain records required to obtain the non-linear scattered shear wave: (a) time record obtained when both sending transducers were operated simultaneously; (b) time record obtained when sending transducers were operated one at a time and the received waveforms added; and (c) non-linear scattered wave, *ie* the difference signal, obtained from subtracting the signals obtained from operating the sending transducers individually from the signal obtained when operating the two sending transducers simultaneously. The theoretically-predicted time of arrival (0.0982 ms) for the difference signal matches closely (~4.7% difference) with the experimentally-observed time of arrival (0.1028 ms). The records are all normalised by the maximum amplitude of the record in (b). The difference signal was scaled up 6 times

The non-linear wave generation parameter, β

Once it is determined that the difference signal has satisfied the selection criteria, the non-linear wave generation parameter β can be computed. Figure 7 shows β for all aged specimens normalised by the average of β_0, corresponding to the virgin mixture. This normalised parameter, β/β_0, indicates the conversion efficiency of the energy transferred from the primary waves interacting to produce the scattered non-linear wave (see Equation (6)). Please note that the stochastic nature of the asphalt concrete causes disparities in the independent measurements, as even a slight variation in the placement of the transducers can alter the travel paths of the travelling waves. It is observed that β/β_0 decreases from 0 to 24 h of ageing and increases exponentially from 24 to 36 h of ageing. This trend has been repeatedly observed in other studies[50,51], in which the behaviour of asphalt concrete as a function of ageing has also been studied. It is

Table 2. Experimentally-obtained and theoretically-predicted frequency ratios corresponding to the maximum amplitude of the scattered wave

Amount aged (h)	Experimentally-recorded mean f_2/f_1	Standard deviation of experimental results (kHz)	Theoretical f_2/f_1	% difference
0	0.572	0.0125	0.600	4.75
12	0.558	0.0212	0.613	8.97
24	0.556	0.0223	0.630	11.82
28	0.679	0.0274	0.650	5.38
32	0.671	0.0288	0.664	0.99
36	0.676	0.0190	0.685	1.17

quite interesting to note that the 24-h laboratory ageing level (at 135ºC) corresponds to the threshold identified by Braham *et al*[49], at which the lab specimens behave similarly to long-term aged field specimens, which exhibit thermal cracking behaviour in the field. This corresponds to a field age level of approximately seven years.
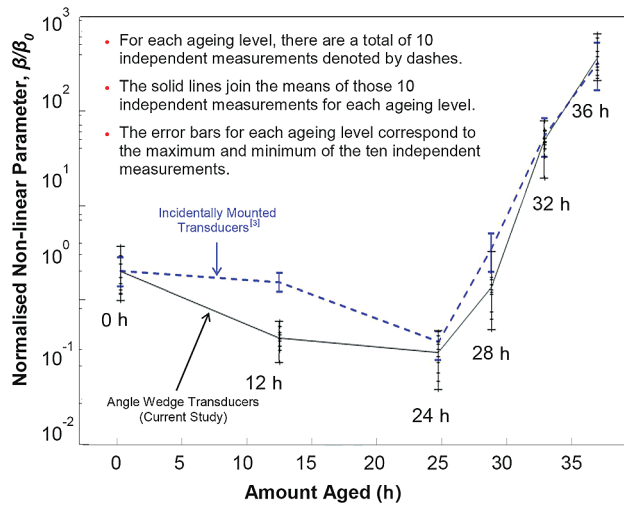
Figure 7. Normalised non-linear parameter, *β*, *versus* different levels of oven ageing. The parameter *β* is normalised with the parameter *β*₀, which corresponds to the virgin, *ie* unaged, mixture. For each ageing level, each of the ten independent measurements required removal of the three sensors, removal of the used couplant, and subsequent application of new couplant, and reposition of the three sensors. The solid line represents currently obtained results and the dashed line represents results obtained in a previous study using incidentally mounted transducers[3]

Furthermore, recalling that the experimental set-up was based on virgin parameters, the non-linear scattered wave will not always strike the receiving transducer's face incidentally and in the centre, because the scattered wave angle changes (*ie* increases) with the amount aged. With an increased amount of ageing, the non-linear scattered wave will strike the transducer's face increasingly off-centre, which may lead to an increasing underestimate of β/β_0 with ageing. The β/β_0 parameter reveals that the asphalt concrete exhibits increasingly strong non-linear behaviour with increasing levels of ageing. This is further evidenced by the fact that the non-linear scattered wave can still be detected, even with such a strong counteracting effect of attenuation.

A comparison of the results from this study with the results of a previous study[3] using test samples of the same material (*ie* the same binder, gradation and levels of oven ageing), but having different geometry, are worth discussing at this point, as they demonstrate the validity of using subsurface waves in the non-collinear wave mixing technique. In the previous study[3], the longitudinal transducers were coupled to the test specimens using normal incidence to launch longitudinal bulk waves by choosing the appropriate geometry for the test specimens. In the current study, the selected interaction angle of the primary ultrasonic beams and the angle for the scattered wave ($\phi = 47º$ and $\gamma = -37º$, respectively) changed slightly from the corresponding angles used in the previous study[3] ($\phi = 31º$ and $\gamma = -42º$), mainly to accommodate positioning of the angle wedge transducers because of the finite width of the test specimens. In doing so, it is noted that the frequency ratios changed according to theory. However, the non-linear wave generation parameter remained nearly the same, as shown in Figure 7. Figure

7 shows the normalised non-linear parameter for increasing levels of oven ageing, where the solid line represents the results obtained in this study and the dashed line represents previously obtained results[3]. Considering: (1) the stochastic nature of aggregates (regarding their shape, size and geometric location/distribution); (2) two sets of specimens with different geometry were used; (3) the potential variability of oven ageing levels (for example potential variability of temperature within the oven and difference in levels of hand stirring the mixtures); and (4) the potential variability in coupling conditions, the agreement between the two studies is very good. This observation lends credence to the claim that the non-linear wave generation parameter is an inherent material property and not a function of the testing set-up. The agreement of the results from these two studies also indicates that subsurface waves can be used successfully to characterise oxidative ageing in asphalt concrete using the non-collinear wave mixing technique.

Further discussion and potential applications

As previously mentioned, it is quite interesting to note that the 24-h laboratory ageing level (at 135ºC) corresponds to the threshold identified by Braham *et al*[49], at which the lab specimens behave similarly to long-term aged field specimens[52]. The long-term field-aged specimens in Braham's study exhibited thermal cracking behaviour in the field, as observed at the Minnesota Road Research Programme. It is therefore hypothesised that the current test and obtained non-linear wave generation parameter could be used for health monitoring of asphalt pavement surfaces. Since asphalt ageing and non-linearity depends on a number of factors (asphalt source(s) and refining technique(s) used, climate/geographical location, air void level, maintenance history, deicing history, traffic history, etc), this technique could potentially be used to accurately assess the surface condition of asphalt pavements, which in turn could be used to identify the most appropriate maintenance or repair technique. For instance, the technique could be used to assess the current ageing state of the asphalt by evaluating the β/β_0 parameter, with reference to the typical evolution of this parameter as depicted in Figure 7. Depending on the level of ageing as assessed by this parameter, different preventive or rehabilitative maintenance strategies could be identified. For example, pavements with β/β_0 parameters on the left-hand side of the vertex shown in Figure 7, *ie* non-severely aged, could be recommended for preventive maintenance treatments, such as rejuvenators or thin surface treatments. On the other hand, pavements with measured β/β_0 values determined to be on the right-hand side of the vertex, *ie* more severely aged, could be recommended for rehabilitation. Depending on the severity of ageing as identified by the β/β_0 parameter, various rehabilitation options, such as surface milling and/or thicker surface treatments, bonded overlays and/or traditional overlays, could be strategically identified, based on data-driven decision making with a rapid, non-destructive and relatively inexpensive test.

7. Conclusions

Asphalt concrete specimens subjected to various amounts of laboratory-induced oven ageing were examined using the non-collinear wave mixing technique. Subsurface longitudinal waves were mixed to produce a scattered subsurface shear wave. The non-linear scattered waves were measured for each aged specimen and used to characterise the inherent non-linearities of the asphalt material as a function of ageing using the non-linear wave generation parameter. Selection criteria were used to verify that the non-linear

scattered waves were generated via the non-collinear wave mixing in the test specimen and not from the testing equipment. It was observed that asphalt concrete behaves increasingly non-linearly with a increasing amount of ageing and that the frequency ratio at which the strongest interaction occurs shifts as a function of ageing. These observations correlate well with results from previous studies. The results from this study suggests the feasibility of mixing subsurface longitudinal waves to interrogate asphalt concrete and assess its amount of oxidative ageing, including durability and damage accumulation due to loading and environmental conditions, for structures where there is only access to one side (for example pavements). Data also suggests that this technique may have the potential to accurately assess the surface condition of asphalt pavements, which in turn could be used to identify the most appropriate maintenance or repair technique.

Acknowledgements

References

1. E R Brown, P S Kandhal, F L Roberts, Y R Kim, D Lee and T W Kennedy, Hot Mix Asphalt Materials, Mixture, Design, and Construction, Third Edition, NAPA Research and Education Foundation and NCAT, Maryland, 2009.

2. R Y Kim (Ed), Modelling of Asphalt Concrete, American Society of Civil Engineers Press and McGraw Hill, Chicago, New York, 2009.

3. M McGovern, W Buttlar and H Reis, 'Characterisation of oxidative ageing in asphalt concrete using a non-collinear ultrasonic wave mixing approach', Insight, Vol 56, No 7, pp 367-374, July 2014.

4. J H Cantre and H Salama, 'Acoustoelastic characterisation of materials', International Materials Review, Vol 36, pp 125-145, 1991.

5. J H Cantrel and W T Yost, 'Non-linear ultrasonic characterisation of fatigue microstructures', International Journal of Fatigue, Vol 23, pp 487-490, 2001.

6. J Kim, J Jacobs, J Qu and J W Littles, 'Experimental characterisation of fatigue damage in nickel-based super alloy using non-linear ultrasonic waves', Journal of the Acoustical Society of America, Vol 120, pp 1266-1273, 2006.

7. C Pruell, J Kim, J Qu and L J Jacobs, 'Evaluation of plasticity driven material damage using Lamb waves', Applied Physics Letters, Vol 91, 231911, 2007.

8. F D Murnaghan, Finite Deformation of an Elastic Solid, John Wiley & Sons Inc, New York, 1951.

9. L D Landau and E M Lifshitz, Theory of Elasticity, Second Edition, Pergamon Press, New York, 1970.

10. Z A Gol'dberg, 'Interaction of plane longitudinal and transverse elastic waves', Soviet Phys Acoust, Vol 6 (3), pp 306-310, 1960.

11. G L Jones and D R Kobett, 'Interaction of elastic waves in an isotropic solid', Journal of the Acoustical Society of America, Vol 35 (1), pp 5-10, 1963.

12. P A Johnson, T J Shankland, R J O'Connell and J N Albright, 'Non-linear generation of elastic waves in crystalline rock', Journal of Geophysical Research, Vol 92 (B5), pp 3597-3602, 1987.

13. P A Johnson and T J Shankland, 'Non-linear generation of elastic waves in granite and sandstone: continuous wave and travel time observations', Journal of Geophysical Research, Vol 94 (B12), pp 17729-17733, 1989.

14. L H Taylor and F R Rollins, 'Ultrasonic study of three-phonon interactions. I. Theory', Physical Review, Vol 136 (3A), pp A591-A596, 1964.

15. F R Rollins, L H Taylor and P H Todd, 'Ultrasonic study of three-phonon interactions. II. Experimental results', Physical Review, Vol 136 (3A), pp A597-A601, 1964.

16. A J Croxford, P D Wilcox, B W Drinkwater and P B Nagy, 'The use of non-collinear mixing for non-linear ultrasonic detection of plasticity and fatigue', Journal of the Acoustical Society of America, Vol 126 (5), pp EL117-EL122, 2009.

17. A Demcenko, R Akkerman, P B Nagy and R Loendersloot, 'Non-collinear wave mixing for non-linear ultrasonic detection of physical ageing in PVC', NDT&E International, Vol 49, pp 34-39, 2012.

18. F R Rollins, 'Phonon interactions and ultrasonic frequencies', Proceedings of the IEEE, Vol 53 (10), pp 1534-1539, 1965.

19. R W Dunham and H B Huntington, 'Ultrasonic beam mixing as a measure of the non-linear parameters of fused silica and single-crystal NaCl', Physical Review, Vol 2 (4), pp 1098-1107, 1970.

20. L K Zarembo and V A Krasil'nikov, 'Non-linear phenomena in the propagation of elastic waves in solids', Soviet Physics, Vol 13, No 6, pp 778-797, 1970.

21. P B Nagy, 'Fatigue damage assessment by non-linear ultrasonic materials characterisation', Ultrasonics, Vol 36, pp 375-381, 1998.

22. R A Guyer and P A Johnson, 'Non-linear mesoscopic elasticity: evidence for a new class of materials', Vol 52, No 4, Physics Today, American Institute of Physics, pp 30-36, 1999.

23. R A Guyer and P A Johnson, Non-linear Mesoscopic Elasticity: The Complex Behaviour of Granular Media including Rocks and Soil, Wiley-VCH Verlag GmbH & Co KGaA, Weinheim, 2009. ISBN: 978 3 527 40703 3.

24. P A Johnson, B Zinszner and P N J Rasolofosaon, 'Resonance and elastic non-linear phenomena in rock', Journal of Geophysical Research, Vol 101 (B5), pp 11553-11564, 1996.

25. M E McGovern and H Reis, 'Linear and non-linear characterisation of limestone rock using non-collinear ultrasonic wave mixing', Health Monitoring of Structural and Biological Systems 2014, Tribikram Kundu (Ed), Proceedings of SPIE, Vol 9064, pp 906404-1/906404-15, 2014.

26. L A Ostrovsky and P A Johnson, 'Dynamic non-linear elasticity in geomaterials', Rivista del Nuovo Cimento, Vol 24, No 7, pp 1-46, 2001.

27. P A Johnson, B Zinszner and P N J Rasolofosaon, 'Resonance and elastic non-linear phenomena in rock', Journal of Geophysical Research, Vol 101, No B5, pp 11553-11564, 1996.

28. J D Ferry, Viscoelastic Properties of Polymers, John Wiley and Sons, New York, 1961.

29. C Y Cheung and D Cebon, 'Deformation mechanisms of pure bitumen', Journal of Materials in Civil Engineering, pp 117-129, 1997.

30. C Y Cheung and D Cebon, 'Thin-film deformation behaviour of power-law creeping materials', Journal of Engineering Materials, pp 1138-1152, 1997.

31. S Kose, M Guler, H U Bahia and E Masad, 'Distribution of strains within hot-mix asphalt binders – applying imaging and finite element techniques', Transportation Research Board, Paper No 00-1391, pp 21-27, 2000.

32. E Masad, N Somadevan, H U Bahia and S Kose, 'Modelling and experimental measurements of strain distribution in asphalt mixes', Journal of Transportation Engineering, Vol 127, No 6, pp 477-485, 2001.

33. E Masad, C-W Huang, G Airey and A Muliana, 'Non-linear viscoelastic analysis of unaged and aged asphalt binders', Construction and Building Materials, Vol 22, pp 2170-2179, 2008.

34. R Delgadillo, 'Non-linearity of asphalt binders and their relationship with asphalt mixture permanent deformation', PhD Thesis, University of Wiscosin, Madison, 2008.

35. E T Hagos, 'The effects of ageing on binder properties of porous asphalt concrete', MS Thesis, Technical University of Delft, The Netherlands, 2008.

36. D E Bray and R K Stanley, Non-Destructive Evaluation – A Tool in Design, Manufacturing, and Service, Revised Edition, CRC Press, New York, 1997.

37. L E Kinsler, A R Frey, A B Coppens and J S Sanders, Fundamentals of Acoustics, Third Editon, John Wiley & Sons, New York, 1984.

38. J Couchman, B Yee and F Chang, 'Energy partitioning of ultrasonic waves beyond the critical angle flat boundaries', Ultrasonics, Vol 12, No 2, pp 69-71, 1974.

39. M Breazeale and L Bjorno, 'Forward and backward displacement of ultrasonic waves relected from a water-sediment interface', Proc Ultrasonics Intern 77, IPC Science and Technology Press, pp 440-447, 1977.

40. J Couchman and J Bell, 'Prediction, detection and characterisation of a fast surface wave produced near the first critical angle', Ultrasonics, Vol 16, No 6, pp 272-274, 1978.

41. L Basatskaya and I Ermolov, 'Theoretical study of ultrasonic longitudinal subsurface waves in solid media', Soviet Journal of Non-Destructive Testing, Vol 16, pp 524-530, 1981.

42. A Pilarski and J Rose, 'Utility of subsurface longitudinal waves in composite material characterisation', Ultrasonics, Vol 27, pp 226-233, 1989.

43. K Langenberg, P Fellinger and R Marklein, 'On the nature of the so-called subsurface longitudinal wave and/or the subsurface longitudinal 'creeping' wave', Research in Non-Destructive Evaluation, Vol 2, pp 59-81, 1990.

44. P Junghans and D Bray, 'Beam characteristics of high-angle longitudinal wave probes', NDE: Applications, Advanced Methods, and Codes and Standards, R N Pangborn (Ed), Proceedings of the Pressure Vessels and Piping Conference, Vol 216 of PVP, Vol 9 of NDE, ASME, pp 39-44, 1991.

45. T Leon-Salamanca and D Bray, 'Residual stress measurement in steel plates and welds using critically-refracted longitudinal (LCR) waves', Research in Non-Destructive Evaluation, Vol 7, pp 169-184, 1996.

46. D Bray and M Dietrich, 'Stress evaluation in high-speed rotating machinery with the LCR ultrasonic technique', Proceedings of the 26th Turbo Machinery Symposium, pp 143-149, 1997.

47. D Bray and W Tang, 'Subsurface stress evaluation in steel plates and bars using the LCR ultrasonic wave', Nuclear Engineering and Design, Vol 207, pp 231-240, 2001.

48. S Chaki, W Ke and H Demouveau, 'Numerical and experimental analysis of the critically-refracted longitudinal beam', Ultrasonics, Vol 53, pp 65-69, 2013.

49. A F Braham, W G Buttlar, T Clyne, M Marasteanu and M Turos, 'The effect of long-term laboratory ageing on asphalt concrete fracture energy', Journal of the Association of Asphalt Paving Technologists, Vol 78, pp 417-454, 2009.

50. M E McGovern, B Behnia, W G Buttlar and H Reis, 'Characterisation of oxidative ageing in asphalt concrete – Part 1: Ultrasonic velocity and attenuation measurements and acoustic emission response under thermal cooling', Insight, Vol 55, No 11, pp 596-604, 2013.

51. M E McGovern, B Behnia, W G Buttlar and H Reis, 'Characterisation of oxidative ageing in asphalt concrete – Part 2: Complex moduli estimation', Insight, Vol 55, No 11, pp 605-609, 2013.

52. M Marasteanu, A Zofka, M Turos, X Li, R Velasquez, X Li, C Williams, J Bausano, W Buttlar, G Paulino, A Braham, E Dave, J Ojo, H Bahia, A Gallistel and J McGraw, 'Investigation of low-temperature cracking in asphalt pavements', Report No 776, Minnesota Department of Transportation, Research Services MS 330, St Paul, MN 55155, USA, 2007.

. . . .

Design of an advanced automatic inspection system for aircraft parts based on fluorescent penetrant inspection analysis

J Zheng, W F Xie, M Viens, L Birglen and I Mantegh

17. G W Budd, 'Surface inspection technology for the detection of porosity and surface imperfections on machined metal surfaces', US Patent 7394530 B2, 1 July 2008.

18. R C Gonzalez, Digital Image Processing, Third Edition, Publishing House of Electronics Industry, China, 2011.

19. S Nashat, A Abdullah and M Z Abdullah, 'A robust crack detection method for non-uniform distributions of coloured and textured image', IEEE International Conference on Imaging Systems and Techniques, pp 98-103, May 2011.

20. X H Liu, L Xu, C J Xiao, M J Cao and J Xiao, 'Identifying the crack of silicon solar cells based on Matlab image processing', Journal of Shanghai Jiaotong University, 44 (7), pp 925-929, July 2010.

21. G Wang and T W Liao, 'Automatic identification of different types of welding defects in radiographic images', NDT&E International, 35, pp 519-528, 2002.

22. Y Tian, D Du, G R Cai, L Wang and H Zhang, 'Automatic defect detection in X-ray images using image data fusion', Tsinghua Science and Technology, 11 (6), pp 720-724, December 2006.

23. N Otsu, 'A threshold selection method from grey-level histograms', IEEE Transactions on Systems, Man and Cybernetics, 9 (1), pp 62-66, 1979.

24. ASTM E433-71, 'Standard reference photographs for liquid penetrant inspection', 2003.

25. ASTM SE-165, 'Methods for liquid penetrant examination'.

26. H Mu, L Li, L Yu, M Zhang and D Qi, 'Detection and classification of wood defects by ANN', Proceedings of the 2006 IEEE International Conference on Mechatronics and Automation, pp 2235-2240, June 2006.

27. S K Ho, R M White and J Lucas, 'A vision system for automated crack detection in welds', Meas Sci Technol, 1, pp 287-294, 1990.

28. Y L Luo, P S Qu and W H Dong, 'Fault diagnosis of aero engine based on digital image processing', Control and Decision Conference 2008, pp 3572-3575, 2008.

Field estimation of oxidative ageing in asphalt concrete pavements using non-collinear wave mixing

M E McGovern, W G Buttlar and H Reis

To facilitate the estimation of the state of oxidative ageing of the top material layer of asphalt concrete pavements, a two-dimensional 'oxidative-ageing non-linear characterisation curve', which uniquely illustrates the non-linear response of asphalt concrete mixtures with increasing levels of oxidative ageing, is presented. Because longitudinal and shear velocities and the corresponding attenuation values in asphalt concrete are dependent upon its level of oxidative ageing, and because these properties are needed for non-collinear wave mixing measurements, a methodology is presented to estimate these properties from the pavement surface only. Results from a blind study are also presented, which indicate that the proposed approach can successfully estimate the level of oxidative ageing from measurements taken from the pavement surface.

1. Introduction

Asphalt concrete (AC) pavements are exposed to a number of harsh damaging elements during service, such as extreme environments in hot and cold regions, oxidative ageing and severe traffic loadings. Oxidative ageing is one of the main contributors to pavement degradation. High levels of oxidative ageing can significantly reduce the performance of the pavement, consequently shortening its service life[1,2]. As a result, AC pavements must be monitored and decisions must be made regarding potential surface treatments, such as the use of rejuvenators and/or overlays[3,4]. Currently, there are no non-destructive evaluation techniques capable of quantitatively assessing the level of oxidative ageing of AC pavements in the field.

The dependence of longitudinal and shear velocities, and the corresponding attenuations, upon levels of oxidative ageing have been investigated by the authors[5]. Based upon these results, the complex moduli were also estimated as a function of ageing levels[6]. As asphalt concrete ages via oxidation, it also displays changes in its non-linear behaviour. This non-linear behaviour can be characterised using an ultrasonic non-collinear wave mixing technique. In this wave mixing approach, two ultrasonic bulk waves are propagated through the medium in a manner such that they cross paths at a certain angle and set of frequencies. For a material that displays non-linear behaviour, these two bulk waves may interact to produce a third non-linear scattered wave.

The longitudinal and shear phase velocities and corresponding attenuation results presented in reference[5] allowed for the estimation of artificially-induced oxidative ageing in asphalt concrete specimens using a non-collinear wave mixing approach[7,8]. In both studies[7,8], the material mixture of the test samples and their increasing levels of laboratory-induced oxidative ageing was the same, only the geometry of the specimens was different. In reference[7], the laboratory asphalt concrete specimens had a special geometry to allow the primary waves to be injected into the specimens using longitudinal sensors mounted in normal incidence and the resultant scattered shear wave to be received with a shear transducer, also mounted in normal incidence. However, in reference[8] the two primary waves were critically-refracted longitudinal waves sent at the surface of the test specimens via variable-angle shear wedges and the resultant shear wave was received via a dilatational transducer mounted onto the surface in normal incidence. Within the margin of experimental error, the results presented in reference[7] were duplicated in reference[8].

Subsurface longitudinal waves are bulk dilatational waves that travel nearly parallel to and along the surface of a solid medium. They can be generated using dilatational transducers mounted on variable-angle shear wedges set to an angle close to the first critical angle[9,10]. From the literature review[11-14], it has been shown that the ideal incident angle to generate these waves is approximately 1° greater than the first critical angle, which can be found using Snell's Law. This angle can be varied about the critical angle for a number of degrees and a longitudinal subsurface wave will still be generated, albeit the path along which it propagates and the resulting beam pattern will change slightly (for example the ray of maximum displacement starts to deviate from being parallel to the free surface).

The significant advantage of having the two sending transducers and the receiving transducer mounted on the same surface is that access to only one side of the AC test specimen is necessary,

Megan E McGovern and Professor Henrique Reis* are with the Department of Industrial and Enterprising Systems Engineering, University of Illinois at Urbana-Champaign, 117 Transportation Building, 104 S Mathews Avenue, Urbana, Illinois 61801, USA. Tel: +1 217 333 1228; Fax: +1 217 244 5705; Email: h-reis@uiuc.edu

Professor William G Buttlar is with the Department of Civil and Environmental Engineering, University of Illinois at Urbana-Champaign, 205 N Mathews Avenue, Urbana, Illinois 61801, USA.

*Corresponding author.

making it useful for non-destructive evaluation of asphalt concrete pavements. However, in both references[7,8], prior knowledge of the longitudinal and shear phase velocities and corresponding attenuations were also known before the test and obtained under ideal laboratory conditions[5].

During application of this technique in the field for *in-situ* pavement evaluation, there is no prior knowledge of the oxidative ageing level of the asphalt concrete, rendering the appropriate incident angle unknown, as well as the longitudinal and shear phase velocities and corresponding attenuations. The purpose of this study is to present a systematic approach to address the issue of the unknown incident critical angle, phase velocities and corresponding attenuations when there is access to only one side of the asphalt concrete pavement. The method allows the technique to be employed by practitioners in the field for pavement evaluation, where the only preexisting knowledge of the pavement is its mixture type.

2. Fundamentals of the non-collinear wave mixing technique using subsurface longitudinal waves

When two monochromatic waves, k_1 and k_2, with frequencies f_1 and f_2, respectively, are propagated in a medium with non-linear elastic constants, such that they intersect at an angle φ, they can generate a scattered wave, k_3, with a sum or difference frequency ($f_3 = f_1 \pm f_2$). The scattered wave propagates at an angle γ with respect to k_1. This scattered wave arises due to the higher-order terms present in the non-linear acoustic wave equation. The type and polarisation of the scattered wave depends on the type and polarisation of the two primary waves. Jones and Kobett[15] found that for interaction to be possible, resonance and polarisation conditions must be met. Consequently, out of 54 potential interaction cases, there are only nine interaction cases that satisfy both the resonance and polarisation conditions. For the case considered in this study, where two dilatational waves interact to produce a shear wave, the resonance and polarisation conditions are met when the following two equations are satisfied:

$$\cos[\varphi] = \left(\frac{c_L}{c_t}\right)^2 \left[1 - \frac{1}{2}\frac{f_1}{f_2}\left(1 - \frac{c_t^2}{c_L^2}\right)\left(\frac{f_2^2}{f_1^2} + 1\right)\right] \quad \text{.............. (1)}$$

$$\tan[\gamma] = \frac{-f_2 \sin[\varphi]}{f_1 - f_2 \cos[\varphi]} \quad \text{.......................... (2)}$$

where c_L and c_t are the dilatational and shear velocities, respectively. Note that the three parameters, $\frac{f_2}{f_1}$, φ and γ, are interdependent in the above equations; once one is chosen (for example φ), the other two are fixed (for example $\frac{f_2}{f_1}$ and γ). The frequencies are defined such that $f_2 < f_1$ and the resultant shear wave, *ie* k_3, has a frequency $f_3 = f_1 - f_2$ and is polarised in the plane parallel to the plane in which the longitudinal waves propagate, *ie* the plane defined by k_1 and k_2. For a more detailed discussion regarding the non-collinear wave mixing technique, and the non-linearities of asphalt concrete with respect to the amount of oxidative ageing, the reader is referred to references[7,8,15-28].

In a previous study[8], it was shown that subsurface longitudinal waves can be used in the non-collinear wave mixing method. Subsurface longitudinal waves can be generated using dilatational transducers mounted on angle wedges set to an angle close to the first critical angle, which is governed by Snell's Law as follows[9,10]:

$$\left[\theta_{inc}\right]_{critical} = \left[\sin^{-1}\left(\frac{c_{wedge}\sin(\theta_R)}{c_L}\right)\right]_{\theta_R=90°} \quad \text{................ (3)}$$

where c_{wedge} is the dilatational velocity of the angle wedge, c_L is the dilatational velocity in the bulk of the specimen material, $[\theta_{inc}]_{critical}$ is the incident angle of the wedge at the first critical angle and θ_R is the refracted angle in the specimen (= 90° for critical refraction). Here, both angles are with respect to the vertical, see Figure 1. Employing subsurface waves in the non-collinear wave mixing method has the advantage that the material can be interrogated with access to only one side.
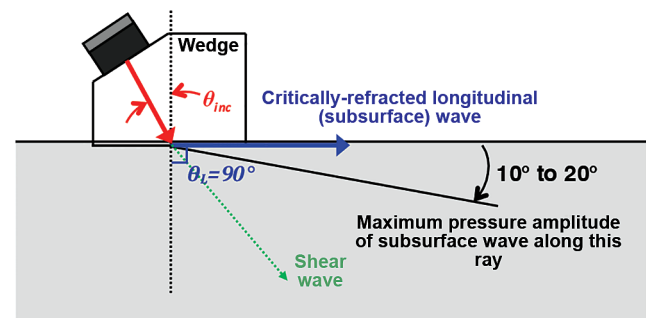

Figure 1. Set-up employing the use of variable angle wedge transducers mounted on the top of the specimen to generate and receive subsurface waves. A subsurface longitudinal wave is generated when θ_{inc} is set close to the first critically-refracted angle. Only one wedge is shown

Selection criteria (established by Johnson and Shankland[20,21]) must be used to verify that the non-linearities are a result of ultrasonic wave mixing between the two primary waves within the medium and not from the testing apparatus. The three selection criteria are: (1) the frequency of the non-linear scattered wave must match the frequency predicted by theory; (2) the amplitude of the non-linear scattered wave must be proportional to the product of the amplitude of the two primary waves; and (3) the propagation direction of the scattered wave must match the direction predicted by theory. Additionally, a time-of-flight (TOF) criterion can be used, where the TOF of the non-linear scattered wave should match that predicted using a straight ray path analysis[7,8].

3. Sample preparation and the 'non-linear characterisation curve'

Two important metrics in the assessment of the non-linearities of a material via the non-collinear wave mixing technique are the normalised non-linear wave generation parameter, β/β_0, and the frequency ratio, f_2/f_1, of the two primary waves from which the non-linear scattered wave is generated. The non-linear wave generation parameter represents the conversion efficiency of the energy transferred from the primary waves interacting to produce the scattered non-linear wave. Thus, the β/β_0 parameter is a good indicator of the material's inherent non-linear behaviour. These parameters, β/β_0 and f_2/f_1, are discussed in more detail in previous studies[7,8], where they are presented with respect to a set of AC specimens subjected to various amounts of oxidative ageing. Neither of these metrics is alone sufficient to uniquely assess the level of oxidative ageing due to a lack of separation at particular ageing levels[7,8]; however, when combined, they provide

a unique characterisation of the oxidative ageing level. Note that for a prescribed angle of interaction of the two primary waves, f_2/f_1 depends only upon the dilatational-to-shear phase velocities' ratio, see Equation (1), *ie* it depends only upon linear measurements. The 'non-linear characterisation curve' is a combination of these two metrics, where f_2/f_1 is plotted as a function of β/β_0, and it represents a trajectory of ageing for a particular mixture in a two-dimensional space defined by f_2/f_1 and β/β_0 parameters.

Ideally, to minimise experimental error, the non-linear characterisation curve should be generated in laboratory conditions using the longitudinal subsurface wave mixing technique, as in McGovern *et al*[7,8], across a sufficient sample size of oxidatively-aged AC specimens. To also minimise the experimental error, the dilatational and shear velocities and corresponding attenuations should be obtained in the laboratory for the entire sample set using incidentally-mounted transducers configured in a through-transmission set-up[5]. The dilatational velocities are used to obtain the appropriate incident angles of the wedges (*ie* 1º above the first critical angle). The attenuations are used in conjunction with the received non-linear scattered wave amplitude to determine the value of β/β_0.

Each non-linear characterisation curve only needs to be generated once for a particular mixture type in the laboratory. A library of non-linear characterisation curves can be generated for different mixture designs (for example different binders, aggregate gradations, aggregate types, etc). Thus, for use in the field, all that needs to be known *a priori* is the type of mixture. It is important that the laboratory testing set-up used to generate the non-linear characterisation curve is kept consistent with that used in the field (*ie* the same testing apparatus, filtering, signal gains, etc) for comparison purposes, since all the data obtained is normalised by the data received from the virgin specimen. Any inconsistencies in the testing apparatus, procedure or data post-processing will render subsequent comparisons with the virgin data invalid.

In a previous study[8], a non-linear characterisation curve was generated for a set of six gyratory-compacted AC specimens with laboratory-induced oxidative oven-ageing levels of 0 h, 12 h, 24 h, 28 h, 32 h and 36 h at 135ºC. The samples were all prepared with the same mixture, which had a target asphalt binder content of 5.9% by weight of the total mixture and 9.5 mm nominal maximum aggregate size. Gyratory-compacted cylinders 17.5 cm tall were prepared, which resulted in 150 × 175 × 50 mm slab specimens after being cut. For the current study, in addition to the six samples characterised in the previous study, three new samples were prepared at the following oven-ageing levels: 18 h, 26 h and 30 h at 135ºC. These samples were prepared with the same mix design. As before, 17.5 cm tall gyratory-compacted cylinders were prepared and cut to produce slab specimens with the same dimensions, *ie* 150 × 175 × 50 mm.

4. Estimation of the incident angle, velocities and attenuations

In the field, because no information regarding the level of pavement oxidative ageing is available, the critically-refracted angle is also unknown as well as the velocities and corresponding attenuations. In this section, methods are proposed to estimate the appropriate incident angle to generate subsurface dilatational waves, as well as to estimate the necessary linear parameters (*ie* velocities and corresponding attenuations) with access to only one side, *ie* the pavement surface. Once the critical refracted angle and linear

parameters are found, the subsurface non-collinear wave mixing technique can be employed as usual[7,8].

4.1 Estimation of the critical refracted angle

The determination of the first critical angle (the incident angle at which the subsurface wave travels parallel to the surface) is an iterative process. Two transducers mounted on variable angle wedges are set-up in a through-transmission configuration so that one sends a square wave at the appropriate frequency (*ie* in the range of f_2 to f_1) and the other receives the signal. Both wedges are set to the same angle. The distance between the wedges should be chosen to be sufficiently small to try to avoid any interference with bulk waves, which may be generated via mode conversion from the wedges and reflected back from discontinuities or large inhomogeneities in the bulk of the medium, see Figure 1. The wedge angle is varied and the amplitude is recorded at each angle. When changing the angle, care should be taken to not disturb the couplant conditions, which will affect the amplitude measurement. The wedges used in the study were limited to an incident angle of 75º. To avoid any interference with waves other than the subsurface wave, the amplitude should be taken from the beginning portion of the signal, as most of the energy in the first arriving signal should correspond to the fastest (*ie* dilatational) wave that travels the shortest path (*ie* closest to the surface). A parabola can then be fitted to the amplitude measurements, which are plotted with respect to the incident angle. The maximum of the parabola corresponds to the ideal incident angle to use in the testing set-up. This angle subtracted by 1º corresponds to the first critical angle (based on a previous study[14], the maximum amplitude will correspond to an incident angle that is 1º greater than the first critically-refracted angle).

4.2 Estimation of velocities and corresponding attenuations

Once the ideal incident angle is found, the mixture velocities and corresponding attenuation can be found. The dilatational velocity can be found using either Snell's Law (assuming critical refraction) or by measuring the time-of-flight of the subsurface waves via a through-transmission set-up with the angle wedges set to the ideal incident angle. The dilatational attenuation can be found using through-transmission subsurface waves over a range of frequencies. Similar to the testing set-up described in the previous section, the distance between the wedges should be chosen to be sufficiently small and the beginning portion of the signal should be windowed to ensure that the velocity and attenuation measurements correspond to the first-arriving subsurface dilatational wave.

To measure the shear wave attenuation, subsurface shear waves are not used due to uncertainty in how the stress-free surface boundary condition affects the propagation and detection of the shear wave. Instead, an empirical relationship between the shear attenuation and the longitudinal velocities for oxidatively-aged AC specimens was found using data obtained from a previous study[5]. As the ageing of the specimen increases, the stiffness of the binder increases and the adhesion between the binder and the aggregates and fine particles decreases. For the specimens aged 0 h to 24 h, the increase in stiffness of the binder dominates the composite behaviour (*ie* increases the stiffness of the composite) and thus the velocity increases from 0 h to 24 h. After 24 h, the loss in adhesion is the dominating effect and the composite stiffness decreases with increasing ageing. Thus, the stiffness can be directly related to the micro-flaw population. As the micro-flaw population increases, the velocity decreases[5,6]. Furthermore, the shear and longitudinal wave

attenuations are directly related to the micro-flaw population. As the micro-flaw population increases, the attenuation also increases. Based on this reasoning, a relationship between the shear wave attenuation and the longitudinal velocity was empirically found using the attenuations and velocities from McGovern *et al*[5], see Figure 2. This relationship was found to be:

$$\alpha_S \left(60 \text{ kHz} \le f \le 90 \text{ kHz} \right) \approx -0.031 c_L + 152.991 \text{ .... (4)}$$
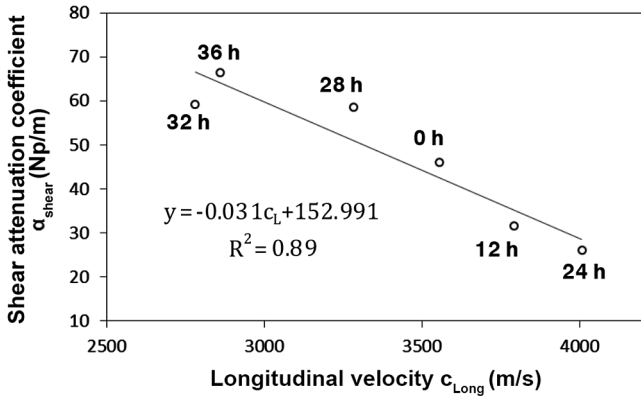

Figure 2. Empirically-derived relationship between the longitudinal velocity and the shear attenuation coefficient. This relationship is only valid for the specific asphalt concrete mixture and aggregate gradation used in this study

The longitudinal velocity is denoted by c_L and is the mean longitudinal velocity from 120 kHz to 200 kHz. Above 120 kHz, the longitudinal velocity is non-dispersive[5]. This empirical relationship is only valid for the AC mixture-type of the sample set used in this study, for α_s in a frequency range of 60 kHz to 90 kHz (which corresponds to the range of the non-linear wave frequencies in this study), and for the longitudinal velocity above the frequency at which it becomes non-dispersive (*ie* frequency independent). There is very little variation between 60 kHz and 90 kHz for α_s. The longitudinal velocity was related to the shear attenuation instead of the longitudinal attenuation because, although α_L is proportional to α_s, the proportionality constant is not the same across the entire sample set of aged specimens.

4.3 Estimation of shear attenuation using Rayleigh wave measurements

An alternative method to estimate the shear wave attenuation is through the use of surface waves, otherwise known as Rayleigh waves. A Rayleigh wave is a combination of dilatational and shear waves. Consequently, the attenuation coefficient of a Rayleigh wave can be written in terms of the dilatational and shear wave attenuation coefficients[29] as:

$$\alpha_R \lambda_R = C \alpha_L \lambda_L + (1 - C) \alpha_S \lambda_S \text{ .... (5)}$$

where:

$$C = \frac{16 \xi^2 \left(1 - \eta^2 \right)}{\eta^2 \left(3 \eta^4 - 16 \eta^2 - 16 \xi^2 + 24 \right)} \text{ ....(5a)}$$

$$\eta = \frac{k_S}{k_R} \approx \frac{0.87 + 1.12 \nu}{1 + \nu} \text{ .... (5b)}$$

$$\xi = \frac{k_L}{k_S} \text{ ....(5c)}$$

where the subscripts R, L and S denote Rayleigh, longitudinal and shear waves, respectively, k denotes the wave number, λ denotes

the wavelength, ν is the Poisson's ratio and α is the attenuation coefficient, which has units of Nepers per unit length. Given that the dilatational attenuation coefficient is already estimated via the use of subsurface waves, the shear attenuation can be readily estimated. For the frequency range used in this study ($f_3 < 100$ kHz), the Poisson's ratio varies from 0.4 to 0.5 as a function of ageing[5,6]. At this range, the $(1 - C)$ term in Equation (5) dominates over the C term and the following approximation can be made:

$$\alpha_R \lambda_R \approx (1 - C) \alpha_S \lambda_S \text{ .... (6)}$$

Thus:

$$\alpha_S \approx \frac{\alpha_R \lambda_R}{(1 - C) \lambda_S} \text{ .... (7)}$$

The Rayleigh wavelength can be found by recording the velocity and dividing it by the frequency of the transmitted wave. The shear wavelength can be estimated via the velocity $\left(\lambda = \dfrac{c}{f} \right)$ by considering that for a Poisson's ratio between 0.4 to 0.5 the Rayleigh velocity varies from $0.94 c_S$ to $0.95 c_S$; thus, an estimate can be made for the shear wavelength by considering the shear velocity to be $\dfrac{c_R}{0.945}$, so that Equation (7) simplifies to:

$$\alpha_S \approx \frac{0.945 \alpha_R}{(1 - C)} \text{ .... (8)}$$

Viktorov[29] provides an excellent and detailed discussion on Rayleigh waves and the above equations.

Rayleigh waves can be generated most efficiently by employing angle wedges set to an incident angle at the third critically-refracted angle. This angle can be found in a manner similar to the iterative method described in Section 3. However, in order to generate the Rayleigh wave via wedges in AC, the ultrasonic velocity in the wedges must be slower than the velocity in AC. The ultrasonic velocity of the more aged specimens is very low[5], so wedges should be made of a material with a sufficiently lower longitudinal velocity than the most expected aged pavements. Rayleigh waves can also be generated by other means, which have the advantage that there is no ambiguity in choosing an incident angle; however, the efficiency is much lower[10,29].

5. Non-collinear wave mixing and the oxidative-ageing non-linear characterisation curve

Once the incident angle, velocities and corresponding attenuations have been estimated, the non-collinear wave mixing technique can be performed as usual[8]. For every measurement, it is crucial to verify that the selection criteria[18,19] are satisfied to ensure that the non-linear interaction has taken place within the bulk of the material. As per the frequency criterion, the interaction should only take place at a particular set of primary wave frequencies (f_1 and f_2) for a chosen interaction angle, φ. This frequency ratio (f_2/f_1) will change with respect to the amount of ageing of the material, and can be found by identifying the point at which the non-linear wave amplitude reaches a maximum as f_2 is swept. The amplitude of the non-linear scattered wave can be described as:

$$A_{age}^{(k_3)} = \beta_{age} A_{sent}^{(k_1)} A_{sent}^{(k_2)} \exp \left[- \left(\alpha^{(k_1)} + \alpha^{(k_2)} \right) D \right] \exp \left[- \alpha^{(k_3)} D_{k_3} \right] ... (9)$$

In the above Equation (9), α denotes the attenuation coefficient for the wave denoted in the superscript, A denotes the amplitude of the transmitted wave denoted in the superscript and β is a

parameter that describes the conversion efficiency of generating the non-linear scattered wave from the interaction between the two primary waves. The f_2/f_1 peak is known once measurements are taken; therefore, the attenuations at the appropriate frequencies (f_1 and f_2) should be used. Note that the propagation distance of the two primary waves is the same, *ie* $D = D_{k_1} = D_{k_2}$. The normalised non-linear wave generation parameter can be found using the estimated attenuations and non-linear scattered wave amplitude, as follows:

$$A_{age}^{*(k_3)} = \frac{A_{age}^{(k_3)}}{\exp\left[-\left(\alpha^{(k_1)}+\alpha^{(k_2)}\right)D\right]\exp\left[-\alpha^{(k_3)}D_{k_3}\right]} = \beta_{age} A_{sent}^{(k_1)} A_{sent}^{(k_2)} \dots (10)$$

so that:

$$\frac{\beta_{age}}{\beta_0} = \frac{A_{age}^{*(k_3)}}{A_0^{*(k_3)}} \quad \dots\dots\dots\dots\dots\dots\dots\dots (11)$$

Prior to taking field measurements, the non-linear wave generation parameter, β_0, of the unaged material should be known, whether it is obtained via laboratory measurements on a mixture of the same type or via measurements taken using a specimen extracted from the bottom protected layer of an extracted field core. Then, the β measured in the pavement can be normalised by β_0 and the point (f_2/f_1, β/β_0) can be plotted on the non-linear characterisation curve to evaluate the level of oxidative ageing.

5.1 Advantages and disadvantages

The biggest advantage to using this technique to characterise the non-linearity of the asphalt concrete is that the normalised non-linear wave generation parameter β/β_0 can be found with some accuracy. Since the optimal angle (*ie* 1º above the first critical refracted angle) is used to generate the subsurface wave, normalising the amplitude to obtain β/β_0 can be readily done by using the estimated attenuations. This technique also offers the advantage that the dilatational velocity can be obtained with relatively good accuracy. Thus, in addition to the f_2/f_1 and β/β_0 parameters, the velocity can also be used as an additional metric to increase the robustness of the technique[5].

One of the disadvantages of this method is that it can be time consuming, since determining the incident angle is an iterative process. Also, although β/β_0 can be calculated using the estimated attenuations, these attenuation estimates are not exact due to beam spread, the fact that the wave is not perfectly parallel to the surface and because of variation in the couplant conditions.

To address the tedious nature of determining the best angle, a phased array approach could be implemented to steer the beam and the process could be automated to find the best angle (*ie* maximum received amplitude). However, it is difficult to say whether or not phased array transducers would function properly in a heterogeneous material such as asphalt concrete, since phased array transducers rely on constructive and destructive interference in the beam patterns to create a steered beam profile.

6. Experimental set-up

In a previous study[8], an 'ideal' testing set-up was found. This testing set-up was based on the unaged parameters for this particular mixture type and was held constant over all aged specimens. It was ensured that, regardless of the ageing of the specimen (within 0 h to 36 h), the scattered wave propagating direction path did not deviate so far as to not encounter the receiving transducer. See McGovern *et al*[7,8] for a more detailed discussion on choosing a suitable testing set-up for a sample set with AC specimens of various oxidative ageing.

Figure 3 shows a schematic diagram of the data acquisition system. A pulser-receiver (Ritec RPR-4000) was used to generate a 15-cycle sinusoidal toneburst at f_1 = 200 kHz, which was sent to a dilatational transducer (Panametrics V413, with a centre frequency of 500 kHz) mounted on a variable angle wedge (Plexiglas, with a dilatational velocity of 2720 m/s). A function generator (Krohn-Hite Model 5920) was used to generate an 8-cycle sinusoidal toneburst, which swept from f_2 =100 kHz to 180 kHz in 1 kHz increments. A gated amplifier (Ritec GA-2500 A) was used to amplify the signal and send it to another dilatational transducer (Panametrics V413, with a centre frequency of 500 kHz), also mounted on a Plexiglas variable angle wedge. The variable angle wedges were set to an incident angle dictated by the experimentally-recorded optimal angle (see Section 4). The two wedges were oriented such that the primary waves (k_1 and k_2) travelled for a distance of 8.2 cm (from the centre of the wedge to the centre of the volume of interaction) and they interacted at an angle of $\varphi = 47º$.
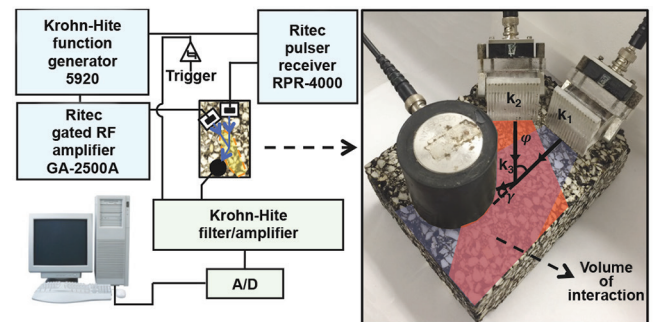

Figure 3. Schematic diagram of the ultrasonic data collection system illustrating the angle of interaction of the two longitudinal waves (*ie* k_1 and k_2) and the location of the shear transducer to receive the generated scattered shear wave, *ie* k_3. The blue and red regions denote the areas of signals k_1 and k_2, respectively, due to beam spread. The region where they overlap is the volume of interaction. Note that the beam spread from k_2 is slightly larger than k_1 due to the difference in frequencies. Note the 5 cm-thick slab-shaped specimen extracted from the gyratory compacted cylinder

Asphalt concrete consists of crushed stone, *ie* aggregates, of different sizes and shapes randomly distributed and held together by thin films of a bituminous binder. As a result of travelling through a highly heterogeneous media, the resulting shear wave goes through a significant level of mode conversion and scattering. This scattering and mode conversion leads to a spatially-incoherent normal particle displacement at the surface. When this random normal displacement distribution is averaged over the large aperture of the receiving longitudinal transducer (Panametrics V1011 with a centre frequency of 100 kHz), it leads to a temporally-coherent but spatially-incoherent output signal. The peak amplitude or total power of this signal can be measured to assess the strength of the resulting shear wave. Maradudin[30,31] and Maugin[32,33] provide an excellent discussion/review of shear horizontal surface acoustic waves in solids.

The receiving transducer was placed on the same surface as the sending transducers and oriented at $\gamma = -37º$ (with respect to k_1) so that it intercepted the non-linear scattered shear wave k_3, which propagated a distance of 4 cm (from the centre of the volume of interaction to the centre of the receiving transducer face). The received signal was amplified and filtered using a second-order Butterworth filter (Krohn-Hite Model 3945). An average of 300 signals were taken to mitigate the effects from scatter.

The following steps were taken for the data collection: (1) the signal is obtained while both transducers are operated simultaneously; (2) the signal is obtained while only one transducer is operated; and (3) the signal is obtained while only the other transducer is operated. The signals obtained from (2) and (3) were then subtracted from the signal obtained in (1) to obtain the non-linear scattered wave.

To ensure that the frequency of the scattered wave matched that predicted by the theory (ie $f_3 = f_1 - f_2$ at the appropriate f_1/f_2), the amplitude of the non-linear scattered wave was monitored as f_2 was swept and f_1 was held constant. The maximum amplitude of the non-linear scattered wave should occur when f_2 reaches the frequency where f_2/f_1 matches the ratio predicted by theory[8]. Figure 4 shows a representative example of the recorded non-linear scattered wave amplitude as f_2 was swept. For the example shown (virgin specimen), the amplitude was predicted to reach a maximum when $f_2/f_1 = 0.6$ (ie $f_2 = 120$ kHz), which differs from the experimentally-obtained value by only 4.1%. Note that the non-linear amplitude should only occur for the theoretically-predicted frequency ratio. In reality, the non-linear amplitude plotted as a function of frequency ratio has a finite width, mainly because many of the assumptions used in the theory are not fully satisfied. For additional discussion on data collection, the reader is referred to McGovern et al[8].
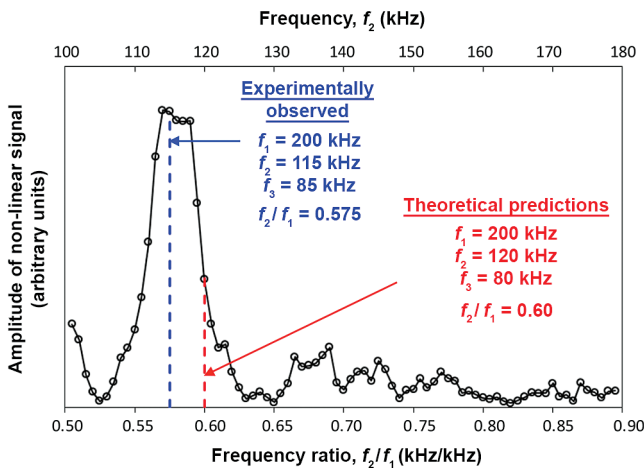

Figure 4. Experimentally-obtained amplitude of scattered shear wave, ie difference signal, ($f_3 = f_1 - f_2$) as f_2 is swept from 100 kHz to 180 kHz ($f_2/f_1 = 0.50$ to 0.90) while f_1 is held constant at 200 kHz. This analysis was performed for all specimens to obtain the data shown in Figures 5 and 7. The plot shown above is from the specimen oven-aged for 12 h and is shown as a representative case. The dashed blue line represents the experimentally-observed maximum and the dashed red line represents the theoretically-predicted maximum, which was obtained using the experimentally-determined velocity data. Figure reproduced from McGovern et al[8]

Figure 5 shows the time domain records for the specimen oven-aged for 36 h as a representative sample. The records shown are: (a) when both transducers were operated simultaneously; (b) when the transducers were operated individually and their time domain records summed; and (c) the difference between the records obtained in (a) and (b). The time-of-flight was calculated assuming a straight ray path. Assuming the shear velocity corresponding to f_3 for the path corresponding to the difference signal, the theoretically-predicted time-of-arrival (0.0982 ms) matches closely (~4.7 difference) with the experimentally-observed time-of-arrival.
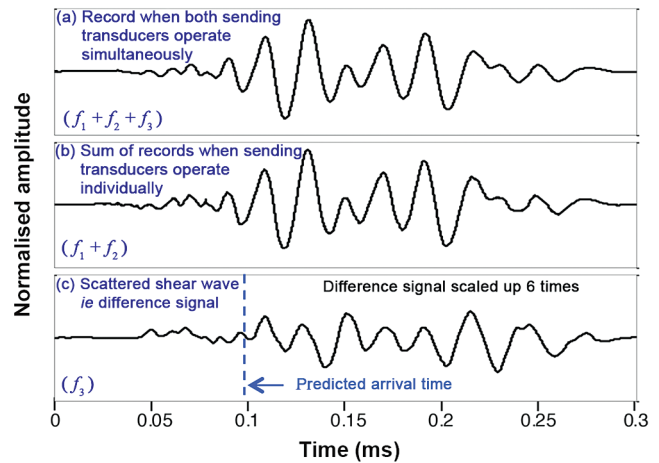

Figure 5. Time domain records required to obtain the non-linear scattered shear wave: (a) time record obtained when both sending transducers were operated simultaneously; (b) time record obtained when sending transducers were operated one at a time and the received waveforms added; and (c) non-linear scattered wave, ie the difference signal, obtained from subtracting the signals obtained from operating the sending transducers individually from the signal obtained when operating the two sending transducers simultaneously. The theoretically-predicted time-of-arrival (0.0982 ms) for the difference signal matches closely (~4.7% difference) with the experimentally-observed time-of-arrival (0.1028 ms). The records are all normalised by the maximum amplitude of the record in (b). The difference signal was scaled up six times. Figure reproduced from McGovern et al[8]

Prior to taking the blind study measurements, the non-linear characterisation curve was generated. In practice, to minimise experimental errors, this oxidative-ageing non-linear characterisation curve can be constructed experimentally in laboratory conditions using either: (a) normally-mounted longitudinal and shear transducers, provided the appropriate geometry of the test specimens is taken into consideration[7]; or (b) critically-refracted subsurface longitudinal waves, which requires only access to one surface of the test specimen[8]. While both approaches should provide the same results, in practice approach (a) should provide more accurate results because the uncertainty regarding the generation of subsurface waves is removed.

Once this non-linear characterisation curve is generated, it need not be generated again as long as the testing set-up and mixture type remain the same. In summary, the following steps should then be taken to assess a pavement of unknown ageing level: (1) Identify the mixture type for the asphalt concrete to be assessed; (2) Determine the optimal incident angle (critical angle +1°) using the iterative technique as described in Section 4; (3) Obtain the dilatational attenuations (across a range of frequencies) and velocity using subsurface waves generated by setting the angle wedge transducers to the incident angle found in Step 2 (see Section 4); (4) Use Equation (4) and the dilatational velocity found in Step 3 to obtain an estimate of the shear attenuation; (5) Perform the non-collinear wave mixing technique[7,8] using the testing set-up described above and the incident angle from Step 2; (6) Determine the f_2/f_1 at which the maximum non-linear wave amplitude occurs; (7) Correct the non-linear wave amplitude for the attenuation at the appropriate frequencies using Equations (9) to (11) and the attenuation estimates obtained in Steps 3 and 4 to obtain β/β_0. The β_0 is known, as it should be previously obtained from a virgin

specimen in the laboratory for this known mixture type using the same testing set-up; (8) Plot the point (f_2/f_1, β/β_0) on the non-linear characterisation curve to evaluate where the point lies to determine the relative amount of oxidative ageing of the pavement.

7. Experimental results

First, the reference curve was obtained by performing non-linear measurements on a set of asphalt concrete specimens subjected to increasing levels of laboratory-induced oxidative oven-ageing. Once the values of f_2/f_1 and β/β_0 were obtained for each specimen, the plots of frequency ratio *versus* level of ageing (Figure 6(a)) and of the normalised non-linear parameter *versus* ageing (Figure 6(b)) were constructed. Based upon these two Figures, the reference plot (in the solid black line) shown in Figure 6(c) was constructed. Note that the experimentally-determined linear acoustic parameters (*ie* critical angles, velocities and attenuations) do not uniquely characterise the binder oxidative ageing, see Figures 6(a) and 6(b). While the linear acoustic parameters can be used as an indicator of the amount of ageing, a unique representation is only achieved when used in conjunction with non-linear measurements, see Figure 6(c). The reference curve only requires knowledge of the existing mixture so the field measurements can be normalised by the parameters

corresponding to the virgin mixture. The reference curve represents the evolution of non-linearities associated with oven-ageing. The trajectory of damage accumulation for an increasing number of hours of oven-ageing is mixture dependent. The solid dots represent an average of 10 independent measurements. The intervals of confidence represent the maximum and minimum of these 10 independent measurements. These values were obtained using the subsurface waves at the respective critical angles for each specimen. These results are discussed in more detail in McGovern et al[8].

Using the procedure outlined in Section 5, a 'blind study' was then performed using the samples in the manner that they would be performed in the field. In other words, it was assumed that there was no knowledge of the specimens' oxidative ageing or linear ultrasonic parameters (*ie* dilatational and shear velocities and corresponding attenuations) *a priori*. Refer to the previous section for the steps taken in the blind study measurements.

The incident angle was found iteratively for each aged sample. Figure 7 shows the amplitude measurements as a function of the incident angle for the virgin specimen. From a previous study, it is known that the critical incident angles will be between 43° and 79° for the range of oxidative ageing (0 h to 36 h) of the sample set of AC specimens used in this study. The measurements were begun by recording the signal for incident angles every 10°, starting at 40°. The amplitude measurement was taken at the beginning portion of the signal, which corresponds to the first arriving subsurface dilatational wave. Later portions of the signal may include other modes, such as surface waves or, in this case due to the finite dimensions of the sample, shear waves reflected from the bottom surface. This process will now be described by way of an example. Consider the case where measurements were taken on the virgin specimen. After taking the first four measurements (at 40°, 50°, 60° and 70°), the amplitudes of the signal were examined at each measurement. From the first four amplitude measurements, a parabolic trend was observed that peaked at 50°. The next two amplitude measurements were taken at 45° and 55°. After these two measurements, the peak was still observed at 50°. The next measurements were taken at 47° and 53°, where the observed peak was then 53°. The peak at 53° did not shift when subsequent measurements were taken for the incident angles of 51°, 52° and 54°. Thus, the optimal incident angle was concluded to be 53°, which corresponds to a critically-refracted angle of 52°.

The above procedure was repeated for all specimens until amplitudes were recorded for a sufficient number of angles. A parabola was then fitted to the measurements and the location (incident angle) of the maximum amplitude was found to the nearest degree. However, for the specimens aged 32 h and 36 h, the first critical angles were near the limitations of the variable angle wedges, making fitting a parabola to the data unfeasible. Thus, in these cases, the maximum value of the data was reported. Table 1 contains the critical angles
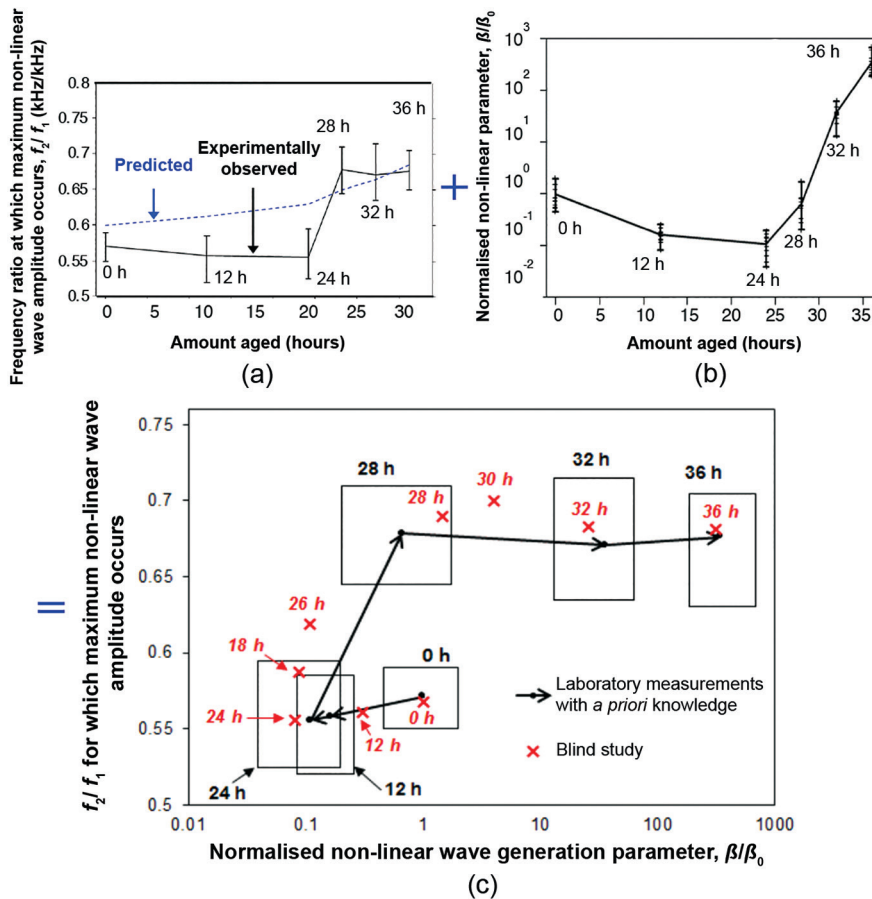

Figure 6. Generation of the reference curve, *ie* the frequency ratio *versus* the normalised non-linear parameter. (a) and (b) are experimentally determined from specimens with increasing levels of controlled oxidative ageing and with knowledge of the velocities and corresponding attenuations for each specimen. The data from (a) and (b) is used to create the reference curve shown in solid black lines in (c). The red crosses represent the average of five measurements taken from the top surface without any prior knowledge of the specimen level of ageing (only the type of mixture was known) using the procedure outlined in Section 5
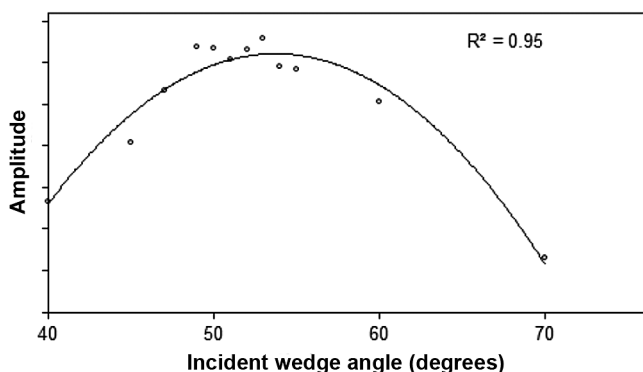
Figure 7. Amplitude of the received wave as the incident angle $\theta_{incident}$ **of the variable angle wedges is set to different angles using the set-up shown in Figure 1. This technique is used to find the first critically-refracted angle when there is no prior knowledge of the material properties. A parabola is fitted to the data to find the maximum. The R^2 of the parabola is 0.95**

found via this approach, along with the theoretically-predicted values (via previous velocity measurements[5]).

Table 1. Theoretically-predicted critical angle +1° based on Snell's Law, and the experimentally-determined critical angle +1°

	Amount aged (h)					
	0	12	24	28	32	36
Theoretically-predicted critical angle +1° *	51°	47°	44°	57°	79°	73°
Experimentally-measured critical angle +1°	53°	50°	45°	55°	75° **	73°
Percent error	3.9	6.4	2.3	3.5	5.1	0.0

*Based on literature, the angle at which the subsurface wave is able to be best detected, *ie* maximum displacement at the surface, corresponds to around 1° above the first critical angle.

**Due to constraints with the angle wedges, the incident angle could not be greater than 75°.

Once the appropriate incident angles were found, the velocities and attenuations were determined, as described in Section 4. Tables 2 and 3 show the dilatational velocity and attenuation estimates, respectively, using the iterative angle technique, along with the percent errors when compared against measurements from a more accurate technique (see McGovern *et al*[5]). It is observed that the velocity estimate using Snell's Law yielded smaller errors

than the estimate using through-transmission of the subsurface waves. Table 4 contains the estimated shear attenuations using the empirical relationship (Equation (4)) with the velocities obtained via longitudinal subsurface waves. Also included in Table 4 are measurements obtained from the more accurate technique (see McGovern *et al*[5]). These errors are higher than desirable; however, they are the best available estimate given the testing set-up constraints (for example access to only one side of the specimen). One major source of error in the linear acoustic measurements arises from the fact that the beam pattern of subsurface waves is different to that generated by incidentally-mounted transducers. Couplant conditions can also add to errors in the attenuation measurements; however, multiple independent attenuation measurements were taken to minimise this error. Also, the attenuation coefficient measurements in the previous study[5] were performed on a different set of samples of the same mixture type. Although care was taken to make the samples in a consistent manner, variability exists due to the stochastic nature of aggregate geometry and aggregate structure, the variability in the oxidative ageing of the mixture and the amount of time spent in the oven while mixing the samples, often referred to as short-term ageing, etc.

Once the non-collinear wave mixing was performed and the non-linear scattered wave signal (*ie* the difference signal) was obtained, Johnson and Shankland's[18,19] selection criteria was used to verify that the non-linear wave arose from interaction of the two primary waves. It was verified that all of the difference signals met the frequency, amplitude, directionality and time-of-arrival criteria.

For each sample, the frequency ratio f_2/f_1 at which the non-linear scattered wave amplitude was greatest was recorded. The normalised wave generation parameter β/β_0 was also found for each specimen using the recorded amplitudes and estimated attenuations, as described in Section 4. The average of five independent measurements for each specimen is superimposed as a red '×' on the laboratory-determined non-linear characterisation curve in Figure 6.

It is observed that the 'blind study' measurements follow closely with the non-linear characterisation curve trend. All of the measurements (0 h, 12 h, 24 h, 28 h, 32 h and 36 h) fall within the error boxes. The measurement with the largest deviation from the expected trend was for the value of f_2/f_1 for the sample oven-aged for 18 h; however, the β/β_0 fell within the expected range. Although care was taken to prepare the samples in a consistent manner, differences in the samples can arise during the ageing process (non-uniformity of the oxidation) and the stochastic nature of the aggregate structure. However, the greatest source of error appears to be in the estimation of the attenuation values, as they were estimated using subsurface waves, which is not as accurate as using a through-transmission set-up with incidentally-mounted transducers.

For the purposes of pavement evaluation and management, it would be advantageous to have a non-destructive technique to determine when an asphalt pavement is no longer able to self-heal or, stated otherwise, to determine when a permanent damage state has been reached in the pavement surface. The accuracy of the proposed method appears to be sufficient to make this determination if applied periodically throughout the life of the top surface layer of the pavement. For instance, a study by Braham *et al*[34] showed that the 24 h oven-ageing level

Table 2. Dilatational velocities using a normal incidence through-transmission technique and the procedure outlined in Section 4

Level of ageing (h)	Velocities using normal incidence (m/s)	Theoretically predicted from Snell's Law (m/s)	Percent error (%)	Experimentally measured from longitudinal subsurface waves in a through-transmission set-up (m/s)	Percent error (%)
0	3554	3452	2.9	3586	0.9
12	3792	3604	5.0	3674	3.1
24	4007	3916	2.3	4389	9.5
28	3284	3362	2.4	3346	1.9
32	2780	2830	1.8	2874	3.4
36	2861	2844	0.6	2667	6.8

Table 3. Dilatational attenuations at different frequencies using a normal incidence through-transmission technique and the procedure outlined in Section 4

Amount aged (h)	Dilatational attenuations							
	Experimentally measured using normal incidence through-transmission set-up[13] (Np/m)			Experimentally measured using critically-refracted longitudinal subsurface waves in a through-transmission set-up (Np/m)				
	120 kHz	160 kHz	200 kHz	120 kHz	Percent error (%)	160 kHz	Percent error (%)	200 kHz	Percent error (%)
0	35.8	35.4	42.2	36.8	2.8	41.7	17.9	48.7	15.4
12	33.0	32.5	39.3	36.1	9.3	38.6	18.8	48.4	23.1
24	32.9	31.6	37.3	33.5	1.7	33.2	5.1	38.4	3.0
28	30.2	33.4	45.4	35.1	16.3	40.9	22.3	50.2	10.5
32	47.1	58.9	77.5	41.8	11.2	59.0	0.2	74.4	3.9
36	59.6	68.0	95.9	70.1	17.6	81.0	19.0	108.2	13.3

Table 4. Shear attenuations for different ageing levels at the corresponding f_3 frequency using a normal incidence through-transmission technique and the procedure outlined in Section 4

Amount aged (h)	Shear attenuations		
	Experimentally measured using normal incidence through-transmission set-up (at corresponding f_3)[13] (Np/m)	Estimated using critically-refracted longitudinal subsurface waves in a through-transmission set-up (Np/m)	Percent error (%)
0	48.1	37.8	21.5
12	33.2	34.9	5.3
24	27.0	33.9	25.7
28	54.6	36.4	33.5
32	54.5	61.1	12.1
36	65.9	74.4	12.8

represented approximately seven years of field ageing. In some of the sections investigated, the field ageing experienced at seven years was sufficient for the development of temperature-induced thermal cracking. This conclusion was based on fracture energy testing of asphalt-aggregate mixtures, where field-aged core samples, field cracking *versus* time data and original materials stored at the time of pavement construction were available. Original materials were oven-aged to develop a fracture energy *versus* time relationship, which was then compared to fracture energy levels of materials sampled from seven-year-aged field sections.

Thus, based on observed field cracking, it appears that the 24 h oven-ageing level represents an ageing level where permanent damage may be retained in the asphalt mixture. This seems to correspond to the shift observed in Figure 6 between the 24 h and 28 h ageing when plotted in the f_2/f_1 *versus* β/β_0 space. Measurements taken on samples aged at 0 h, 12 h and up to 24 h fell in the lower plateau range, with 24 h of oven-ageing representing a breakpoint between the lower and upper plateau regions in Figure 6. A possible application of this technique in pavement engineering might involve the use of non-linear ultrasonics to assess and maintain treatments on asphalt pavement surfaces, such as the use of penetrating rejuvenators, to retain material behaviour safely in the right-hand side of the lower plateau (healing region), *ie* in the 0-12 h equivalent oven-ageing regime. This would prevent the pavement surface ageing to a condition where permanent damage and the

vulnerability towards large, discrete crack formation (such as thermal and block cracks) occurs.

8. Conclusions

A method has been introduced that allows for the non-collinear wave mixing technique to be used in the field to estimate the level of oxidative ageing in the top material layer of asphalt concrete (AC) pavements. The method requires only prior knowledge of the mixture type of the AC pavement. The method involves an iterative approach for finding the appropriate incident angle to generate subsurface longitudinal critically-refracted waves using shear wedges and longitudinal transducers. An approach is also presented to estimate the longitudinal and shear phase velocities and corresponding attenuations of the top material layer of the pavement. These material properties, which are also dependent upon the oxidative ageing level of the pavement material, are needed to estimate the non-linear response of the pavement material. The non-linear scattered waves, which arose from the wave mixing, were checked to ensure they arose from the wave mixing within the material and not from non-linearities in the testing apparatus by using Johnson and Shankland's selection criteria[19,20]. A two-dimensional space is introduced by cross-plotting f_2/f_1 *versus* β/β_0, *ie* the frequency ratio at which the maximum amplitude of the non-linear wave occurs and the normalised non-linear generation parameter, respectively. This leads to an 'oxidative-ageing non-linear characterisation curve' that is characteristic of each mixture type regarding its non-linear response to increasing levels of oxidative ageing. A blind study is also presented and the results indicate that the approach can be used in the field to evaluate the oxidative ageing levels of pavements once the mixture 'non-linear ageing characterisation curve' is known.

or recommendations expressed in this publication are those of the authors and do not necessarily reflect the views of the sponsoring agency.

References

1. D Y Lee, 'Development of a durability test for asphalts', Iowa Highway Research Board Project HR-124, Final Report ISU-ERI-72125, Engineering Research Institute, Iowa State University, 1972.

2. D Y Lee, 'Weathering of asphalts as characterised by infrared multiple internal reflection spectra', Applied Spectroscopy, Vol 27, No 6, pp 435-440, 1973.

3. E R Brown, P S Kandhal, F L Roberts, Y R Kim, D Lee and T W Kennedy, Hot Mix Asphalt Materials, Mixture, Design and Construction, Third Edition, NAPA Research and Education Foundation and NCAT, Maryland, 2009.

4. R Y Kim (Ed), Modeling of Asphalt Concrete, American Society of Civil Engineers Press, Chicago, and McGraw Hill, 2009.

5. M E McGovern, B Behnia, W G Buttlar and H Reis, 'Characterisation of oxidative ageing in asphalt concrete – Part 1: Ultrasonic velocity and attenuation measurements and acoustic emission response under thermal cooling', Insight, Vol 55, No 11, pp 596-604, 2013.

6. M E McGovern, B Behnia, W G Buttlar and H Reis, 'Characterisation of oxidative ageing in asphalt concrete – Part 2: Complex moduli estimation', Insight, Vol 55, No 11, pp 605-609, 2013.

7. M E McGovern, W G Buttlar and H Reis, 'Characterisation of oxidative ageing in asphalt concrete using a non-collinear ultrasonic wave mixing approach', Insight, Vol 56, No 7, pp 367-374, 2014.

8. M E McGovern, W G Buttlar and H Reis, 'Estimation of oxidative ageing in asphalt concrete', Insight, Vol 57, No 1, pp 25-34, 2015.

9. D E Bray and R K Stanley, Non-Destructive Evaluation, Revised Edition, CRC Press Inc, Boca Raton, 1997.

10. J L Rose, Ultrasonic Waves in Solid Media, Cambridge University Press, New York, 1999.

11. L Basatskaya and I Ermolov, 'Theoretical study of ultrasonic longitudinal subsurface waves in solid media', Soviet Journal of Non-Destructive Testing, Vol 16, pp 524-530, 1981.

12. A Pilarski and J Rose, 'Utility of subsurface longitudinal waves in composite material characterisation', Ultrasonics, Vol 27, pp 226-233, 1989.

13. K Langenberg, P Fellinger and R Marklein, 'On the nature of the so-called subsurface longitudinal wave and/or the subsurface longitudinal 'creeping' wave', Research in Non-Destructive Evaluation, Vol 2, pp 59-81, 1990.

14. S Chaki, W Ke and H Demouveau, 'Numerical and experimental analysis of the critically-refracted longitudinal beam', Ultrasonics, Vol 53, pp 65-69, 2013.

15. G L Jones and D R Kobett, 'Interaction of elastic waves in an isotropic solid', Journal of the Acoustical Society of America, Vol 35, No 1, pp 5-10, 1963.

16. F D Murnaghan, Finite Deformation of an Elastic Solid, John Wiley & Sons Inc, New York, 1951.

17. L D Landau and E M Lifshitz, Theory of Elasticity, Second Edition, Pergamon Press, New York, 1970.

18. Z A Goldberg, 'Interaction of plane longitudinal and transverse elastic waves', Soviet Physics: Acoustics, Vol 6, No 3, pp 306-310, 1960.

19. P A Johnson, T J Shankland, R J O'Connell and J N Albright, 'Non-linear generation of elastic waves in crystalline rock', Journal of Geophysical Research, Vol 92 (B5), pp 3597-3602, 1987.

20. P A Johnson and T J Shankland, 'Non-linear generation of elastic waves in granite and sandstone: continuous wave and travel time observations', Journal of Geophysical Research, Vol 94 (B12), pp 17729-17733, 1989.

21. L H Taylor and F R Rollins, 'Ultrasonic study of three-phonon interactions. I. Theory', Physical Review, Vol 136 (3A), pp A591-A596, 1964.

22. F R Rollins, L H Taylor and P H Todd, 'Ultrasonic study of three-phonon interactions. II. Experimental results', Physical Review, Vol 136 (3A), pp A597-A601, 1964.

23. A J Croxford, P D Wilcox, B W Drinkwater and P B Nagy, 'The use of non-collinear mixing for non-linear ultrasonic detection of plasticity and fatigue', Journal of the Acoustical Society of America, Vol 126 (5), pp EL117-EL122, 2009.

24. A Demcenko, R Akkerman, P B Nagy and R Loendersloot, 'Non-collinear wave mixing for non-linear ultrasonic detection of physical ageing in PVC', NDT&E International, Vol 49, pp 34-39, 2012.

25. F R Rollins, 'Phonon interactions and ultrasonic frequencies', Proceedings of the IEEE, Vol 53, No 10, pp 1534-1539, 1965.

26. R W Dunham and H B Huntington, 'Ultrasonic beam mixing as a measure of the non-linear parameters of fused silica and single-crystal NaCl', Physical Review, Vol 2, No 4, pp 1098-1107, 1970.

27. L K Zarembo and V A Krasil'nikov, 'Non-linear phenomena in the propagation of elastic waves in solids', Soviet Physics, Vol 13, No 6, pp 778-797, 1970.

28. P B Nagy, 'Fatigue damage assessment by non-linear ultrasonic materials characterisation', Ultrasonics, Vol 36, pp 375-381, 1998.

29. I A Viktorov, Rayleigh and Lamb Waves, Plenum Press, New York, 1967.

30. A A Maradudin, 'Surface acoustic waves', In: Nonequilibrium Photon Dynamics, W E Brown (Ed), Plenum Press, New York, pp 395-599, 1985.

31. A A Maradudin, 'Surface acoustic waves on real surfaces', Preprint, Department of Physics, University of California, Irvine, pp 82-147, 1985.

32. G A Maugin, 'Shear horizontal surface acoustic waves in solids', In: Wave Phenomena, Proceedings of European Mechanics Colloquium 226, D F Parker and G A Maugin (Eds), University of Nottingham, UK, pp 158-172, 1987.

33. G A Maugin, 'Elastic surface waves with transverse horizontal polarisation', Advances in Applied Mechanics, J W Hutchinson (Ed), Academic Press, New York, Vol 23, pp 373-434, 1983.

34. A F Braham, W G Buttlar, T Clyne, M Marasteanu and M Turos, 'The effect of long-term laboratory ageing on asphalt concrete fracture energy', Journal of the Association of Asphalt Paving Technologists, pp 417-454, Vol 78, 2009.

Effectiveness of Rejuvenators on Aged Asphalt Concrete using Ultrasonic Non-collinear Subsurface Wave Mixing

by Megan E. McGovern[*], Nicholas Farace[*], William G. Buttlar[†], and Henrique Reis[‡]

ABSTRACT

Rejuvenators are products that aim to restore the physical and chemical properties of aged bitumen. To evaluate rejuvenators' restorative properties of aged asphalt concrete, artificially oven-aged (for 36 h at 408 K [135 °C]) asphalt concrete specimens were coated with a rejuvenator (10% by weight of the binder) and left to dwell for the following prescribed amounts of time: 3 to 6 days in 1-day increments, 1 to 8 weeks in 1-week increments, and 12 weeks. After its dwell time, each specimen was evaluated using non-collinear mixing of critically refracted dilatational ultrasonic waves. The frequency ratio, f_2/f_1, at which the interaction took place and the normalized nonlinear wave generation parameter, β/β_0, were recorded and compared against a reference plot. The reference plot was created using asphalt concrete samples (with no rejuvenator) subjected to increasing levels of oxidative oven-aging. It was observed that the samples with a dwell time of five weeks and greater exhibited material response similar to the reference virgin specimen. From one to four weeks, the nonlinear parameters become closer to the virgin parameters with each successive week. The approach appears to be capable of estimating the rejuvenators' capacity of restoring the material response of the original asphalt concrete with increasing dwell time. Potential application to pavement maintenance is presented and discussed.

KEYWORDS: asphalt concrete pavements, oxidative aging, oven-aging, ultrasonics, nonlinear ultrasonics, non-collinear wave mixing, rejuvenators.

Introduction

Oxidation—the main mechanism behind aging of asphalt concrete, and hence, pavement deterioration—changes certain chemical properties of the asphalt binder; specifically, it changes its asphaltenes-to-maltenes ratio. Asphaltenes are defined by their insolubility in pentane and function as bodying agents, whereas maltenes are the residual constituents after asphaltene precipitation (Boyer, 2000; Buenrostro-Gonzales et al., 2001; Karlsson and Isacsson, 2006; Long, 1982). Types of maltenes include polar compounds/nitrogen bases (peptizers for the asphaltenes), acidiffins (solvent for the peptized asphaltenes), and paraffins (saturated hydrocarbons that act as a gelling agent) (Boyer, 2000; Buenrostro-Gonzales et al., 2001; Long, 1982; Shen et al., 2007). The asphaltenes-to-maltenes ratio influences the rheology of bitumen; as oxidation occurs, polar compounds and acidiffins are converted into asphaltenes, thus increasing the asphaltenes-to-maltenes ratio, resulting in a stiffer, more brittle asphalt binder. The reaction rate of oxidation can be accelerated at high temperatures or by high exposure to ultraviolet light. The amount of oxidation is also positively correlated to how much asphalt is exposed to air; therefore, stockpiling recycled asphalt materials may result in additional oxidation (Karlsson and Isacsson, 2006). Products have also been developed to counteract the effects of oxidation. Depending on the use of the products (preventative, corrective, maintenance, or recycling) these products have been called different names such as "service life extenders," "softening agents," "rejuvenator seals," and "recycling agents/additives" (Karlsson and Isacsson, 2006). For consistency, any such product is referred to as a "rejuvenator" in this study.

[*] M.S., Department of Industrial and Enterprise Systems Engineering, University of Illinois at Urbana-Champaign, 104 S. Mathews Ave., Urbana, Illinois 61801.

[†] Ph.D., Department of Civil and Environmental Engineering, University of Illinois at Urbana-Champaign, 205 N. Mathews Ave., Urbana, Illinois 61801.

[‡] Ph.D., Department of Industrial and Enterprise Systems Engineering, University of Illinois at Urbana-Champaign, 104 S. Mathews Ave., Urbana, Illinois 61801; (217) 333-1228; fax 217-244-5705; e-mail h-reis@illinois.edu.

Rejuvenators, as the name implies, are products that mostly aim to restore the physical and chemical properties of aged bitumen. Rejuvenators address the issue of oxidative hardening by softening the aged asphalt via the restoration of the original asphaltenes-to-maltenes ratio as discussed in the preceding paragraph (Buenrostro-Gonzales et al., 2001; Garcia et al., 2011; Shen et al., 2007). Some examples of rejuvenators are refined tallow, waste vegetable or frying oils, waste motor oils, lube extracts, extender oils, emulsions, soft virgin binders, and bio-binders (Buenrostro-Gonzales et al., 2001; Nahar et al., 2014; Oldham et al., 1988). Rejuvenators are generally applied to the surface of existing pavements; therefore, it is essential for the rejuvenator to have the ability to penetrate the surface and diffuse through the aged asphalt. If the rejuvenator lacks this ability, not only will the aged asphalt be unaffected, but the unabsorbed rejuvenator will reduce skid resistance (Brown, 1988; Garcia et al., 2011). To avoid creating slick, over-coated surfaces, it is often good practice to apply rejuvenators in several coats at a lower application rate (Boyer, 2000). Rejuvenators penetrate the pavement via capillary action and gravity; as a result, their penetration depends upon the pavement pore structure and tortuosity. During the diffusion process, the rejuvenator first forms a low-viscosity film around the layer of aged binder, which coats the aggregate. Then, the rejuvenator starts to diffuse into the aged binder, thus softening it. Eventually, all the rejuvenator penetrates into the aged binder. The inner layer becomes less viscous, and the outer layer becomes more viscous as the mixture approaches a state of equilibrium (Brown, 1988; Garcia et al., 2011). A 1974 study found that the rate of diffusion could be increased by adding diluents or by increasing temperature (Oliver, 1974). Thus, the environment in which rejuvenators are applied is of critical consideration, especially in terms of application rate. After a sufficient dwell time, the performance of the rejuvenator can be evaluated. For additional reading on rejuvenators, the reader is referred to the references (Lin et al., 2012; Rostler and White, 1970; Scofield and Timothy, 1986; Shen et al., 2006).

The ability of rejuvenators to improve pavements' durability is typically evaluated by: (1) estimating the penetration by comparing the penetration at 298 K (25 °C) in the asphalt binder extracted from untreated and treated cores; (2) comparing the viscosity at 333 K (60 °C) of the asphalt binder extracted from untreated and treated cores, and; (3) comparing the percentage loss of aggregate when untreated and treated samples are subjected to a pellet abrasion test (Boyer, 2000; Brown and Johnson, 1976). Mainly because these tests are cumbersome and time consuming, they are not often used. There exists a need for a more reliable technique for determining the effectiveness of rejuvenating agents. The non-collinear wave-mixing technique has been shown to be a reliable technique for assessing the amount of oxidative aging present in asphalt concrete (McGovern et al., 2014a; McGovern et al., 2014b). In this study, the effectiveness of rejuvenators, that is, the effective amount of aging of the asphalt concrete after rejuvenator application, is assessed via the non-collinear wave-mixing technique as a function of the dwell time.

## Oxidative Age Assessment of Pavements via Non-collinear Wave Mixing

Non-collinear wave mixing of critically refracted (that is, subsurface) dilatational waves can be used to assess the level of oxidative aging in asphalt concrete mixtures when access to only one side is available, that is, the top surface of a pavement (McGovern et al., 2014a; McGovern et al., 2014b). Two nonlinear parameters are measured via the non-collinear wave-mixing technique and compared with a reference plot to determine the amount of oxidative aging present in the material. The reference plot (or calibration curve) is mixture dependent, and was generated in a previous study by characterizing the nonlinear parameters of asphalt concrete specimens subjected to increasing levels of laboratory induced oxidative aging (McGovern et al., 2014a).

When two monochromatic, plane, sinusoidal waves, k_1 and k_2, with frequencies f_1 and f_2, respectively, propagate in a nonlinear elastic medium such that they intersect at an angle, φ, it is possible that they may interact to produce a third wave, $k_3 = k_1 \pm k_2$, with frequency $f_3 = f_1 \pm f_2$. This third wave is referred to as the nonlinear scattered wave. The polarization, direction of propagation, and frequency of the scattered wave depend on the polarization, direction of propagation, and frequency of the two interacting waves, termed the primary waves. The two primary waves may be dilatational or shear polarized in or out of the k_1-k_2 plane. The scattered wave may have a sum ($f_3 = f_1 + f_2$) or difference ($f_3 = f_1 - f_2$) frequency. Out of 54 potential interaction cases, only 8 satisfy the necessary resonance and polarization conditions for interaction to take place and a scattered wave to occur (Jones and Kobbett, 1963). In this study, the case where two dilatational waves interact was used, which generated a shear wave polarized in the k_1-k_2 plane with a difference frequency $f_3 = f_1 - f_2$. The reader is also referred to the references for a review of nonlinear elasticity and higher order elastic constants (Landau and Lifshitz, 1970; Murnagan, 1951).

A dilatational transducer mounted on variable angle wedge can be used to generate a dilatational wave, which propagates close to and nearly parallel to the surface by setting the incident angle close to the first critical refracted angle. It has been shown that an incident angle of 1° greater than the first critical angle is the optimal angle for generating a wave which propagates parallel to the surface; see Figure 1 (Chaki et al., 2013). These critically refracted dilatational waves are often also referred to as subsurface dilatational waves. The reader is referred to the references for more detailed information on subsurface waves (Basatskaya and Ermolov, 1981; Bray and Stanley, 1977; Chaki et al., 2013; Langenberg et al., 1990; Pilarski and Rose, 1989; Rose, 1999).
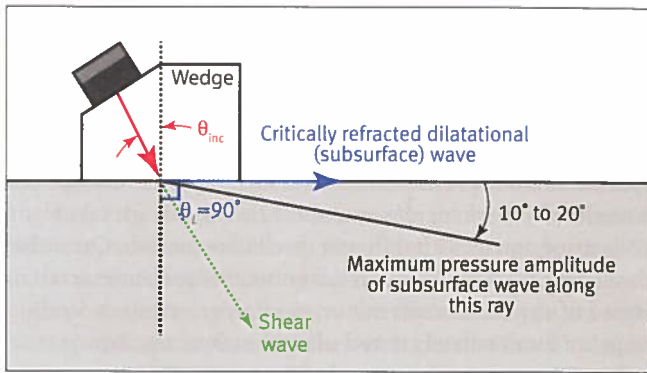
Figure 1. Schematic illustrating the use of dilatational transducers mounted on shear wedges to launch critically refracted dilatational waves. A subsurface dilatational wave is generated when θ_{inc} is set close to the first critically refracted angle.
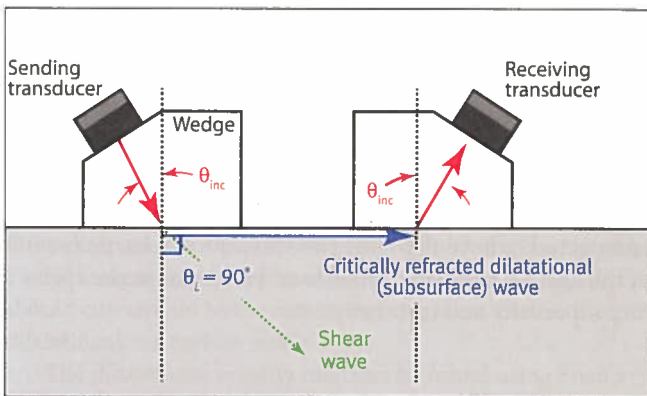
Figure 2. Schematic of through-transmission setup used to obtain experimental measurements of dilatational velocity and corresponding attenuation. The sending and receiving transducers are both mounted on wedges set to the same incident angle, θ_{inc}, to generate and receive a critically refracted dilatational subsurface wave, respectively.

To implement non-collinear wave mixing of subsurface dilatational waves, two dilatational transducers mounted on angle wedges can be oriented such that they generate two subsurface dilatational waves, k_1 and k_2, which intersect at an angle, φ (McGovern et al., 2014b). The two dilatational waves interact to generate a shear wave, k_3, which propagates in the direction γ with respect to k_1. This interaction takes place when the following conditions are met:

$$(1) \qquad \cos(\varphi) = \left(\frac{c_L}{c_S}\right)^2 \left(1 - \frac{1}{2}\frac{f_1}{f_2}\left[1 - \frac{c_S^2}{c_L^2}\right]\left[\frac{f_2^2}{f_1^2} + 1\right]\right)$$

$$(2) \qquad \tan(\gamma) = \frac{-f_2 \sin(\varphi)}{f_1 - f_2 \cos(\varphi)}$$

where

c_L and c_S are the dilatational and shear wave velocities of the medium, respectively (Jones and Kobbet, 1963).

If k_1 and k_2 are propagating close and parallel to the surface, k_3 will also propagate close and parallel to the surface. A good review of nonlinear acoustics and non-collinear wave mixing is provided by outside studies (Croxford et al., 2009; Demcenko et al., 2012; Goldberg, 1960; Nagy, 1998; Rollins, Jr., 1965; Rollins, Jr., et al., 1964; Taylor and Rollins, 1964).

Two parameters are of importance for assessing oxidative aging via the non-collinear wave-mixing technique: the frequency ratio, f_2/f_1, at which interaction occurs, and the normalized nonlinear wave generation parameter, β/β_0. Both f_2/f_1 and β/β_0 change with increasing levels of oxidative aging in asphalt concrete, making these parameters ideal for assessing the level of aging (McGovern et al., 2014a). The frequency ratio at which the interaction occurs can be determined by holding one of the frequencies constant (for example, f_1) and monitoring the amplitude of the nonlinear scattered wave as the other frequency (for example, f_2) is swept. The frequency ratio at which the nonlinear scattered wave amplitude reaches a maximum corresponds to the frequency ratio at which the interaction takes place. The β parameter describes the conversion efficiency at which energy is converted from the primary waves to the scattered nonlinear wave via the interaction and is found as:

$$(3) \qquad \frac{\beta_{age}}{\beta_0} = \frac{A_{age}^{*(k_3)}}{A_0^{*(k_3)}}$$

where

$$(4) \qquad A_{age}^{*(k_3)} = \frac{A_{age}^{(k_3)}}{\exp\left(-\left[\alpha^{(k_1)} + \alpha^{(k_2)}\right]D\right)\exp\left(-\alpha^{[k_3]}D_{k_3}\right)}$$

where

$A_{age}^{(k_3)}$ is the recorded amplitude of k_3,

$\alpha^{(k_n)}$ is the experimentally determined attenuation coefficient of wave k_n,

D_{k_n} is the distance traveled by wave k_n.

For this study, the propagation distance of the two primary waves is the same. The "age" subscript denotes the amount of oxidative oven-aging in hours, where "0" corresponds to a virgin specimen with no oxidative aging.

For the particular asphalt mixture used in this study, a reference curve was generated to characterize the f_2/f_1 and β/β_0 using laboratory aged specimens with increasing levels of oxidative aging (McGovern et al., 2014a). Prior to taking field measurements, the virgin nonlinear wave generation parameter, β_0, should be known. This can be accomplished by performing either laboratory measurements on a mixture of the same type or by taking measurements using specimens from the bottom protected layer of an extracted field core. Then, the β parameter, measured from the oxidized pavement

surface can be normalized by β_0, and the point $(f_2/f_1, \beta/\beta_0)$ can be plotted on the reference curve to estimate the level of the pavement oxidative aging.

Sample Preparation

Gyratory compacted asphalt concrete specimens were prepared using PG 64-22 binder with a target asphalt content of 5.9% by weight of the total mixture, and with a 4% air void content. The aggregate structure had a nominal maximum aggregate size of 19.5 mm, and it consisted of aggregates from four different stockpiles: 65% of coarse aggregate (CM16), 23% of manufactured sand (FM20), 10.5% of manufactured sand (FM02), and 1.5% of mineral filler. This mixture design followed Superpave guidelines.

The asphalt concrete mixtures were mixed using a standard bucket mixing procedure at a temperature of 428 K (155 °C). Then, the mixtures were oxidatively aged by placing the uncompacted mixtures in an oven at 408 K (135 °C) for 36 h. To ensure uniformity of the aging process (that is, uniform exposure to oxygen), the mixtures were hand-stirred every 12 h. A gyratory compactor was used to compact the loose mixture into cylinders with a nominal height of 175 mm and radius of 150 mm.

Test specimens (with approximate dimensions of $150 \times 175 \times 50$ mm) were then obtained by cutting 50 mm thick slabs along the longitudinal dimension of the gyratory specimens. Rejuvenator (in the amount of 10% of binder by weight) was applied to one of the two 150×175 specimen faces, after which the specimens were kept horizontal with their rejuvenator treated face on top. Care was taken to apply the rejuvenator in a thin, even layer across the entire face of the specimen. Each coated specimen was left to dwell for a specific amount of time: 3 to 6 days in 1-day increments, 1 to 8 weeks in 1-week increments, and 12 weeks for a total of 13 test specimens with different dwell time periods. Once the dwell time reached the desired amount, the specimen was wiped of any excess rejuvenator, to improve couplant conditions, and immediately tested using the ultrasonic non-collinear wave-mixing approach. The specimens were weighed before and after wiping the rejuvenator to determine how much rejuvenator was removed during the wiping process, as reported in Table 1.

The samples with low dwell times (< 5 days) had the greatest rejuvenator loss, because the rejuvenator did not have time to penetrate fully into the sample. It was observed that the rejuvenator penetrated some samples quicker than others, and it did not always penetrate the sample uniformly. The variability in rejuvenator penetration can be attributed to variability in porosity and tortuosity in the specimens. While the specimens were all compacted to have the same porosity, the stochastic nature of the asphalt concrete causes local variations in the specimens' porosity and tortuosity.

TABLE 1
Rejuvenator lost from wiping excess off the surface for samples after the various dwell times, and linear and nonlinear characterization values for the rejuvenator coated samples with different dwell times

Dwell time (weeks)	Rejuvenator lost (%)	Experimentally determined critical angle (°)	Dilatational velocity* (m/s)	Dilatational attenuation[†] k_1 (Np/m)	Dilatational attenuation[†] k_2 (Np/m)	Shear attenuation[‡] k_3 (Np/m)	Frequency ratio at which maximum nonlinear wave amplitude occurs (f_2/f_1)	Normalized nonlinear wave generation parameter (β/β_0)
0.50 (≈ 3 days)	34.1	72	3287	35.4	42.2	64.82	0.99	0.687
0.70 (≈ 4 days)	19.5	62	3445	64.14	61.28	57.49	0.64	0.706
0.78 (≈ 5 days)	7.5	55	3316	40.30	37.71	50.06	0.63	0.697
0.93 (≈ 6 days)	7.5	55	3468	53.00	57.00	50.06	0.61	0.674
1	2.0	50	3276	60.08	60.89	42.92	0.16	0.543
2	2.0	50	3687	31.29	31.64	42.92	0.03	0.594
3	5.7	54	3234	17.94	11.74	53.33	0.91	0.520
4	12.5	45	3215	52.18	47.23	38.05	0.41	0.581
5	9.3	56	3621	54.70	52.47	40.73	0.48	0.609
6	14.7	44	3708	47.11	46.68	33.74	1.07	0.587
7	7.5	55	3465	35.78	26.29	33.74	1.39	0.581
8	9.3	56	3754	55.98	41.01	51.28	0.24	0.555
12	1.8	52	3385	57.94	56.61	45.99	1.45	0.534

* The dilatational velocity was measured using the experimentally measured critical angle with Snell's Law; † the dilatational attenuation was measured experimentally via subsurface waves in a through-transmission configuration; ‡ the shear attenuation was estimated using an empirical relationship between the shear attenuation and dilatational velocity.

Linear Characterization

Prior to implementing the non-collinear wave-mixing technique, the asphalt concrete samples must be characterized with linear acoustics to determine the dilatational and shear phase velocities and corresponding attenuations, and the appropriate incident angles. Recall that the optimal incident angle corresponds to the case where the transmitted waves are subsurface dilatational waves, which propagate nearly parallel to the surface. Implementing the testing setup with the optimal incident angle allows for the dilatational velocity and corresponding attenuation to be determined with a fair degree of accuracy with access to only one side. Because no prior knowledge of the specimen is known, the incident angle is found experimentally. This is accomplished by mounting two dilatational transducers on variable angle wedges in a through-transmission setup, as illustrated in Figure 2. Both wedges are set to the same angle, and the signal is transmitted and recorded for various angles. The angle at which the amplitude reaches a maximum corresponds to the optimal incident angle to be used in future measurements for that aged mixture. It is important to window the beginning portion of the signal for data analysis, because reflections from the back surface may interfere with the measurements because of the finite dimensions of the test samples. Windowing the signal is a valid technique, as the first arriving portion of the signal should correspond to the fastest-arriving wave, that is, the dilatational, subsurface wave.

The dilatational velocity can then be found using Snell's law with the experimentally determined incident angle, θ_{inc}, as follows:

$$(5) \qquad c_L = \left(\frac{c_{wedge} \sin[\theta_R]}{\sin[\theta_{inc}]} \right)_{\theta_R = 90°} = \frac{c_{wedge}}{\sin(\theta_{inc})}$$

where

c_{wedge} is the dilatational velocity for the angle wedge,
θ_{inc} is the experimentally determined critical angle.

The refracted angle, θ_r, is 90° for the case of critical refraction. Alternatively, the dilatational velocity can be determined by measuring the time of flight of the first arriving portion of the through-transmission signal, and comparing it with a signal obtained in the same fashion for the angle wedges positioned at a different distance apart. The dilatational attenuation is found by filtering the signal about the appropriate frequency and measuring the amplitudes for signals obtained at two (or more) different distances apart. The shear attenuation is estimated using an empirical relationship with the dilatational velocity.

$$(6) \qquad \alpha_s (60 \text{ kHz} \leq f \leq 90 \text{ kHz}) \approx -0.031 c_L + 152.991$$

This empirical relationship is only valid for the asphalt concrete mixture-type of the sample set used in this study, for α_s in a frequency range of 60 to 90 kHz (which corresponds to the range of the nonlinear wave frequencies in this study), and for the dilatational velocity above the frequency at which it becomes non-dispersive (that is, frequency independent) (McGovern et al., 2013). There is very little variation between 60 and 90 kHz for α_s. Please note that the shear attenuation could also be estimated using the attenuation of surface waves in conjunction with the attenuation of the dilatational wave (Viktorov, 1967).

Experimental Setup and Procedure

Two dilatational transducers (center frequency of 500 kHz) were mounted on variable angle wedges oriented such that the transmitted waves, k_1 and k_2, propagated a distance of 8.2 cm (from the center of the wedge to point of intersection) and intersected at an angle of $\varphi = 47°$. The angle wedges (dilatational velocity = 2720 m/s) were set to an incident angle that corresponded to the experimentally found optimal incident angle described in the previous section.

Asphalt concrete consists of crushed stone (aggregates) of different sizes and shapes randomly distributed and held together by thin films of a bituminous binder. As a result of travelling through a highly heterogeneous media, the resulting shear wave goes through a significant level of mode conversion and scattering. This scattering and mode conversion lead to a spatially incoherent normal particle displacement at the surface. When this random normal displacement distribution is averaged over the large aperture of the receiving dilatational transducer (center frequency of 100 kHz), it leads to a temporally coherent but spatially incoherent output signal. The peak amplitude or total power of this signal can be measured to assess the strength of the resulting shear wave. A 1987 work provides a good discussion/review of shear horizontal surface acoustic waves in solids (Maugin, 1987). The receiving transducer was incidentally mounted on the same face of the asphalt specimen such that it was positioned 4 cm from the center of the intersection of the two waves (to the center of the transducer), at an angle of $\gamma = -37°$ with respect to k_1; see Figure 3.

A pulser receiver was used to generate and amplify k_1, a 15 burst sinusoidal signal at $f_1 = 200$ kHz. A function generator and a gated amplifier were used to generate and amplify k_2, an 8 burst sinusoidal signal, which was swept from $f_2 = 100$ to 180 kHz in 1 kHz increments. The number of cycles in the tonebursts was chosen to guarantee intersection between the two waves. A second-order butterworth filter was used to apply a gain to the received signal, as well as filter out any very low frequencies. Each received signal was averaged 300 times.

The size of the interaction region is important because the larger the interaction volume the higher the amplitude and directionality of the nonlinear wave. The volume of interaction is a function of the specimen dimensions and transducer beam divergence (see Figure 3 for an illustration of the interaction region). Considering the beam divergence, as the angle

between the transducer centerline and the point where the signal is half its strength, a characteristic length of the volume of interaction can be estimated at the point where the two primary beams intersect. The most limiting case corresponds to the specimen aged 24 h, which corresponds to the longest wavelengths. Comparing this characteristic length with the number of possible signal wavelengths within the region of interaction, the characteristic length of the volume of interaction is always greater than 3.5× the largest signal wavelength, that is, k_2, for the entire test sample set.

The experiment was carried out as follows: first, data were collected when the two transducers were operated simultaneously; second, data were collected when only one transducer was operated individually; and third, data were collected when the other transducer was operated individually. To obtain the nonlinear signal, the time-domain records obtained in the second and third steps were subtracted from the time-domain record obtained in the first step. The resulting signal is termed the difference signal and primarily consists of the nonlinear scattered wave resulting from the primary wave interaction. Some of the primary wave energy still exists in the difference signal because the subtraction is imperfect. Some of the energy in the primary waves is converted to the scattered shear wave in the interaction; therefore, the amplitude from the signal obtained with the transducers operating simultaneously is slightly smaller than the sum of the amplitudes obtained when the transducers are operated individually. A filter is then applied to the difference signal to remove most of the primary wave signals still remaining after the subtraction.

It is essential to verify that the difference signal satisfies the selection criteria to ensure that the nonlinearities result from the primary wave interaction and not from the testing apparatus (Johnson et al., 1987; Johnson et al., 1989). These selection criteria include: amplitude criterion—the nonlinear scattered wave should have an amplitude that is proportional to the product of the primary wave amplitudes; frequency criterion—the nonlinear scattered wave should have a frequency, f_3, which matches that predicted by theory (that is, $f_3 = f_1 - f_2$); and directionality criterion—the nonlinear scattered wave should propagate in the direction predicted by theory (that is, γ with respect to k_1). A time of flight criterion is also used, where the predicted time of flight (assuming a straight-ray path) should coincide with the observed time of flight.

Experimental Results

As described in the previous sections, the non-collinear wave-mixing technique can be used to determine the level of oxidative aging of asphalt concrete. First, the procedure is described by way of an example. The technique is then used to evaluate the effectiveness of rejuvenator in restoring the aged mixture for increasing periods of dwell time.

Assessment of Oxidative Aging via Non-collinear Wave Mixing

To assess the amount of oxidative aging in a sample, the nonlinear parameters, f_2/f_1 and β/β_0, can be measured and compared against a reference plot for that mixture type. The reference plot was generated in a previous study by characterizing the nonlinear parameters of a sample set of asphalt concrete specimens subjected to controlled amounts of oxidative aging (McGovern et al., 2014a). To illustrate the characterization of the samples' oxidative aging via the non-collinear wave-mixing approach, the characterization of the unaged virgin sample is described here in detail.

Recall that the data collection consists of three steps. Figure 4 shows the time-domain records obtained during data collection on the virgin sample. As f_2 is swept, the amplitude of the difference signal is recorded, as shown in Figure 4c.
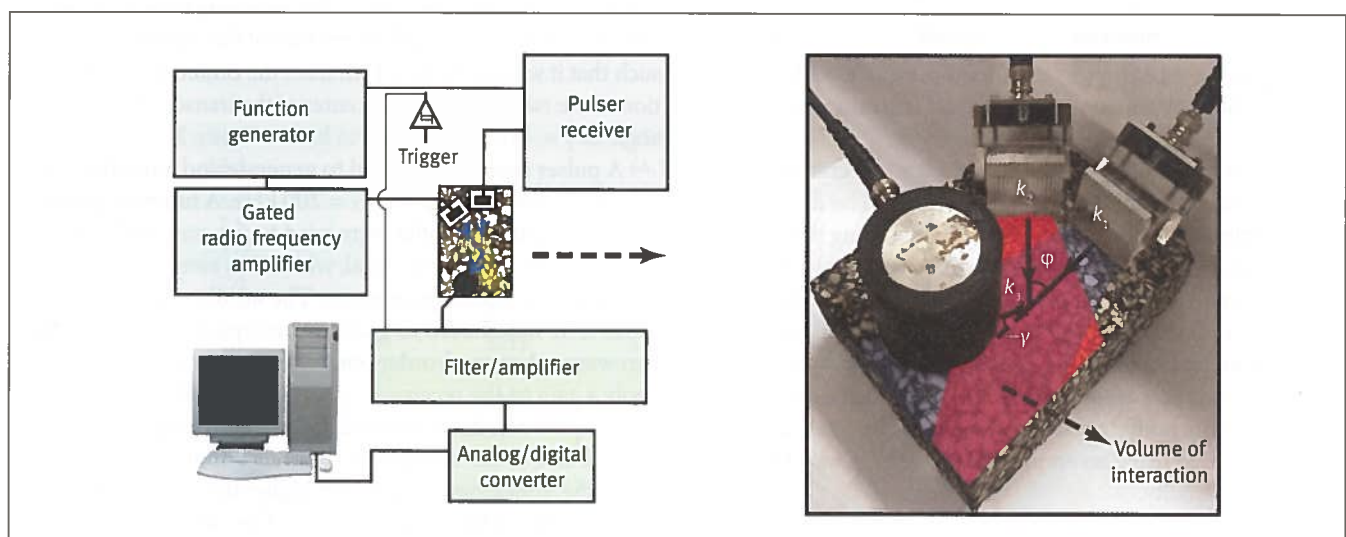
Figure 3. Schematic of the ultrasonic data collection system illustrating the angle of interaction of the two dilatational waves and the location of the receiving transducer to receive the generated scattered shear wave. The blue and red regions denote the areas of signals k_1 and k_2, respectively, due to beam spread. The overlap is the volume of interaction. Note, the beam spread from k_2 is slightly higher than k_1 because of the difference in frequencies. Note also the geometry of the test samples and that access to only one surface is needed.

The point at which it reaches a maximum corresponds to the frequency ratio, f_2/f_1, at which the interaction occurs. Figure 5 shows a representative example of the amplitude measurements of the difference signal as f_2 is swept. The observed and theoretically determined frequency ratio matches closely

(≈3.3% error). Please note that the time-domain records shown in Figure 4 correspond to the signals obtained when the nonlinear scattered wave reached maximum amplitude. The theoretically predicted time of arrival of 0.103 ms for the difference signal matches closely (≈9.7% difference) with the
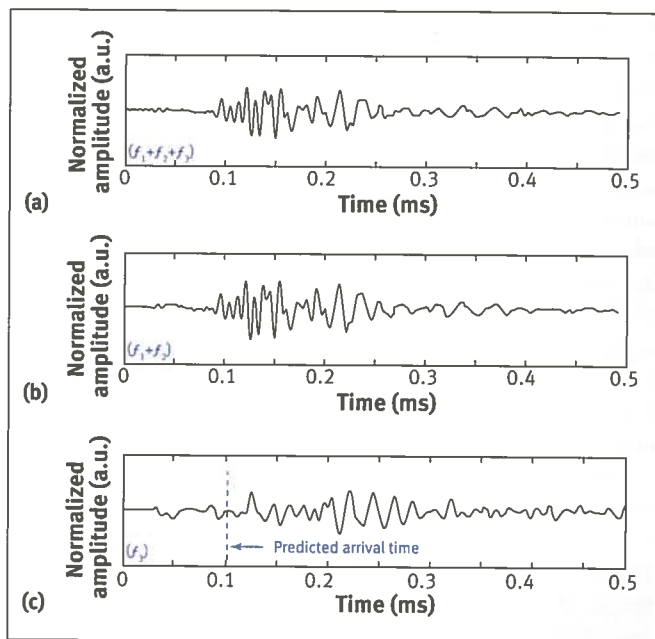

Figure 4. Time domain records required to obtain the nonlinear scattered shear wave: (a) when both sending transducers were operated simultaneously; (b) when sending transducers were operated one at a time and the received waveforms added; and (c) nonlinear scattered wave (the difference signal) obtained from subtracting the signals obtained from operating the sending transducers individually from the signal obtained when operating the two sending transducers simultaneously. Records are normalized by the maximum amplitude of that in Figure 4b. The difference signal was scaled up 10 times.
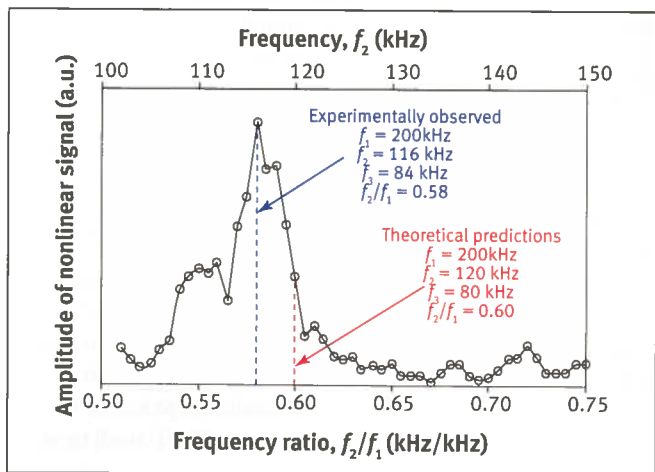

Figure 5. Experimentally obtained amplitude of scattered shear wave, that is, difference signal, ($f_3 = f_1 - f_2$) as f_2 is swept from 100 to 180 kHz ($f_2/f_1 = 0.50$ to 0.90) while f_1 is held constant at 200 kHz for the unaged virgin specimen.
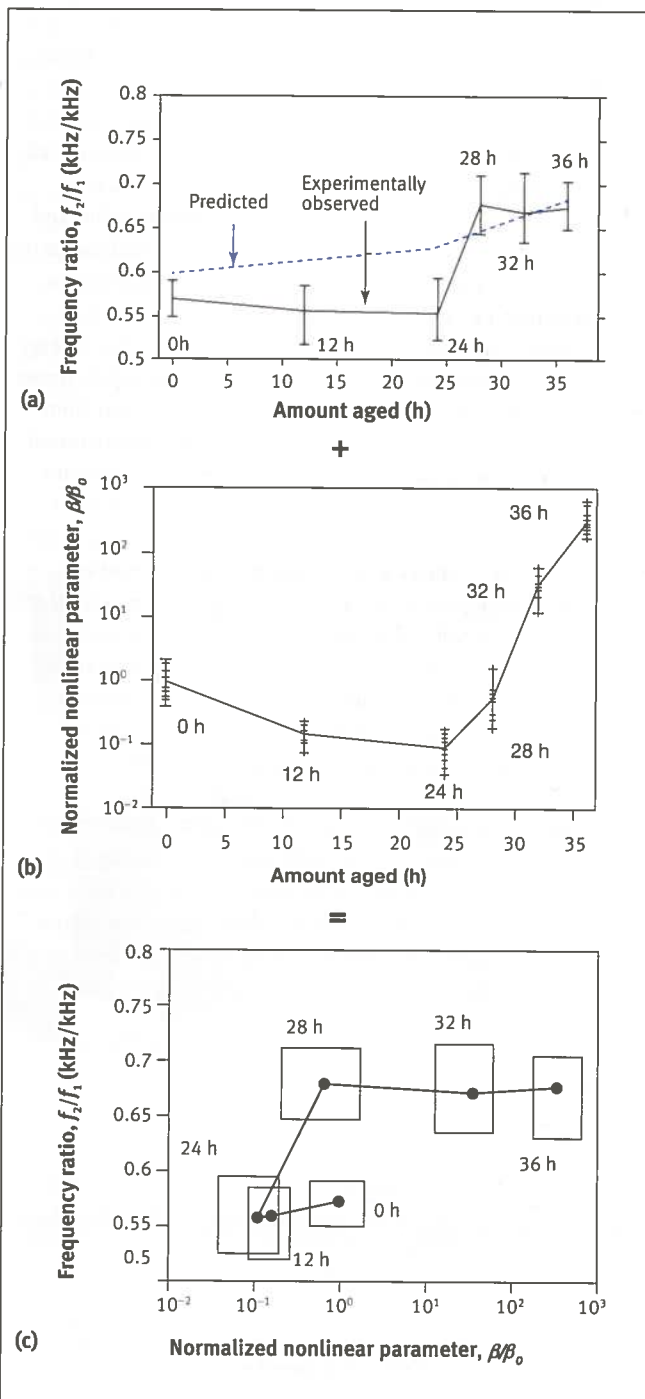

Figure 6. Generation of the reference curve: (a) frequency ratio at which maximum nonlinear wave amplitude occurs, f_2/f_1; (b) normalized nonlinear parameter, β/β_0; and (c) the created reference curve. Note that Figure 6a and b are experimentally determined from specimens with increasing levels of controlled oxidative aging and are used to create Figure 6c.

experimentally observed time of arrival of 0.113 ms. The time of flight measurement is not necessary to characterize the sample's nonlinearities; rather, it indicates that the difference signal is a result of the nonlinear interaction and not from system nonlinearities.

Figure 5 shows the experimentally obtained amplitude of scattered shear wave, that is, difference signal, ($f_3 = f_1 - f_2$) as f_2 is swept from 100 to 180 kHz ($f_2/f_1 = 0.50$ to 0.90) while f_1 is held constant at 200 kHz for the unaged virgin specimen. The dashed blue line represents the experimentally observed maximum and the dashed red line represents the theoretically predicted maximum. The same set of measurements was repeated for the set of asphalt concrete specimens subjected to various amounts of laboratory-induced controlled oxidative aging. Once the values of f_2/f_1 and β/β_0, were obtained for each specimen, the plots of frequency ratio versus level of aging (Figure 6a) and of the normalized nonlinear parameter versus aging (Figure 6b) were constructed. Based upon these two figures, the reference plot shown in Figure 6c was then constructed. Please note that the experimentally determined linear acoustic parameters (that is, critical angles, velocities, and attenuations) do not uniquely characterize the binder oxidative aging; see Figure 6a. Thus, while the linear acoustic parameters can be used as an indicator of the amount of aging, a unique representation is only achieved when used in conjunction with nonlinear measurements; see Figure 6c. In Figures 6a–c, the data points (dots) represent an average of ten independent measurements for each level of oxidative aging, and the error bars represent the maximum and the minimum of these ten independent measurements.

Rejuvenator Treated Specimens and Rejuvenator Effectiveness

Prior to implementing the non-collinear wave-mixing technique, the optimal incident angles were measured experimentally and were found to vary with the dwell time; see Figure 7 and Table 1. In a previous study, the optimal angle for a virgin specimen (that is, no rejuvenator or oxidative aging) and for
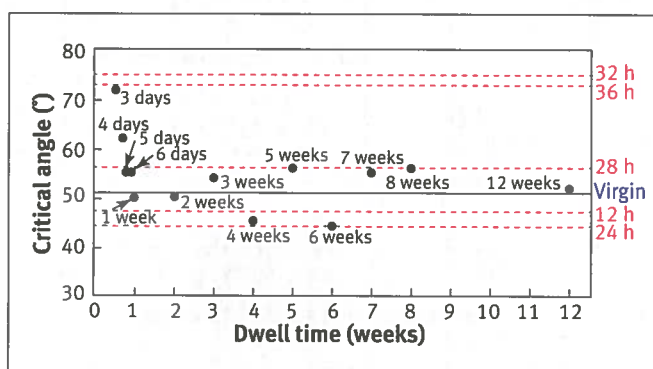

Figure 7. Experimentally measured critical angles of asphalt concrete samples with different dwell times after being treated with rejuvenator. For comparison, lines indicating critical angles of specimens subjected to various amounts of aging (with no rejuvenator) are also shown.

oven-aged specimens for 36 h (with no rejuvenator) was found to be 51 and 73°, respectively. For specimens with a dwell time of 3 to 5 days, the optimal angle approached the virgin specimen optimal angle with each successive day. For specimens with a dwell time greater than 5 days, the optimal angles varied about the virgin optimal angle within a ±7° range. These angles were all observed to be closer to the angle corresponding to the virgin sample than that of the 36 h, indicating that the rejuvenator is having a restorative effect on the aged specimens. For the specimens with a dwell time greater than 5 days, the largest difference (14.7% difference with respect to the virgin angle of 51°) corresponded to the sample with a dwell time of 6 weeks, which had an experimentally determined optimal angle of 44°. It is interesting to note that the samples with 5, 7, and 8 weeks dwell time had incident angles of 56° (55° for the 7 week sample), which was larger than the virgin incident angle. This suggests that the oxidative damage was not fully reversed. This suggests that the rejuvenator did not penetrate as thoroughly as in the other samples, leaving regions of low porosity of unrestored binder.

The dilatational velocity and corresponding attenuation values were found using subsurface dilatational waves in the through-transmission configuration, as described in Figure 2. The shear attenuation coefficient was calculated using the empirical relation from Equation 6. This empirical relation was derived in a previous study using data obtained using bulk waves in a traditional through-transmission setup, where sending and receiving sensors were placed on opposite parallel sides of the specimen (McGovern et al., 2013). Subsurface dilatational waves have a different beam profile than traditional bulk waves, which may result in discrepancies in the shear attenuation estimate with the actual shear attenuation. Refer to Table 1 for a summary of the experimentally determined linear acoustic parameters.

Non-collinear wave mixing with subsurface dilatational waves was carried out for each specimen using the experimentally determined optimal incident angles. The f_2/f_1 and β/β_0 values were determined for each specimen and plotted on the reference curve, which was found in a previous study (McGovern et al., 2014b). Figure 8 shows selected data from some of the rejuvenator coated specimens (red crosses) superimposed on the reference curve, where not all of the data was plotted to facilitate viewing (Table 1 shows the nonlinear parameters measured for the entire sample set). In Figure 8, each data point (red crosses) represents the average of five independent measurements. It is observed that past 4 weeks of dwell time, the samples have f_2/f_1 and β/β_0 values that are within experimental error of the nonlinear parameters for the virgin specimen. For the specimen with a dwell time of 8 weeks, there was a large amount of excess rejuvenator that was wiped off; see Table 1. This explains why the nonlinear parameters deviated from the virgin nonlinear parameters further than the specimens with a lower dwell time of 5 and 6 weeks. For the specimens with a dwell time of
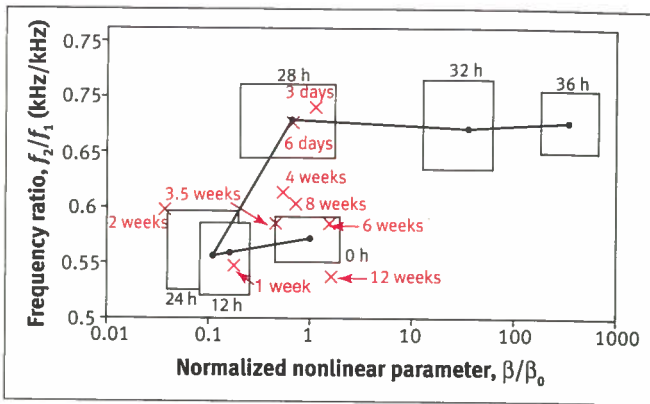
Figure 8. Frequency ratio f_2/f_1 versus the normalized nonlinear wave generation parameter, β/β_0, for the rejuvenated specimens (red crosses), plotted against the reference curve for the mixture. Each of the red crosses represents an average of five measurements. The reference curve represents the evolution of the oxidative oven-aging damage and is mixture dependent.

4 weeks and under, the nonlinear parameters deviated further from the virgin parameters in a manner that may be correlated with the dwell time. From 0.5 to 4 weeks, the nonlinear parameters become closer to the virgin parameters with each successive week.

Figure 9 shows some representative selected data that were used to find the f_2/f_1 values. Recall that f_2/f_1 is found by holding f_1 constant, monitoring the amplitude of k_3 ($f_3 = f_1 - f_2$) as f_2 is swept, and determining the point at which k_3 reaches maximum amplitude. Figure 9a shows the amplitude of k_3 as f_2 was swept for a few selected samples. For some samples (for example, the samples with dwell times of 4 days, 1 week, and 2 weeks), the process was relatively straightforward: the peak amplitude was located with respect to the f_2/f_1 ratio. However, the presence of multiple peaks in some samples makes the analysis more difficult (for example, the samples with dwell times of 6 days, 4 weeks, 6 weeks, and 8 weeks). Multiple peaks can occur due to non-uniformity of
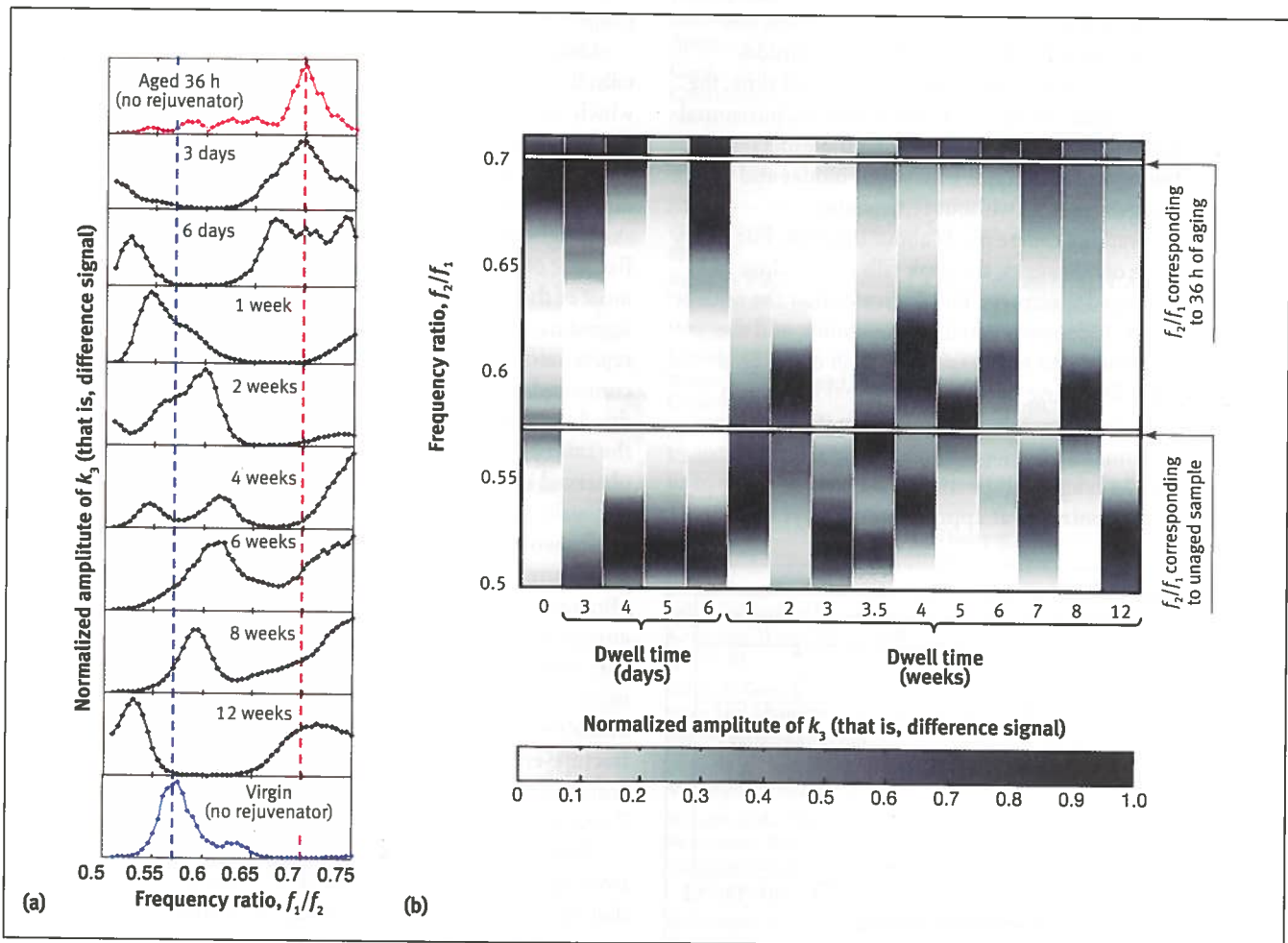

Figure 9. Normalized amplitude of the scattered waves: (a) the normalized amplitude of the scattered wave versus frequency ratio, f_2/f_1, for different dwell times; and (b) the frequency ratio versus dwell time in one plane and the normalized amplitude (using a gray scale) in the axis perpendicular to the plane. Amplitudes are normalized for each sample using the maximum value for that sample; see normalized bar code of the difference signal. This was done to enhance visualization of the results but prevents comparison of the difference signal amplitudes among the test specimens. Note that at each dwell time, the color code is normalized from 0 to 1.

the rejuvenator penetration in the finite interaction volume; see Figure 3. Within this volume, as expected, the rejuvenator does not necessarily penetrate and act on the binder in a uniform manner, which may result in pockets of unaffected, aged binder and pockets of rejuvenated binder. Thus, interactions will occur at different f_2/f_1 ratios, since the binder properties vary with location within the interaction region. The non-uniformity of the degree of binder restoration has the effect of lowering the experimentally measured velocity and increasing the experimentally measured attenuation, because the primary waves and resulting scattered wave may travel through both areas of unaffected binder and rejuvenated binder before being received by the receiving transducer.

Figure 9b shows the normalized amplitude of the scattered wave with respect to the dwell time and frequency ratio f_2/f_1, where the amplitude is depicted as a gray scale in the axis perpendicular to the plane. For each sample, these amplitudes are normalized using the maximum value for that sample (see normalized bar code of the difference signal). This was done to enhance visualization of the results, but prevents comparison of the difference signal amplitudes among the test specimens. Note that for each dwell time, the gray scale is normalized from 0 to 1. For reference, horizontal lines are superimposed on the plot showing the expected location of the peaks for samples with virgin binder and for samples oven-aged for 36 h without rejuvenator.

A few observations can be made about this plot. For a very short dwell time of 0.5 weeks, the peak falls at 0.7, close to that of the 36 h aged specimen. This indicates that the rejuvenator has not yet discernably acted on the binder, and the specimen still very much behaves as the 36 h oven-aged sample. For the following days, multiple peaks begin to appear, one at approximately $f_2/f_1 = 0.67$ to 0.7 and the other at approximately $f_2/f_1 = 0.52$, which correspond to 36 h and 12 to 24 h aged, respectively. At 1 week, most of the energy is concentrated at approximately $f_2/f_1 = 0.55$,

which corresponds to 12 to 24 h of oven aging. From 1 to 4 weeks, there are very broad, and sometimes multiple sets of peaks at approximately $f_2/f_1 = 0.53$ to 0.61. From 5 to 8 weeks, most of the energy seems to converge about one peak centered at $f_2/f_1 = 0.59$, which corresponds to 0 h of oven aging, that is, virgin. Note that there is still some energy at $f_2/f_1 = 0.7$, which indicates that portions of the binder remain unaffected by the rejuvenator. For this reason, measurements were also taken after 12 weeks of dwell time to determine whether these portions of unaffected binder were completely isolated from the rejuvenator or if the rejuvenator was still acting on the binder. It was observed that the 12 week sample exhibited two peaks at $f_2/f_1 = 0.53$ and $f_2/f_1 = 0.7$, where the peak at $f_2/f_1 = 0.53$ was more dominant. The presence of the peak at $f_2/f_1 = 0.7$ may indicate that portions of the binder do remain unaffected by the rejuvenator. The peak at $f_2/f_1 = 0.53$ corresponds to a sample oven-aged for 12 to 24 h. This may indicate that the rejuvenator did not fully restore the entire material volume to its original properties.

Once the frequency ratio, f_2/f_1, is determined experimentally, the velocity ratio, c_S/c_L, can also be found from Equation 1, which shows that for a fixed angle of interaction the value of f_2/f_1 depends only upon the ratio c_S/c_L, that is, depends only upon linear measurements. Figure 10 shows the corresponding velocity ratios as a function of the dwell time. Figure 10 sheds light onto the rejuvenator effect upon the binder. Because of the mesoscopic nature of the asphalt concrete, most of the deformation occurs in the binder. Because of the aggregate interlocking, the softening of the binder due to the rejuvenator has smaller influence upon the shear velocity (as compared to the dilatational velocity). This implies that as the dwell time increases, the dilatational velocity decreases and the ratio c_S/c_L increases, which explains some of the results observed in Figures 9 and 10, for example, the sample with 12 weeks of dwell time.

Previous study has shown that the 24 h of oven-aging level represents approximately seven years of field aging (Braham et al., 2009). This conclusion was based on fracture energy testing of asphalt-aggregate mixtures, where field-aged core samples, field cracking versus time data, and original materials stored at the time of pavement construction were available. Original materials were oven-aged to develop a fracture-energy-versus-time relationship, which was then compared to fracture energy levels of materials sampled from 7-year aged field sections.

Based on observed field cracking, it appears that the 24 h oven-aging represents an aging level where permanent damage may be retained in the asphalt mixture, that is, the mixture loses the self-healing property. This seems to correspond to the shift observed in Figure 8 between the 24 and 28 h aging when plotted in the f_2/f_1 versus β/β_0 space. Measurements taken on the rejuvenated samples after 4 weeks of dwell time (some earlier depending upon porosity) all fell in
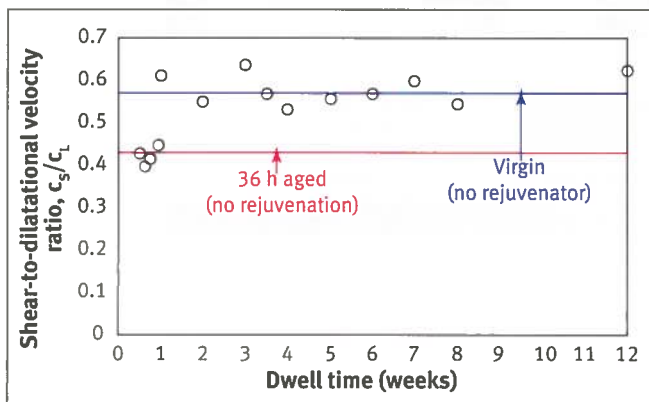

Figure 10. Velocity ratio, c_S/c_L, for each dwell time as determined by the experimentally measured frequency ratios, f_2/f_1. For reference, the blue solid and red dashed lines denote the values for the virgin, and 36 h of aging specimens, respectively, without exposure to rejuvenator.

the lower plateau range, with 24 h of oven aging representing a breakpoint between the lower and upper plateau regions on Figure 8. A possible application of this technique in pavement sustainability might involve treatments on asphalt pavement surfaces using penetrating rejuvenators to retain material behavior safely in the right-hand side of the lower plateau (self-healing region), that is, in the 0 to 24 equivalent oven-aging regime. This would prevent allowing the pavement surface to age to a condition where permanent damage and the vulnerability towards large, discrete crack formation (such as thermal and block cracks) can occur.

Conclusion

Asphalt concrete specimens subjected to 36 h of laboratory-induced oxidative oven-aging, and coated with rejuvenator (10% by weight of the binder), were ultrasonically tested using the non-collinear wave mixing of critically refracted dilatational waves after the following prescribed amount of dwell time periods: 3 to 6 days in 1 day increments, 1 to 8 weeks in 1 week increments, and 12 weeks. The frequency ratio, f_2/f_1, at which the wave interaction took place and the normalized nonlinear wave generation parameter, β/β_0, were recorded and compared against a reference plot for the mixture, which was created using asphalt concrete samples (with no rejuvenator) subjected to increasing amounts of oxidative oven aging. It was observed that the samples with a dwell time greater than 4 weeks exhibited nonlinear characteristics similar to the reference virgin specimen. From 0.5 to 4 weeks, the nonlinear parameters become closer to the virgin parameters, indicating that it takes time for the rejuvenator to penetrate the specimen and chemically act upon the aged binder. Also, it was observed that the rejuvenator penetrates the specimens in a non-uniform manner, which has the effect of also acting on the binder non-uniformly. In the field, to overcome the effects of the observed variability (due to the stochastic nature of the asphalt concrete), it is recommended that an average of several measurements be taken at different locations on the pavement.

REFERENCES

Basatskaya, L., and L.N. Ermolov, "Theoretical Study of Ultrasonic Longitudinal Subsurface Waves in Solid Media," *Soviet Journal of Nondestructive Testing*, Vol. 16, 1981, pp. 524–530.

Boyer, R.E., "Asphalt Rejuvenators 'Fact, or Fable'," Asphalt Institute, Panama City, Florida, 2000.

Braham, A.F., W.G. Buttlar, T.R. Clyne, M.O. Marasteanu, and M.I. Turos, "The Effect of Long-term Laboratory Aging on Asphalt Concrete Fracture Energy," *Journal of the Association of Asphalt Paving Technologists*, Vol. 78, 2009, pp. 417–454.

Bray, D.E., and R.K. Stanley, *Nondestructive Evaluation*, revised ed., CRC Press, Boca Raton, Florida, 1997.

Brown, E.R., "Preventive Maintenance of Asphalt Concrete Pavements," Report No. 88-1, National Center for Asphalt Technology, Auburn, Alabama, 1988.

Brown, E.R., and R.R. Johnson, "Evaluation of rejuvenators for Bituminous Pavements," *AFCEC-TR-76-3*, Air Force Civil Engineering Center, Tyndall Air Force Base, Florida, 1976.

Buenrostro-Gonzalez, E., H. Groenzin, C. Lira-Galeana, and O. C. Mullins, "The Overriding Chemical Principles that Define Asphaltenes," *Energy Fuels*, Vol. 15, No. 4, 2001, pp. 972–978.

Chaki, S., W. Ke, and H. Demouveau, "Numerical and Experimental Analysis of the Critically Refracted Longitudinal Beam," *Ultrasonics*, Vol. 53, No. 1, 2013, pp. 65–69.

Croxford, A.J., P.D. Wilcox, B.W. Drinkwater, and P.B. Nagy, "The Use of Non-collinear Mixing for Nonlinear Ultrasonic Detection of Plasticity and Fatigue," *Journal of the Acoustical Society of America*, Vol. 126, No. 5, 2009, pp. EL117–EL122.

Demcenko, A., R. Akkerman, P.B. Nagy, and R. Loendersloot, "Non-collinear Wave Mixing for Non-linear Ultrasonic Detection of Physical Aging in PVC," *NDT&E International*, Vol. 49, 2012, pp. 34–39.

García, Á., E. Schlangen, and M. Van de Ven, "Properties of Capsules Containing Rejuvenators for their Use in Asphalt Concrete," *Fuel*, Vol. 90, No. 2, 2011, pp. 583–591.

Goldberg, Z.A., "Interaction of Plane Longitudinal and Transverse Elastic Waves," *Soviet Physical Acoustics*, Vol. 6, No. 3, 1960, pp. 306–310.

Jones, G.L., and D.R. Kobett, "Interaction of Elastic Waves in an Isotropic Solid," *Journal of the Acoustical Society of America*, Vol. 35, No. 5, 1963, pp. 5–10.

Johnson, P.A., T.J. Shankland, R.J. O'Connell, and J.N. Albright, "Nonlinear Generation of Elastic Waves in Crystalline Rock," *Journal of Geophysical Research*, Vol. 92, No. B5, 1987, pp. 3597–3602.

Johnson, P.A., and T.J. Shankland, "Nonlinear Generation of Elastic Waves in Granite and Sandstone: Continuous Wave and Travel Time Observations," *Journal of Geophysical Research*, Vol. 9, No. B12, 1989, pp. 17729–17733.

Karlsson, R., and U. Isacsson, "Material-related Aspects of Asphalt Recycling—State-of-the-art," *Journal of Materials in Civil Engineering*, Vol. 18, No. 1, 2006, pp. 81–92.

Landau, L.D., and E.M. Lifshitz, *Theory of Elasticity*, second ed.. Pergamon Press, New York, New York, 1970.

Langenberg, K., P. Fellinger, and R. Marklein, "On the Nature of the So-called Subsurface Longitudinal Wave and/or the Subsurface Longitudinal 'Creeping' Wave," *Research in Nondestructive Evaluation*, Vol. 2, 1990, pp. 59–81.

Lin, J., P. Guo, L. Wan, and S. Wu, "Laboratory Investigation of Rejuvenator Seal Materials on Performances of Asphalt Mixtures," *Construction and Building Materials*, Vol. 37, December 2012, pp. 25–41.

Long, R.B., "The Concept of Asphaltenes," Chapter 2, *Chemistry of Asphaltenes*, 1982, pp. 17–27.

Maugin, G.A., "Shear Horizontal Surface Acoustic Waves in Solids," *Wave Phenomena: Recent Developments in Surface Acoustic Waves*, Proceedings of European Mechanics Colloquium 226, University of Nottingham, U.K., 2–5 September 1987, pp. 158–172.

McGovern, M., B. Behnia, W.G. Buttlar, and H. Reis, "Characterization of Asphalt Concrete Oxidative Aging – Part 1: Acoustic Emission Response and Ultrasonic Velocity and Attenuation Measurements," *Insight – Nondestructive Testing and Condition Monitoring*, Vol. 55, No. 11, 2013, pp. 1–9.

McGovern, M., B. Behnia, W.G. Buttlar, and H. Reis, "Characterization of Oxidative Aging in Asphalt Concrete using Non-collinear Ultrasonic Wave Mixing" *Insight – Nondestructive Testing and Condition Monitoring*, Vol. 56, No. 7, 2014a, pp. 367–374.

McGovern, M.E., W.G. Buttlar, and H. Reis, "Estimation of Oxidative Aging in Asphalt Concrete Pavements using Non-collinear Wave Mixing of Critically Refracted Longitudinal Waves," *Insight – Nondestructive Testing and Condition Monitoring*, Vol. 57, No. 1, 2014b, pp. 25–34.

Murnaghan, F.D., *Finite Deformation of an Elastic Solid*, John Wiley & Sons, Inc., New York, New York, 1951.

Nagy, P.B., "Fatigue Damage Assessment by Nonlinear Ultrasonic Materials Characterization," *Ultrasonics*, Vol. 36, Nos. 1–5, 1998, pp. 375–381.

Nahar, S.N., J. Qiu, A.J.M. Schmets, E. Schlangen, M. Shirazi, M.F.C. Van de Ven, G. Schitter, and A. Scarpas, "Turning Back Time: Rheological and Microstructural Assessment of Rejuvenated Bitumen," *Journal of the Transportation Research Board*, 2014, pp. 52–62.

Oldham, D.J., E.H. Fini, and T. Abu-Lebdeh, "Investigating the Rejuvenating Effect of Bio-binder on Recycled Asphalt Shingles," *Transportation Research Board 93rd Annual Meeting Compendium of Papers*, 2014.

Oliver, J.W.H., "Diffusion of Oils in Asphalts," *Industrial & Engineering Chemistry Product Research and Development*, Vol. 13, No. 1, 1974, pp. 65–70.

Pilarski, A., and J. Rose, "Utility of Subsurface Longitudinal Waves in Composite Material Characterization," *Ultrasonics*, Vol. 27, No. 4, 1989, pp. 226–233.

Rollins, Jr., F.R., L.H. Taylor, and P.H. Todd, Jr. "Ultrasonic Study of Three-phonon Interactions. II. Experimental Results," *Physical Review*, Vol. 136, No. 3A, 1964, pp. A597–A601.

Rollins, Jr., F.R., "Phonon Interactions and Ultrasonic Frequencies," *Proceedings of the IEEE*, Vol. 53, No. 10, 1965, pp. 1534–1539.

Rose, J.L., *Ultrasonic Waves in Solid Media*, Cambridge University Press, New York, New York, 1999.

Rostler, F.S., and R.M. White, "Rejuvenation of Asphalt Pavements," Technical Report, Materials Research and Development, Inc., Oakland, California, 1970.

Scofield, L., and W.M. Timothy, "Product Evaluation: Bituminous Pavement Rejuvenator," Arizona Transportation Research Center, Phoenix, Arizona, 1986.

Shen, J., S. Amirkhanian, and B. Tang, "Effects of Rejuvenator on Performance-based Properties of Rejuvenated Asphalt Binder and Mixtures," *Construction and Building Materials*, Vol. 21, No. 5, 2006, pp. 958–964.

Shen, J., S. Amirkhanian, and J. Aune Miller, "Effects of Rejuvenating Agents on Superpave Mixtures Containing Reclaimed Asphalt Pavement," *Journal of Materials in Civil Engineering*, Vol. 19, No. 5, 2007, pp. 376–384.

Taylor, L.H., and F.R. Rollins, Jr., "Ultrasonic Study of Three-phonon Interactions. I. Theory," *Physical Review*, Vol. 136, No. 3A, 1964, pp. A591–A596.

Viktorov, I.A., *Rayleigh and Lamb Waves: Physical Theory and Applications (Ultrasonic Technology)*, Plenum Press, New York, New York, 1967.